



UNIVERSITY OF
BIRMINGHAM

**Carbon black and graphene supported
Pt catalysts for intermediate
temperature polymer electrolyte fuel
cells**

by

HAITAO YU

A thesis submitted to the University of Birmingham for the degree of
MSc by Research

Supervisor: Prof. Robert Steinberger-Wilckens

PEFC Research group

School of Chemical Engineering

University of Birmingham, B15 2TT, UK

October 2014

UNIVERSITY OF
BIRMINGHAM

University of Birmingham Research Archive

e-theses repository

This unpublished thesis/dissertation is copyright of the author and/or third parties. The intellectual property rights of the author or third parties in respect of this work are as defined by The Copyright Designs and Patents Act 1988 or as modified by any successor legislation.

Any use made of information contained in this thesis/dissertation must be in accordance with that legislation and must be properly acknowledged. Further distribution or reproduction in any format is prohibited without the permission of the copyright holder.

Abstract

A Polymer Electrolyte Fuel Cell (PEFC) is an electrochemical cell which can transfer chemical energy of hydrogen fuel into electrical energy directly, with high efficiency and little environmental impact. PEFCs have attracted a lot of interest due to the advantages, such as; good response to load change, quick start up times and high efficiency value. During its operation process, hydrogen is oxidized at the anode and oxygen is reduced at the cathode. As the most significant problem, the cost of platinum catalyst is an obstacle in the commercial application of PEFC. This study focused on the utilization of different catalyst support materials (Carbon black, RGO and a mixture of them) and the fabrication process of catalysts, in order to reduce the platinum amount used in electrodes and get better electrochemical performance in both ex-situ and in-situ tests. The microwave-assisted polyol process (MWAPP) was used to fabricate catalysts in a quick way, involving only Pt precursor and support materials in polyol solution.

In our research, numerous attempts have been made to achieve the improvement of the Pt catalyst properties. Briefly, the serious stacking of RGO sheets is observed in the SEM image of Pt/RGO. However, as to our Pt/(RGO+C) catalysts, the addition of carbon black has solved this problem very well. The carbon black particles encircle the RGO sheets to prevent them from stacking. According to the TEM images of Pt/(60%RGO+40%C), it is clear that, the Pt nanoparticles only grew on the surface of RGO. Moreover, a majority GO sheets have been changed into little pieces by strong ultrasonic treatment. The rare remaining RGO sheets are much thinner than the RGO sheets in Pt/RGO. Compared to TKK, our catalysts with the mixture support material of RGO and C have similar nanoparticle sizes and are more uniform with stable Pt distribution. The largest ex-situ ECSAs of the Pt/C catalyst and Pt/RGO catalyst were

ca. $80 \text{ m}^2\text{g}^{-1}$ and ca. $45 \text{ m}^2\text{g}^{-1}$ respectively. At 800W in MWAPP, the best reaction duration is clearly illustrated to be 50 s. Through various attempts of the heat treatment at different temperatures, the best temperature of the heat treatment to the Pt/RGO catalysts comes to be about $140 \text{ }^\circ\text{C}$. As to the promising Pt-RGO-C catalysts made in-house, they illustrated excellent performances in both ex-situ and in-situ test, which is much better than TKK and JM-0165.

Contents

Carbon black and graphene supported Pt catalysts for IT-PEFCs	1
Abstract	2
1. Introduction.....	6
1.1. Fuel cell.....	6
1.2. PEFC	8
1.2.1. Collector plates	10
1.2.2. Gas channels	12
1.2.3. Gas diffusion layers	14
1.2.4. Catalyst layer	15
1.2.5. Polymer Electrolyte Membrane	23
1.2.6. PEFC Applications.....	28
1.3. Research goals and strategy	29
2. Experimental Work	31
2.1. Synthesis	31
2.1.1. Pt/C	31
2.1.2. Pt/RGO.....	32
2.1.3. Pt/(RGO+C).....	32
2.2. Characterisation	33
2.2.1. Thermogravimetric analysis (TGA).....	33
2.2.2. X-ray photoelectron spectroscopy (XPS)	33
2.2.3. Fourier transform infrared (FT-IR)	34
2.2.4. Environment Scanning Electron Microscopy (ESEM).....	34
2.2.5. Transmission Electron Microscopy (TEM)	35
2.3. Electrochemical Testing.....	36

2.3.1. Cyclic voltammograms (CV).....	36
2.3.2. Linear sweep voltammetry (LSV)	38
2.4. MEA Fabrication and Fuel Cell Testing	39
3. Results and Discussion	42
3.1. TGA	42
3.2. XPS	44
3.3. FT-IR.....	45
3.4. SEM	47
3.5. TEM	52
3.6 CV and LSV.....	56
3.6.1 Pt/C	56
3.6.2. Pt/RGO.....	63
3.6.3 Pt/(RGO+C)	74
3.7. MEA testing (in-situ testing).....	79
4. Conclusions and Further Work	94
5. References.....	99
6. Appendix	106

1. Introduction

1.1. Fuel cell

A fuel cell is an electrochemical device which can turn chemical energy of fuels into electrical energy directly, with a high efficiency and little environmental impact. Fuel cells have attracted a lot of interest recently due to the potential for clean energy, high efficiency and high power density. Compared with typical conventional power generation methods, fuel cells avoid the intermediate processes of mechanical work and heat loss. As a result, fuel cells get rid of the thermodynamic limitation experienced by heat engines, i.e. the Carnot efficiency. Furthermore, different from batteries, fuel cells are continuously supplied with the reductant and oxidant so that they can keep working. As long as fuel is supplied, fuel cells show more significant resemblance to electrolyzers. Fuel cells can be operated in reverse for energy storage. In principle, a wide range of fuels and oxidants can be used in fuel cells. The major reductants used are common fuels, such as hydrogen, carbon monoxide, methane and the major oxidant is air.

The components of all fuel cell power systems comprise three parts. The first one is unit cells, which is the site of the electrochemical reactions. The second one is stacks, in which the separate unit cells are modularly connected together. Finally, there are some components for the system balance, such as thermal management, electric power and feed stream conditioning. Among these components, unit cells are the core in fuel cells. This is where the chemical energy of the fuel is converted into electrical energy.

The basic structure of the fuel cell includes an electrolyte layer, with a cathode and an anode on either side. A schematic of the ion conduction, electrons and reactant/product gases flow in an individual fuel cell is shown in Fig.1.1

(Hirschenhofer, Stauffer, Engleman, & Klett, 1998). Typically, in a fuel cell, fuel and oxidant (usually air) are separately fed into the negative electrode (anode) and the positive electrode (cathode) respectively. The electrode is the place for the electrochemical reactions to occur, with ions transport through the electrolyte and complementary electric current through the external load.

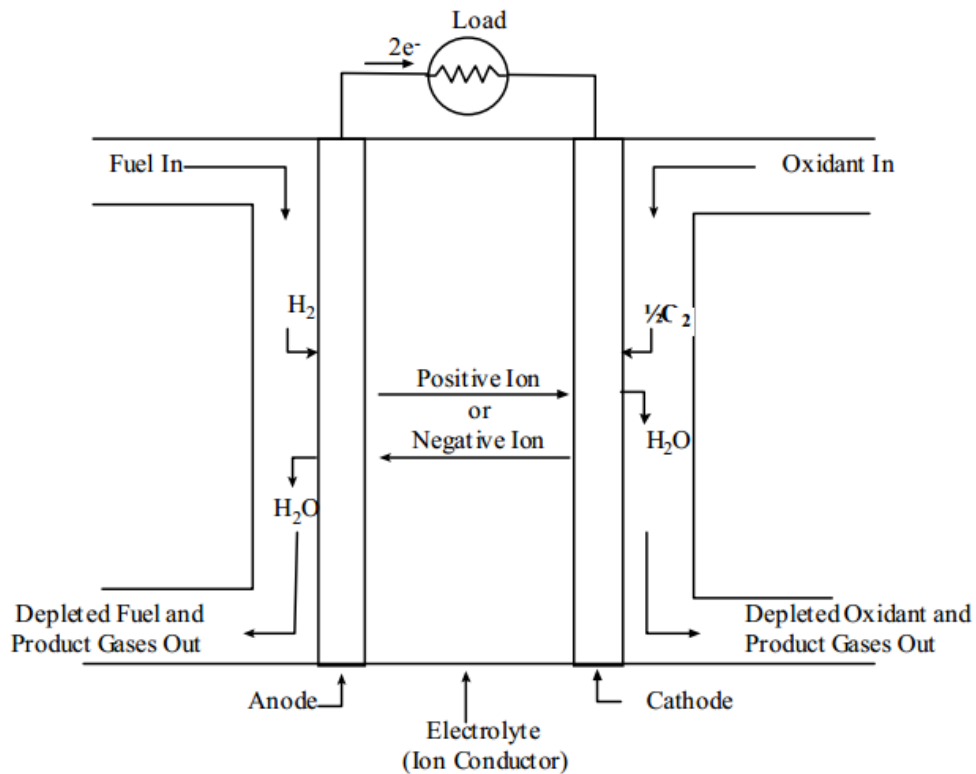


Figure.1.1. Schematic of an individual fuel cell in hydrogen operation

Though there are many aspects in common between a fuel cell and a battery, a fuel cell still has several different features from a battery. In the battery, the energy available is stored in the reductant before it works. Explained in another way, the battery is an energy storage device. When the energy stored in chemical reactants is used up, it can't continue to work anymore. While, the fuel cell essentially is an energy conversion device, which can continue to export electric energy as long as the fuel and air are supplied. Generally, the type of fuel cells is identified by the use of the electrolyte. At the same time, the fuel and electrolyte in the fuel cell can also determine the reactions in

the electrode and the ion transportation in the electrolyte.

1.2. PEFC

Polymer Electrolyte Fuel Cells (PEFCs) are seen as the replacement for the internal combustion engine as they have good response to load change, quick start up times and high efficiency value. In the 1960s, as an auxiliary power sources (APU), the first PEFC was applied in the Gemini space flights (SONE, 2004). After this, technology developments in the PEFC area were stagnant. Since then, the fundamental design of PEFC went through a period of redesign because of new fabrication methods in the late 1980s.

As the most significant problem, the cost of platinum catalyst is an obstacle in the application of PEFC. In original PEFCs, the amount of platinum loading (4 mg/cm^2 in the first generation PEFC) (Pak & Kang, 2010) was so large that the PEFC could not achieve commercialization. Thus, this reconfiguration was focused on electrode employed materials, especially on reducing the platinum amount used in electrodes. The research in this area still continues to be paid lots of attention.

PEFC is one kind of electrochemical cells, in which hydrogen is fed and oxidized at the anode and oxygen is fed and reduced at the cathode. During operation, hydrogen is oxidized; the protons are released and conducted to the cathode through the proton exchange membrane (PEM). The protons combine with oxygen ions to generate water at the cathode. Meanwhile, since the PEM in PEFCs doesn't conduct electrons, the electrons released in the anode have to travel to the cathode along the electrical detour provided. So an electrical current is generated in this way. PEFCs operate at $\sim 80 \text{ }^\circ\text{C}$ and require high purity hydrogen as a fuel. The principles described above are

schematically shown in Fig. 1.2 (Litster & McLean, 2004). The membrane electrode assembly (MEA) is composed of a PEM, catalyst layers, and gas diffusion layers (GDLs). When fabricating the MEA, these three components are made separately and then pressed together in the environment of high temperatures and pressures. The MEA works as a heart of the PEFC. We can also see the MEA schematically in Fig.1.2. Usually there are two flowfield plates mirrored to build a bipolar plate, used in order to get higher voltages by stacking MEAs in series. The MEA is typically sandwiched by these plates (Kreuer, 2013). The electrodes consist of catalyst layers and gas diffusion layers. The electrodes connect the membrane surface with gas channels and current collectors.

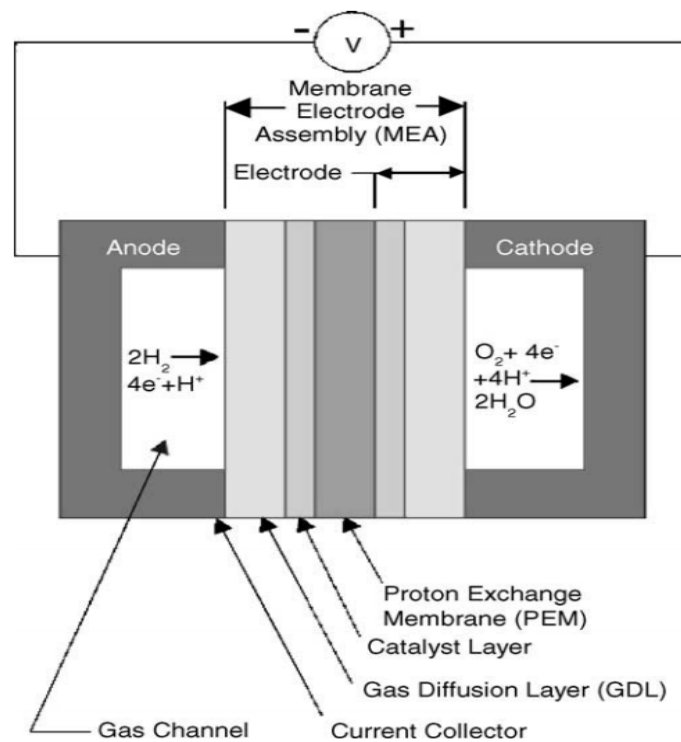


Figure.1.2. Schematic of a single typical proton exchange membrane fuel cell

As shown in Fig.1.2 (Litster & McLean, 2004), an effective electrode ought to realize the balances of the different transport process as which happen in an operational PEFC. Generally, the transport processes in PEFC can be divided into three categories. The three processes are proton transport, electron transport and gas transport.

Specifically, proton transport to/from the membrane from/to the catalyst; electrons move to/from the current collector to the catalyst through the gas diffusion layer; and the gases in the reactant, and product transport from catalyst layer and gas channels to the environment. The three phases usually refer to protons, electrons, and gases in a catalyst layer. In order to reduce the losses in transport processes, some attempts have been tried to distribute the volume amount of the catalyst layer for each phase among the transport media correctly to achieve the electrode design optimization (Mehta & Cooper, 2003). In addition, at the catalyst particle, an intimate intersection of the different transport processes is vital for an effective PEFC (Curnick, Mendes, & Pollet, 2010).

1.2.1. Collector plates

In most PEFC, multiple cells are connected in series by collector plates (bipolar plates). Collector plates work as electron conductors in the fuel cell. The current is transferred between one cell's anode and another cell's cathode. Furthermore, the air/oxygen and the fuel gas are distributed evenly over the cathode and the anode respectively along a flowfield. The collector plate in the anode and cathode are both in contact with the porous material (the anode GDL and cathode GDL, Fig.1.2) which is coated with hydrophobic polytetrafluorethylene (PTFE).

The designs to construct fuel cells and the materials used are various. This is a significant topic because the collector plates occupy the most volume and mass (about 80%) in fuel cell stacks (Murphy, Cisar, & Clarke, 1998). Moreover, a high percentage of the cost is used at the collector plates. It is only, in some small cells, where bipolar plates are not necessary.

For the design of bipolar plates, one simple flowfield pattern uses parallel grooves. There are some other patterns as well. Overall, there is no clear conclusion to choose

which one is the best. Different flow field patterns have their own supposed problems. For example, in the parallel systems, it is quite easy for reactant impurity or water to block the channels. By this, it will create an area that can't be supplied with reactants. It can be guaranteed there isn't the blockage in the serpentine systems. However, the path length and turns increases in the system, which will need more excessive power to push the reactants through the cells. Based on the understanding of these flow field systems, a compromise design which makes gases swirling over the surface of the electrode has been utilized to shift the block region of impurity gases. But for water, it is still possible to form a droplet and exist in the bipolar plates. Generally, the height and width of grooves are controlled no more than 1 mm. As to the water drop, it requires that the pressure decline along the channel needs to be larger than the surface tension of the water. In this situation, if blockage caused by water and other gases happen, sufficient pressure can drive them away again.

The requirements of the material used as bipolar plates usually follow these aspects. First, the material should own excellent electrical and heat conductivity (more than 10 S cm^{-1} and $20 \text{ W m}^{-1} \text{ K}^{-1}$ respectively). Second, because the material will contact with oxygen, hydrogen, electrolyte, water and heat directly, it should be corrosion resistant to these infections. Moreover, it needs to be fairly stiff, with flexural strength more than 25 Mpa, and impermeable to gas. Finally, the cost is better at a reasonably low level (Büchi, F., et al 2002). After getting suitable materials, the requirements of the bipolar plate fabrication process should be light and slim, in order to get the minimum weight and volume of the fuel cell stack. Besides, the duration of the manufacture should be as short as possible. During the fabrication process of the bipolar plates, these two aspects – materials and manufacturing methods - need to be considered together. Generally, graphite is used as the material to manufacture collector

plates due to its good electrical conduction, low density compared with metal, and its reasonable plasticity. The collector plate made of graphite sheet has shown an excellent power density in fuel cell stacks. On the other hand, there are also some disadvantages of using graphite. First of all, the bipolar plates are required to be several millimeters thick to separate the reactant gases because of the porosity of the graphite. Meanwhile, some machining processes still take a rather long time and high charge. Furthermore, graphite is so brittle that it asks for careful operation in practical application. As to metal materials, they can be utilized to fabricate collector plates as well. Compared with the carbon materials, metals have shown good electrical and heat conduction, they are much easier to be machined and can achieve keeping the reactants apart by only using very thin materials. Corrosion is the main problem in the metal collector plates. The atmosphere in PEFCs usually contains oxygen, water and warmth, sometimes acid exists as well. In order to prevent the metal from being corroded, some special materials, such as hydrophobic PTFE, can be coated on the surface of collector plates. By this way, some advantages of the machining materials will be lost.

Nowadays, according to the research, various machining materials and methods of the PEFC collector plates have been introduced. While, as stated before, there isn't any strategy that fully satisfies to every requirement, it still presents a huge space of the improvement in the collector plate technique.

1.2.2. Gas channels

Gas channels act as the reactant suppliers in the fuel cell. The anode reactant gas is usually hydrogen. While, the cathode reactant gases are oxygen or air. The principle of reactant gases transport in the gas channels is by gas convection and diffusion. Except few PEFCs are supplied with pure oxygen at the cathode, it is generally using the air as the cathode reactant. When the air goes through the PEFC, it achieves driving the

product water out of the cell. Thus, the rate of the actual air flow is always higher than that of the necessary oxygen supply. If the air flow was fed at the exact stoichiometric rate of oxygen, the oxygen would be completely used up in the fuel cells. As a result, the depletion of the oxygen in the exit air will cause serious concentration losses. In practice, the stoichiometric rate is usually more than 2.

Other problems in the air are its drying effect which is influenced by the temperature in a non-linear way. In this situation, the effects in terms of saturated vapour pressure and relative humidity need to be precisely designed and analyzed. Specifically, the definition of saturated vapour pressure is the partial pressure of water vapour at the situation that the mixture of liquid water and air comes to be equivalent. That is to say, when the partial pressure of vapour reaches saturated, the rate of liquid water evaporation and steam condensation are the same. As the temperature of the PEFC goes up, the variety of saturated vapour pressure tends to increase more and more quickly, instead of growing in a linear way. This physical characterization makes it more complicated to achieve the adjustment of the saturated vapour pressure in PEFCs. Moreover, at the cathode, the control of the relative humidity will have a huge affect to the PEFCs as well. In order to retain the electrolyte membrane at suitable water content, it generally requires the humidity of air to be more than 80%. While it can't also be too wet, another significant function of the air is to carry the product water out of the PEFCs, in order to ensure that the collection of liquid water won't happen in the electrodes. In this aspect, it needs the air dry enough to take up the liquid water in the cells. So far, most methods used to increase the humidity are utilizing the water out of the cells. In practice, the method and level of the humidification needs to be designed and varied based on the other effects, such as the volume of the PEFC, the fuel source and system pressure. For the cell system, it requires good balance among many effects

to achieve the improvement and optimization.

1.2.3. Gas diffusion layers

The gas diffusion layers (GDL), also called porous backing layers, are typically composed of carbon materials (carbon paper or cloth), with a thickness from 100 μm to 300 μm . In PEFC, two gas diffusion layers sandwich the polymer membrane. The main functions of the gas diffusion layers contain four aspects: gas diffuser, electrical transfer, mechanical support and driving water out of the electrodes. Specifically, the porous GDLs transport reactants/products diffusing to and from the catalyst layer effectively both in the anode and cathode. The reactant gas components (hydrogen gas in the anode and the air mixture in the cathode) from the gas channels will go through the gas diffuser to the catalyst layer. In this process, the driving forces for the reactant gases to transport through the pores of the GDL are concentration and pressure gradients and the momentum transport. Meanwhile, the graphite matrix of the GDL is the electrical conductor to transport electrons between the catalyst layers and the collector plates.

For the materials of the GDL, it typically uses carbon in the configuration e.g. felt-like or non-woven pressed carbon fiber. In addition, the GDL manages the water amount to be suitable in reaching and being held in the membrane. As in the collector plate, hydrophobic polytetrafluorethylene is used in the backing plates as well. GDLs are typically covered with a PTFE coat. The main aim to incorporate hydrophobic materials in GDL is to prevent water from filling the pore volume. Therefore, it can make sure that the catalyst and the gases have a good contact in PEFCs. Meanwhile, in the cathode, it has more advantages in removing the product water easier by forming non-wetting surface of the passages.

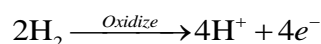
For the water management, the ideal statement is that the production water at the cathode can keep the hydration of the electrolyte in the PEFC at the best level. At the

same time, air will provide the necessary oxygen and take the extra water from the cells. In principle, the thickness of the electrolyte membrane is so thin that sometimes it is possible to achieve this ideal status by excellent design.

The water management is influenced by several factors. One effect is that when proton transfers from the anode to the cathode, each proton usually carries between one and five water molecules (Ren & Gottesfeld, 2001; Zawodzinski, 1993). This phenomenon is described as electro-osmotic drag. Based on this principle, it means, when the current density is high, the anode tends to be dried out, though the cathode is hydrated well. Meanwhile, as stated in the former section, the air at the condition of high temperature has a strong efficiency to dry out the electrodes. It is worth motioning that, before the gases were transferred into the cells, it is necessary to humidify them. Though it may seem bizarre to add by-product to the reaction system, it is certified to improve the performance greatly in this way in PEFCs.

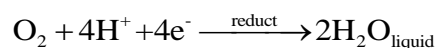
1.2.4. Catalyst layer

The catalyst layer which directly contacts with the GDL and the membrane is the active layer in PEFC. No matter in the anode or cathode, both the half-cell reactions take place in the catalyst layer. In the anode catalyst layer, there is an oxidation reaction of hydrogen gas, which comes from the anode gas diffuser, based on the following reaction equation.

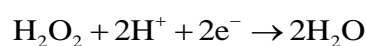
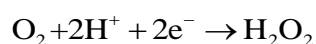


Protons released in this reaction will impregnate the PEM by dissolving in the trapped water. In contrast, there is a reduction reaction of the oxygen, which comes from the cathode gas diffuser, taking place with the protons and electrons based on the reaction equation in the cathode. The E_0 of the reduction reaction vs. hydrogen electrode (NHE) is +1.229 V. The protons are released by the PEM and the electrons are

transported through the external circuit. Because of the sluggish oxygen reduction reaction in the cathode, this reaction acts as the limitation of the overall reaction rate in a PEFC. Meanwhile, it is also the main reason that causes the loss of cell voltage and efficiency during the PEFC application.



The oxygen reduction reaction (ORR) that directly transfers four electrons is what we design and prefer to get in the cathode. Actually, besides transferring four electrons to get water directly, there is also a half-cell redox existing during the electron transfer process. This half-cell redox is hydrogen peroxide continues to accept two electrons to form water. As shown below, with E_0 at +0.695 V and +1.776V vs.NHE respectively, hydrogen peroxide is produced and consumed during the process. The decrease of the E_0 lets the cell voltage drop significantly in the reaction. Moreover, hydrogen peroxide plays an obvious harm to the polymer in PEM, so it will reduce the durability of the MEA dramatically. Therefore, for cathode catalysts design and fabrication, we prefer to get the catalysts with higher electron transfer number in ORR.



Generally, the catalyst layer is fabricated by painting the catalyst on the GDL or the membrane. In either fabrication way, the common objective is to combine the catalyst particles (mostly platinum or platinum alloys), which is shown as black spots in Fig.1.3 (Litster & McLean, 2004), with the proton conducting media closely.

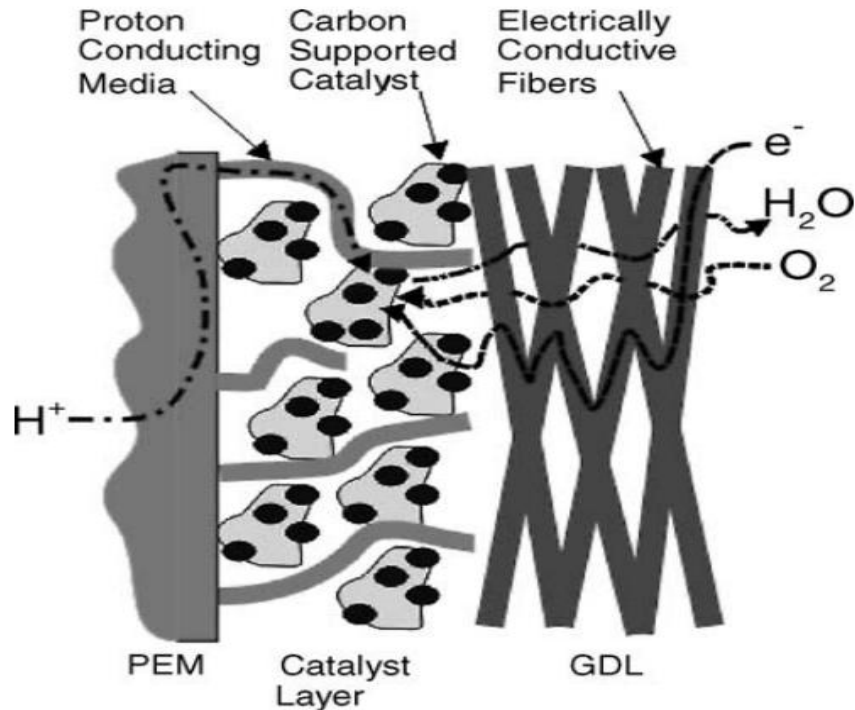


Figure.1.3. Transport of protons, electrons and gases in PEFC electrode

The first generation catalyst was PTFE-bound Pt black electrocatalyst. When it was used in PEFCs, the fuel cell exhibited an excellent cycling performance. The cost of the first generation PEFC is prohibitively high because of commonly high-priced platinum loading of 4 mg/cm^2 (Pak & Kang, 2010). Based on the high cost, a great amount of research work has been done to reduce the Pt loading to below 0.4 mg/cm^2 . During the research process, increasing the utilization of the platinum by advancing the methods is an effective way to achieve the target of reducing Pt loading. There are two common strategies to maximize the available surface area of electrocatalysts. One strategy is to control the particle size of catalysts to the nano-size. The other practice is to disperse the Pt nanoparticles onto support materials for retaining its nano-scale. Recently, a quite low Pt loading catalyst (0.014 mg/cm^2) was produced by a novel sputtering process (Zabihian, Davari, & Osei-Prempeh, 2013). As a result of the Pt loading reduction, now the main problem of PEFC commercialization is not the high cost of Pt catalyst anymore. The utilization of Pt catalysts has drawn more and more

attention. In PEFC, the overall performance is influenced by many properties of the catalyst layer, such as electrical and ionic conductivity, hydrophobicity and reactant diffusivity. So a good balance among these aspects should be researched to get the optimization of the catalyst layer in a PEFC.

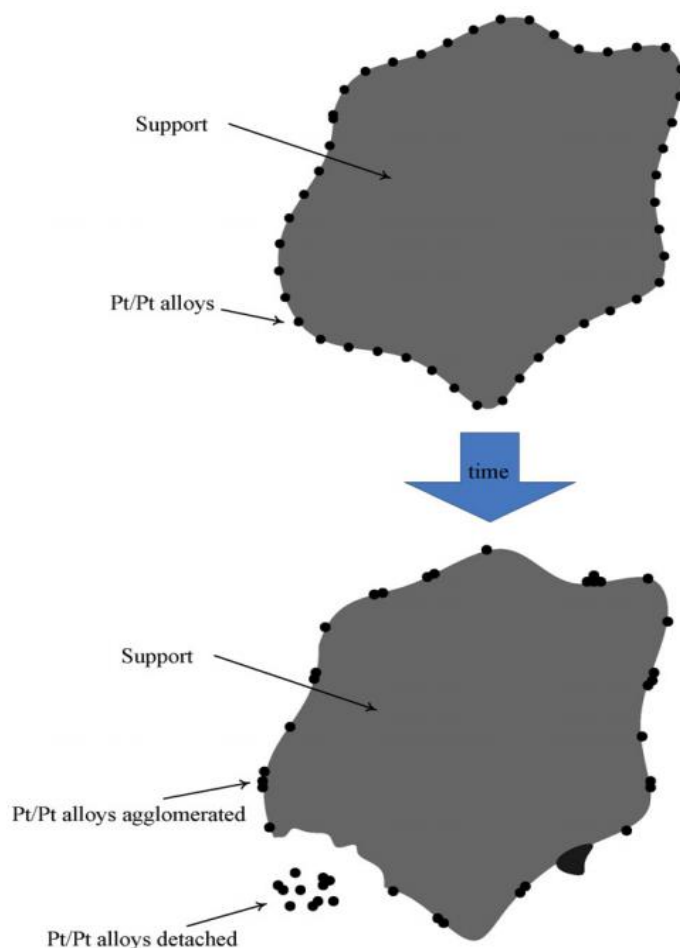


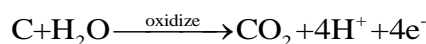
Figure.1.4. Schematic of the cause to the degradation of Pt nanocatalysts

The cycle life of PEFC is one of the most significant properties, which not only represents the operation life, but also demonstrates the reliability and reduce the cost of the cell. High requirements of long lifetime are shown in many applications, such as the durations of car, bus and stationary applications are about 5000, 20000 and 40000 hours respectively. The main factor which decides the cycle life of PEFC is the degradation of the platinum catalyts. Specifically, the electrochemical activity of the Pt nanoparticles in the MEA is the only determinant to the electrode reactions. Therefore, the more

electrochemically active of the catalysts which can be characterized by electrochemical surface area (ECSA), the better performance the PEFC has. It is generally accepted that, as it is shown in Fig.1.4 (Shao, Yin, & Gao, 2007), Pt nanoparticles tend to agglomerate or drop off from the support materials during the PEFC operation. This process will result in the deterioration of the performance dramatically by decreasing the ECSA of Pt nanoparticles. Meanwhile, the oxidation of the carbon support materials also degrades the cycle life.

A great deal of research has been done in this area, while, the discrepancies of the durability in PEFC catalysts, especially in Pt/C catalysts, are still extensively existing. According to the state-of-art research, the size of Pt nanoparticles on the carbon support materials is usually distributed from 2 nm to 6 nm. Because of the high specific surface energy of the nanoparticles, they tend to agglomerate during the operation process. When the size of the nanoparticle is smaller, its ECSA is higher and it is more possible to agglomerate. Moreover, the reason for the degradation of the catalyst is the harsh conditions during the PEFC operation. As it can be seen, the PEFCs usually work at the high temperature, high humidity and low pH. In addition, the anode and the cathode are exposed in the strong hydrogen and oxygen atmosphere respectively. Meanwhile, in order to achieve high efficiency, it generally requires the potential should be more than 0.6 V (versus the standard hydrogen electrode), sometimes even reach 1.2 V for a short duration. High operating voltage will not only decreases the performance of Pt catalyst in the ORR, but also deteriorates the degradation.

For the degradation mechanisms of Pt catalysts, it contains two aspects - support materials (Carbon) and catalytic metals (Pt), which each have influence to the other. Specifically, as to the support material, carbon is usually oxidized based on the electrochemical reaction shown as below.



The E_0 of this electrochemical oxidation reaction vs. NHE is only +0.207 V. Therefore, from the thermodynamic analysis, the carbon in the support materials is possible to be oxidized when the potential is above +0.2 V. Moreover, based on the investigation of differential electrochemical mass spectroscopy (DEMS), in the Pt catalysts, carbon will be oxidized to CO and CO₂, when the voltage is over 0.3 V and from 0.6 V to 0.8 V respectively. On the other side, another reaction also results in the degradation of the carbon, especially Pt existing in the environment.



Meanwhile, the corrosion of carbon declines the available support materials for the Pt nanoparticles, which leads to the drop of Pt nanoparticles from carbon support and the decrease of the ECSA of catalyst. At the same time, as the reaction products of two reactions, CO will poison the Pt in the catalysts. Besides, in the oxidative atmosphere, oxygen containing functional groups tend to be formed on the surface of the carbon supports, which will both reduce the conductivity and accelerate the Pt agglomeration. Furthermore, the carbon corrosion will also influence the performance of PEFC in many aspects, such as hydrophilicity, gas permeability, electrode resistance and electric contact.

As to the catalyst metal (Pt), the ECSA is a very significant parameter to characterize the performance of an electrode. Commonly, the value of ECSA reflects the amount of available Pt catalyst sites in the electrochemical reactions. Thus, an excellent electrode catalyst should have a large ECSA in both ex-situ test and in-situ test. It is reported that the decrease of ECSA in electrodes is the main cause to the degradation of PEFC. As it is said before, the decrease of ECSA is due to the agglomeration of Pt, the dissolution of Pt into the polymer electrolyte and the drop of

Pt nanoparticles from the support materials. While, the percentage of each factor that contributes in the Pt degradation is still uncertain. Specifically, the pathways of Pt sintering take place in the three kinds of processes. The first one is the dissolution and redeposition process of Pt nanoparticles. The second one is that the Pt atoms move on the support materials. The last one is the migration of Pt nanoparticles through nanocrystallite to result in the agglomeration. The specific degradation mechanisms are different when the operation conditions are varied. For instance, under the loading cycle process, the dissolution and redeposition of Pt tend to be more prevalent. Nowadays, the mechanism of the degradation and the approaches to improve the performance of the catalysts are still being searched and explored.

Ideal support materials usually have four advantages, excellent electrical conductivity, large available surface area, mesoporous structure and good adhesion between catalyst particles and the support. Commercial carbon black support materials, such as Vulcan XC-72 carbon black, which consist of amorphous carbon spheres with Pt nanoparticles, have shown good performance in PEFCs. However, there are still several issues in some aspects, such as low thermochemical stability, poor durability and the nanoparticles trap of micropores (Curnick et al., 2010; Ferreira et al., 2005; Takahashi & Kocha, 2010). These problems can be improved by using novel material supports such as graphene oxide (GO).

Reduced GO (RGO) is a modified GO with some surface oxygen groups removed. According to Liao's research (Liao, Liao, Tso, & Shy, 2011), the size of Pt/RGO nanoparticles is decided by the reaction time in one-pot microwave assisted polyol process (MWAPP). The shorter times made the Pt particles smaller, more uniform and better separated on the GO sheets. On the contrary, the longer times let Pt particles disperse denser and more agglomerate.

The polyol process is the most common method to grow nanoparticles on the support materials by using polyol solutions (Chu, Wang, Gu, & Yin, 2010). In the usual fabrication procedure, catalyst precursor and support materials in a polyol solution were heated under reflux. However, this procedure is time intensive and it is pretty hard to precisely control the particle size (Lee, Lim, Chun, & Lee, 2012). Compared to the common polyol process and other synthesis methods, MWAPP has many advantages such as fast reaction speed, high efficiency and homogeneous heating process. The MWAPP can also achieve a more precise adjustment of Pt size distribution by controlling reaction time in minutes rather than hours. Specifically, when the MWAPP is used to fabricate Pt/RGO electrocatalysts as illustrated in Fig.1.5, the fast heating process and the formation of evenly dispersed particles can prevent the nanoparticles from agglomerating, thus increasing the surface area of the electrocatalyst. The size and distribution of Pt particles on the RGO play decisive roles in the performance of PEFCs.

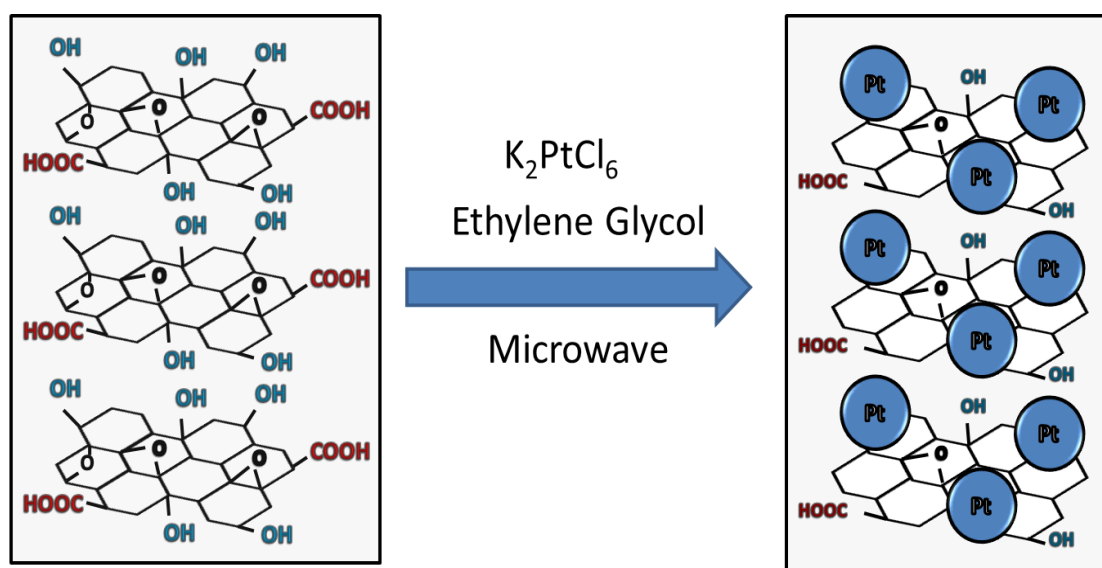


Figure.1.5. Schematic of the microwave polyol process as applied to the growth of Pt nanoparticles on Graphene Oxide

the hydrogen of the polyethylene is replaced by fluorine to modify its property. This process is usually named as perfluorination, which is widely applied to many aspects. After the modification, the polymer we get is polytetrafluoroethylene (PTFE) which is named as Teflon as well. The monomer of PTFE is tetrafluoroethylene, in which, 'tetra' means that all of the four hydrogens in ethylene have been substituted by fluorine. Because of its special molecular structure, illustrated in Fig.1.7 (Larminie & Dicks, 2003), PTFE plays a significant role in many fuel cell areas, not only in PEFCs, but also in alkali and phosphoric acid fuel cells. Specifically, in PTFE, there are strong chemical bonds existing between the carbon atom and the fluorine atom, which gives it high chemical stability. In other words, it is resistant and durable to most chemical attack. Furthermore, when it is used in PEFC, its property of strong hydrophobicity gives it great advantages at forbidding fuel cells from flooding by driving water out. Furthermore, in order to get an electrolyte, the PTFE polymer needs to be modified by sulphonation. In other words, one fluorine in PTFE is replaced by a side chain which ends with a sulphonic acid group (HSO_3). As we know, it is widely used for some complex chemicals to be 'sulphonated' in the processing, such as the fabrication of detergents. As to the manufacture of Nafion, various types of Nafion have different details of the side chains. One structure is shown in Fig.1.8 (Larminie & Dicks, 2003).

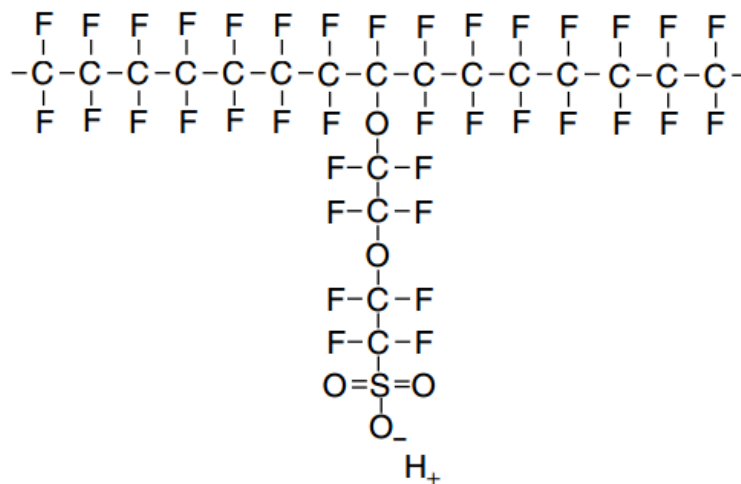


Figure.1.8. One molecular structure of Nafion

Actually, the connection in HSO_3 is ionic bond, so the side chain is ended by a SO_3^- ion, instead of HSO_3 . This characteristic makes the side chains in Nafion material tend to gather. Therefore, when the hydrophilic functional group- sulphonic acid clusters in Nafion, it means that we have created some hydrophilic regions within the hydrophobic materials, which will bring us some creative results. The hydrophilic regions created by HSO_3 clusters own strong ability in the absorption of water, which can increase the maximum weight up to 50% of its dry mass. It forms a micro-phase separated morphology in Nafion, in which the water collected by the hydrophilic side chains exists in stable and tough hydrophobic main structure. The specific configuration of this morphology is illustrated in Fig.1.9 (Larminie & Dicks, 2003). Meanwhile, as it is said before, the ionic bond between H^+ and SO_3^- is relatively weak within these hydrophilic regions. Overall, although actually all the hydrated regions do not contact directly, proton still has the ability to transfer through the polymer molecule structure. The larger hydrated regions, the better transfer of the protons it has. Generally, as a level of well hydrated electrolyte, each sulphonic side chain usually needs almost 20 water molecules to achieve the conductivity at 0.1 S cm^{-1} . The fall of the conductivity and water molecules content are nearly in linear relationship.

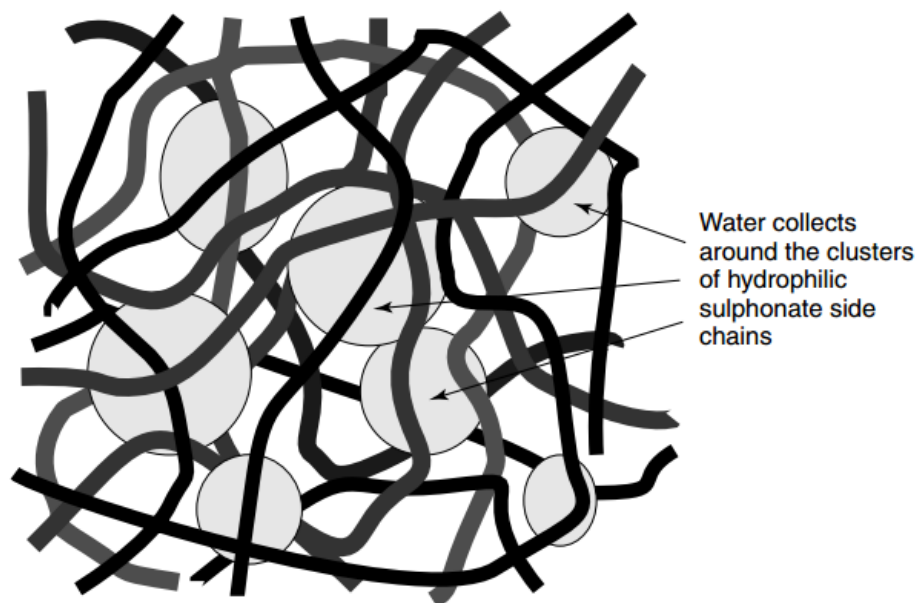


Figure.1.9. The morphology of water in Nafion membrane materials

Equivalent weight which is inversely related to the ion exchange capacity (IEC) is used for characterizing the membrane. Typically, the range of equivalent weight is from 800 to 1100 milliequivalents per gram (dry polymer). In PEMFC, the fully fluorinated Teflon®-based family is the standard electrolyte material, which is similar to the space application product of E.I. DuPont de Nemours in the mid-1960s. In the past, the membrane usually used was a melt-extruded membrane (Nafion®No. 117) fabricated by DuPont. The PFSA membranes exhibit remarkably high stability in chemical and thermal aspects. Specifically, the PFSA membranes can bear chemical attack in the FC environment, such as strong oxidizing and reducing conditions, strong bases, H₂, O₂ and Cl₂ up to 125 °C. Similar to Teflon®, Nafion consists of a fluoropolymer backbone with some sulfonic acid groups chemically bonded side chains. Nafion membranes have shown excellent stack life in the application aspect, especially in selected applications, electrochemical applications and operating conditions (Passalacqua, Lufrano, Squadrito, Patti, & Giorgi, 2001; Sasikumar, Ihm, & Ryu, 2004). Nafion membranes have exhibited a long lifetime which is over 50,000 hours in the selected

tests and water electrolysis system.

The polymeric structure of the electrolyte membrane produced by The Dow Chemical Company (XUS 13204.10) is very similar to that of Nafion, except the length of the side chain is shorter. These shorter side-chain membranes also have excellent performance and stability. However, because of the change in side chain length, some membrane properties have been influenced. For example, the water interactions are raised to a higher degree. As a result, when the Dow's membrane is used, particularly in a thinner form, ohmic resistance turns to be lower than Nafion. However, Dow no longer produced this kind of short side-chain membranes. Nafion also fell into engineering and expense issues. Now new kinds of PEMs are being researched by numerous companies. From the view of Nafion and other PEMs, there are several common features among them. First, they have high chemical resistance and mechanical strength. Second, they can generate protons and absorb numerous water molecules. At last, in well hydrated condition, they can transfer H^+ quite easily.

The process which we normally use is the melt-extruded film technique. With the development of the solution-cast film process, it is moving to take place of melt-extruded film because of its advantages in reduction of costs and improvement of the manufacturing throughput efficiency. In the solution-cast film process, the polymer in ionic form is dissolved in alcoholic solution, and then it is fabricated into desired the film. Before the solubilization step, the non-ionic polymer is transformed to an ionic phase, which is ready to be used in PEFC. Another development of the membrane manufacture techniques is the use of internal support layer in enhancing the mechanical strength of the thin polymer electrolyte membrane.

1.2.6. PEFC Applications

The applications of PEFCs usually contain two main aspects, transportation applications and stationary applications. PEFCs are used as a kind of prime powers in cars and light trucks. As we know, among different types of fuel cells, PEFC is the only one designed in on-road cars. The PEFC systems which utilize integrated fuels of gasoline, hydrogen and methanol have been attempted by many car producers. In America and Japan, even some PEFC vehicles from Honda and Toyota have been used by specific customers. However, in order to enlarge the PEFC application in transportation and achieve widespread use, there are still several aspects needed to be improved further. First of all, the improvement of PEFCs in cycle life and reliability is necessary. Meanwhile, we need to continue reducing the weight, volume and cost of the PEFC systems by developing fuel cell technology. The structure of PEFC systems are required to be more robust for being operated under all the expected conditions of the cars. At last, the safety level of PEFC vehicles also needs to be paid much attention.

As to the stationary applications during the PEFC development, distributed generation in small scale, from 1 to 10 kW AC, using natural gas or hydrogen is the major aim of many efforts. There are hundreds of PEFC stationary units located in Europe, Japan and America. Through considerable research, significant improvement on system integration and stand-alone operation has been achieved. The typical system efficiency of PEFC is about 30%, which can be raised to about 80% by recovering heat from the water at 50 to 70 °C. The cycle life of a single system has been enhanced to 8000 hours, with a degradation rate at approximately 5% per 1000 hours.

1.3. Research goals and strategy

During our study, in order to reduce the platinum amount used in electrodes and get better electrochemical performance in both ex-situ and in-situ test, we try to broaden the utilization of electrode support materials (Carbon black, RGO and the mixed material of them) and achieve the fabrication and optimization of catalysts.

According to the state-of-art researches, the degradation of electrical property in the catalyst is due to three aspects: the agglomeration of Pt, the dissolution of Pt into the polymer electrolyte and the drop of Pt nanoparticles from the support materials. Based on these difficulties of catalysts, ideal support materials are usually required to own the following advantages: excellent electrical conductivity, large available surface area, mesoporous structure and good adhesion between catalyst particles and the support. Though carbon black consisted of amorphous carbon spheres has good performance as the support material in PEFCs, novel material supports RGO is considered to have more advantages at many aspects, such as larger surface area, higher thermochemical stability, longer durability and stronger Pt nanoparticles trap ability. Promising mixture support materials of C and RGO are designed and researched in this thesis as well. As to the fabrication process, the MWAPP was used to fabricate catalysts in a quick way, involving only Pt precursor, support materials and polyol solution.

Numerous attempts were tried and analyzed to achieve the improvement of the Pt catalyst properties. Briefly, this report describes the variety of support materials; the optimization of MWAPP at pH value, heating power, reaction duration and other aspects; heat treatment at different temperatures to the catalyst; the design, optimization and selection of the best carbon content among the Pt-RGO-C catalysts. The composition and structure of the catalysts synthesized are characterized via TGA,

XPS, FT-IR, SEM and TEM. The electrochemical characterizations are performed in both ex-situ and in-situ systems.

2. Experimental Work

2.1. Synthesis

As it is shown below, the MWAPP fabrication process is an efficient way to produce Pt nanocatalysts on support materials, certified by our experiments and optimizations. Pt catalyst that has the nanoparticles of Pt distributed on the support materials such as carbon and reduced graphene oxide (RGO) was synthesized by taking 50 mg support materials, which was suspended in Ethylene Glycol (EG) (24 mL) and Isopropanol (IPA) (6 mL) (EG:IPA=4:1 in volume). Then suspension was ultrasonically treated for 60 minutes. Upon completion, 31.24 mg hexachloroplatinate (K_2PtCl_6 , 0.05 M (Sigma, $\geq 99\%$)) was added into the suspension. The suspension was then mixed further by ultrasonication and mechanical mixing for a further hour in order to make sure that there is a good dispersion of Pt salt throughout the mixture. The pH of the mixture was adjusted by sodium hydroxide (NaOH)-EG solution to about 12 which was monitored by utilizing universal indicator paper. Stir for another 30 minutes in N_2 atmosphere before it was set in the microwave oven and microwaved (CEM MARS Xpress) (800W) for the desired duration (40s). Then adjust the pH of mixtures back to less than 2 by adding nitric acid (HNO_3) and stir for another 12 hours to separate out and settle the Pt nanoparticles. The black precipitate product was washed several times with distilled water (18.2 M Ω) by high speed centrifuge (21,000 revolutions per minute, 4 °C) before being dried in vacuum oven at 60 °C for several hours.

2.1.1. Pt/C

As the commercial carbon black (Vulcan XC-72) was used as support material, in order to get a reproducibly productive process for Pt/C, different Pt content samples

were designed and fabricated by controlling the MWAPP conditions (650W, 140s and 800W 40s) and the mass rate of K_2PtCl_6 and C. Besides, after we got the Pt/C samples, they are heat treated for 2 hrs at 150 °C to enhance the performance of catalyst in ex-situ test.

2.1.2. Pt/RGO

During this part of the experiments, the support material was changed to commercial GO. Numerous attempts have been made to improve the performance of Pt/RGO catalysts, such as the adjustments of pH value (8 and 12), power (800W and 300W) and reaction duration (30, 40, 50, 60, 80, 120 and 160 s) of the MWAPP process. After this, a heat treatment at different temperatures (60, 100, 150, 180, 200, 250, 300 °C) for 2 hours was used to improve the catalyst performance. Moreover, for improving the catalyst property, before the commercial GO were used as support material, a strong ultrasonic treatment (100W, 30 mins) was attempted, working as 30s on – 10s off, in order to reduce its size and make it disperse better in solution.

2.1.3. Pt/(RGO+C)

In this part, the mixture of RGO and C were used as the support materials. The mass percentage of C in the support materials changed as 10%, 20%, 30%, 40% and 50%. It is worth mentioning that GO was also treated by high ultrasonic power as it was used in producing Pt/RGO samples before mixing with K_2PtCl_6 . And the calculated carbon was added after the MWAPP in all sample fabrications. Besides, the research on adding carbon before MWAPP and using commercial GO directly without strong sonic treatment have been tried as well.

All chemicals used were purchased from Sigma. The information of synthesis equipments is shown in table. 2.1. A commercially available Pt/C catalyst was used as

a reference (47 wt% Pt/C from Tanaka Kikinzoku Kogyo, ECSA=73.0 m²/g, electron transfer number=3.75).

Table.2.1. Synthesis equipments

Machine name	Model	Producer
Microwave oven	MARS 240/50	CEM Co.
High speed centrifuge	Sigma 3K30	Suquip Ltd.
Rotor	12150H	
Furnace	Lenton	Lenton Thermal Design Ltd.
Ultrasonic generator	VCX 130	Sonics and Materials Inc.
Magnetic stirrer	RS 232/0-10V	Heidolph Ltd.

2.2. Characterisation

2.2.1. Thermogravimetric analysis (TGA)

Thermogravimetric analysis (TGA) was tested on a Netzch Tg 209 Fi in-house. The environment of test process was 30 mL min⁻¹ of air and 30 mL min⁻¹ of Nitrogen with heating rate at 10 or 30 °C/min from 25 °C to 900 °C.

2.2.2. X-ray photoelectron spectroscopy (XPS)

X-ray photoelectron spectroscopy (XPS) could obtain the relative content of different groups or valences through the change of element's binding energy. XPS test was carried out at University of Leeds EPSRC Nanoscience and Nanotechnology Equipment Facility (LENNF). The machine used for XPS was a high resolution VG Escalab 250 which is equipped with a high intensity monochromatic Al K α X-ray

source.

2.2.3. Fourier transform infrared (FT-IR)

The principles of infrared (IR) spectrometry are the variety of the dipole moment in molecules influenced by molecular rotations and vibrations. In infrared spectroscopy, IR radiation is utilized on the samples to create molecular fingerprint of the specimen. Specifically, during the irradiating process, some infrared radiation will transmit the sample and some will be absorbed by the sample. The absorption happens when the frequency of radiation and vibration of the molecule match. The absorption of infrared radiation will result in the change of vibration amplitude, which illustrates a peak in the IR spectrum. Therefore, the spectrum carries the information of the molecular transmission and absorption (Nicolet, 2001; Tschida, n.d.).

In our experiment, the samples were performed on ATR-FTIR spectrometer for the qualitatively identification of the characteristic infrared groups at Chemistry Department in University of Birmingham.

2.2.4. Environment Scanning Electron Microscopy (ESEM)

Typical SEM is composed by electron column, sample chamber, detectors and viewing system. Each component has its corresponding function. Specifically, electron beam is created at electron column and interacts with the specimen in the sample chamber; detectors monitor numerous signals from the interaction of electron beam and samples; signal images of samples are displayed in viewing system. Different from optical microscope, there is not real images formed in SEM. The virtual image is constructed by scanning electron beam line, which is emitted by the specimen, with rectangular pattern. Electron beam only illuminates a single point in the rectangular pattern. The signals vary as the beam moves to reflect the

characteristic of samples. ESEM (Environmental Scanning Electron Microscope) with its higher resolution and lower requirement of vacuum degree has great potential in SEM aspect due to its unique electron detectors and pumping systems (Carrassi & Abati, n.d.; Legends, 2AD).

Our samples were tested by FEG-ESEM of XL30 with a maximum acceleration voltage of 100kV at Metallurgy and Materials Department in University of Birmingham.

2.2.5. Transmission Electron Microscopy (TEM)

Transmission electron microscopy (TEM) is consisted by three main components (illumination system, objective lens/stage and image system). Specifically, the illumination system, which plays the role as transferring the electrons from light source to the specimen, can be divided up into the gun and condenser lenses. As the important components in TEM, the lenses not only acts in using electron beam to form images, but also works in focusing the beam at a spot. The resolution of the electron lens stands for the minimum length which is resolvable in the object. Based on the principle of electron optic, when the specimen is settled in front of objective stage, an electron density distribution image is formed at the surface of the sample. Then, after the diffraction pattern is created at the back focal plane, an image is formed in the image plane of objective lens by recombining the diffracted beams. At last, the electrons are converted into visible signal by the fluorescent screen (Alexander, n.d.; Zaluzec, n.d.).

The ink preparation for TEM test is to disperse 1 mg catalyst into 1mL IPA by sonication for 30 mins. The copper grip is held by tweezers to immerse into the catalyst ink and dried. Our samples were performed by using a Philips CM200 FEGTEM field emission gun at University of Leeds EPSRC Nanoscience and

Nanotechnology Equipment Facility (LENNF) and HRTEM of JEM-2100 at Metallurgy and Materials Department in University of Birmingham.

2.3. Electrochemical Testing

The ex-situ test was conducted using a potentiostat (Autolab PGSTAT302N) to get cyclic voltammetry (CV) and linear sweep voltage (LSV) results. The principle of electrochemical testing is based on the conventional three electrodes system. During the testing process, the glassy carbon electrode (GCE) (5 mm diameter, 0.196 cm²) was coated in catalyst by dropping 10 μ L of catalyst ink and was used as the working electrode. For the ink preparation, 1.4 mg catalyst (ca. 20 wt % Pt) was dispersed in the solution, which contains 0.247 mL IPA, 0.748 mL H₂O and 0.005 mL Nafion. The corresponding Pt loading on the working electrode is 14.5 μ g/cm². The Pt mesh and the reversible hydrogen electrode (RHE) utilized as the counter electrode and reference electrode separately. The solution for the testing is 0.1 M HClO₄. Prior to dropping the catalyst ink on GCE, the GCE was polished thoroughly by using alumina powders in 1.0, 0.3 and 0.05 μ m successively, washed by UHQ water and dried under infrared light. Before the working electrode used for testing, the catalyst ink is dried in oven at 40°C for 12 hours.

2.3.1. Cyclic voltammograms (CV)

The definition of ECSA is the available catalyst surface area for the occurrence of electrochemical reactions. In the catalyst layer of PEFC, it reflects the available area of triple phase boundary for reactions. During our experiments, the ECSAs of Pt catalysts are measured through cyclic voltammograms (CV) both in ex-situ test and in-situ test. ECSA can be calculated by using the equation below:

$$ECSA = \frac{Q}{\Gamma \times L_{Pt} \times A_{geo}} \quad (\text{m}^2 \text{ g}^{-1})$$

Q: hydrogen desorption charge (μC) Γ : $210 \mu\text{C}/\text{cm}^2$

L_{Pt} : the Pt loading ($\text{g}_{Pt}/\text{cm}^2$) A_{geo} : the GCE geometric area (cm^2)

In this thesis, Q which is used in this equation is hydrogen desorption charge, shown as the upper area in Fig.2.1(Li & Lane, 2011). In order to characterize the electrochemical properties of our catalysts, CVs were performed at different voltage scan speeds (10, 20, 40, 60, 80, 100 mV s^{-1}) between 0.0 V and 0.5 V vs RHE in HClO_4 solution which was saturated by N_2 . For making comparisons among different samples, in the ex-situ test, we only illustrate the CV curves performed at 20 mV s^{-1} in a N_2 saturated solution of 0.1 M HClO_4 . The ECSA data was the average of the ECSA results at 10, 20, 40, 60, 80 and 100 mV s^{-1} .

We also did the CV in the in-situ test, CVs were obtained at 25 °C with gas relative humidity of 100% in the MEA, at the scanning rate of 10, 20, 30, 40 and 50 mV s^{-1} . In this thesis, we use the CV at 40 mV s^{-1} to calculate ECSA of catalysts in the in-situ system.

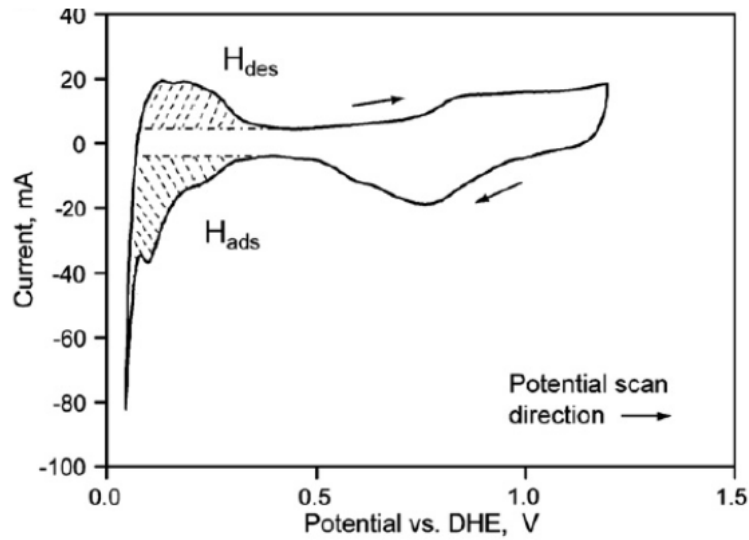


Figure.2.1. Cyclic Voltammogram of Pt nanocatalyst

2.3.2. Linear sweep voltammetry (LSV)

Linear sweep voltammetry (LSV) was tested through the oxygen reduction reaction (ORR) in saturated oxygen solution. The current density measured in the ORR needs to be corrected by using the famous Koutecky-Levich equation to characterize the activity of catalyst.

$$\frac{1}{j} = \frac{1}{j_k} + \frac{1}{j_d} \quad (\text{Koutecky-Levich equation})$$

j : the measured O_2 reduction current density

j_k : the mass-transport corrected kinetic ORR current density

j_d : the diffusion limiting current density

As it is shown in Fig.2.2 (Hasch *et al.*, 2012), it is a typical plot of LSV tested in 0.1 M $HClO_4$ O_2 saturated solution at 1600 rpm. In our experiment, LSV was tested at the rotation speeds of 400, 800, 1200, 1600 and 2000 in N_2 and O_2 saturated solution respectively.

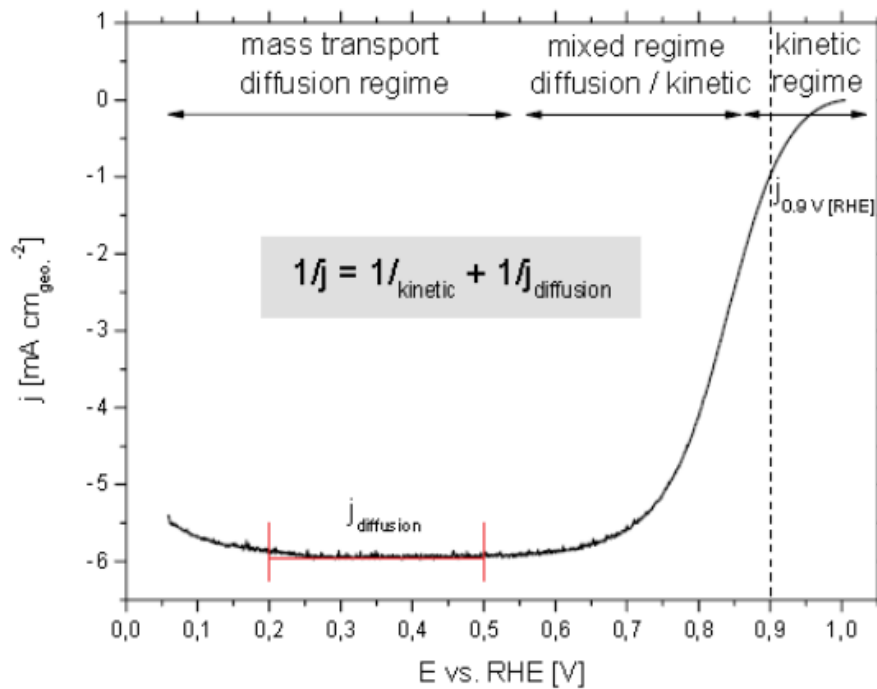


Figure.2.2. A typical LSV of Pt nanocatalyst

2.4. MEA Fabrication and Fuel Cell Testing

MEA was fabricated with the method given by Kim, Lee et al (Wee, Lee, & Kim, 2007). Catalyst inks were prepared by sonicating the quantitative mixture of Pt catalyst, solvent (isopropanol (IPA) and UHQ water) and 10 wt% Nafion solution for 30 mins. Then this ink was hand painted onto a GDL (Freudenberg H2315C4) to fabricate a gas diffusion electrode with the designed Pt loading (0.25 mg/cm^2). Specifically, the hand painting process began with painting two layers of catalyst ink. The brushstrokes of two layers were perpendicular to each other. Then the two layers were dried before painting another two layers. Repeated this procedure until all the premixed catalyst ink was painted onto the GDL. In the same way, the same quantity of 10 wt% Nafion solution (Nafion dry weight of 0.6 mg cm^{-2}) was painted on commercial Johnson Matthey Gas Diffusion Electrode (GDE). The GDE we made in-house with catalyst ink and the

commercial GDE were placed on the either side of the commercial membrane (Nafion 212). After this, two GDEs and the membrane went through the hot pressing process at 125 °C and 600 psi for 120 s to get the MEA. For the in-situ test, polarization curves are obtained to illustrate the properties of catalysts. As it is shown in Fig.2.3, there are usually three apparent drops of the voltage in typical PEFC polarization curve. Different drops correspond to the different reasons, such as kinetic losses, ohmic losses and mass transfer losses.

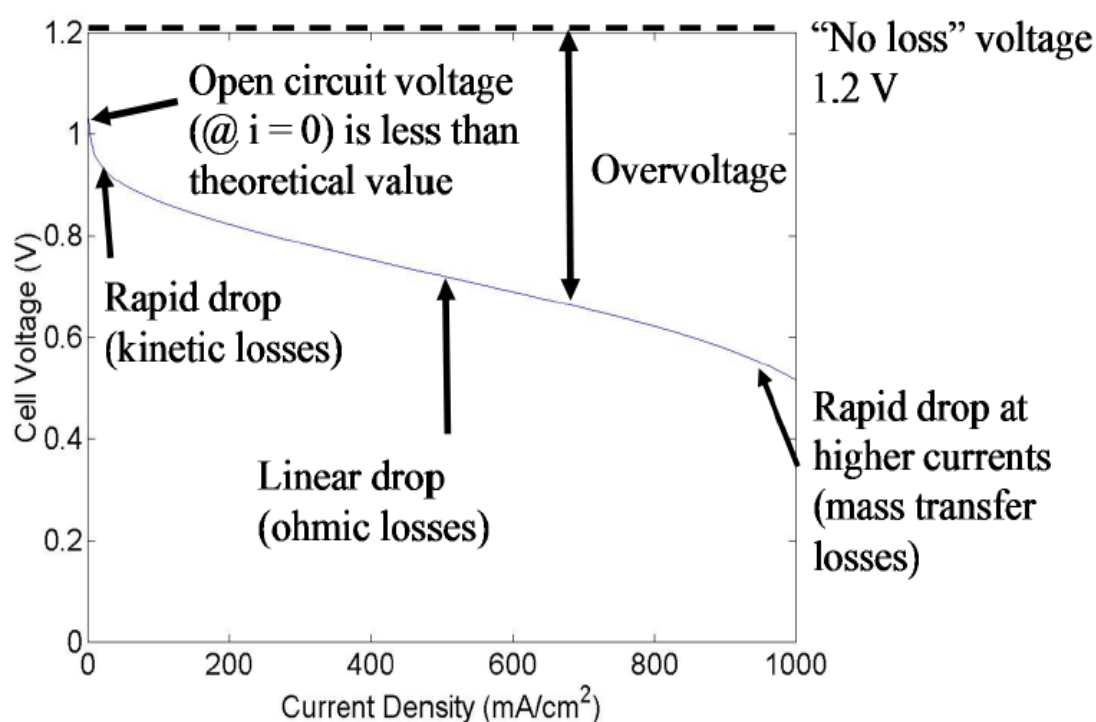


Figure.2.3. A Schematic of typical fuel cell polarization curve

During the experiment, the active area of all MEAs was 5 cm². The characterizations of the MEA produced in-house were tested on a Scribner 850e with EIS capabilities. The MEAs were measured at 80 °C, 90 °C, 100 °C, 110 °C and 120 °C with a gas relative humidity of 100% at the cathode and anode sides in air and H₂ respectively, at 1.8 bar gas back pressure.

In our experiments, the current densities at 0.6 V in polarization curves are utilized to value the performance of different catalysts. The commercial Johnson

Matthey GDE (Pt loading 0.4 mg/cm^2) and the commercial catalyst TKK (Pt loading 0.4 mg/cm^2) were used as the reference to show the performance level of our catalysts which made in-house.

3. Results and Discussion

3.1. TGA

The TGA results of samples are shown in Fig.3.1. Here, the percentage remaining after the temperature increase is the Pt content of the catalysts. The specific Pt content of Pt/C sample 1, Pt/C sample 3, Pt/RGO and Pt/(80%RGO-20%C) is 40.2%, 18.4%, 21.3% and 19.2%, respectively. According to the TGA curves, for the Pt/C catalysts, it remains stable under 400 °C, and then the linear decrease is illustrated from 400 °C to 800 °C because of the loss of C. When all the carbon is oxidized by the air, it reaches a plateau again between 800 °C and 900 °C. As to the Pt/RGO and Pt/(80%RGO-20%C) catalysts, the existence of remaining oxygen functional groups and water absorbed in the catalysts causes the sample to lose weight at the start of heating. Specifically, in the Fig.3.2, the mass change (4.58%) under 100 °C is considered as the loss of water in the Pt/(80%RGO-20%C), and the weight loss speed after 400 °C is faster than that before 400 °C. Meanwhile, there is also evidence that the actual Pt contents in Pt/RGO (19.2 wt%) and Pt/(80%RGO-20%C) (21.3 wt%) are almost the same to our design (ca. 20 wt%) before the fabrication process. Therefore, it is reliable to calculate Pt content of catalyst as 20 wt% in the following experiment process.

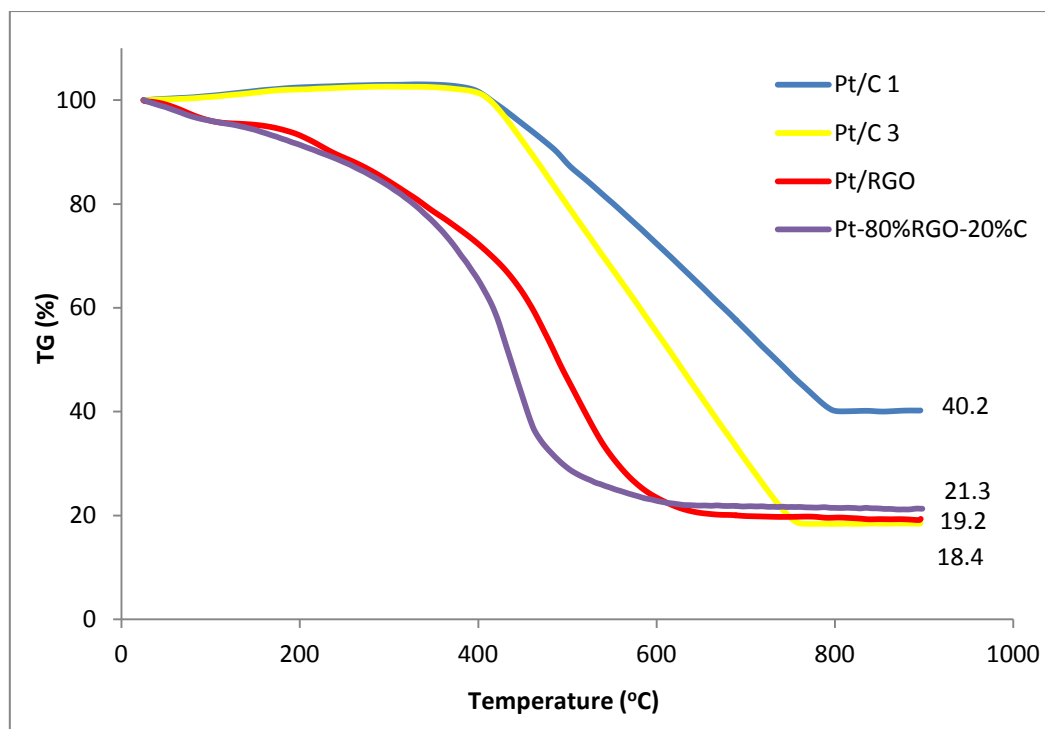


Figure.3.1. TGA of Pt catalysts made in-house

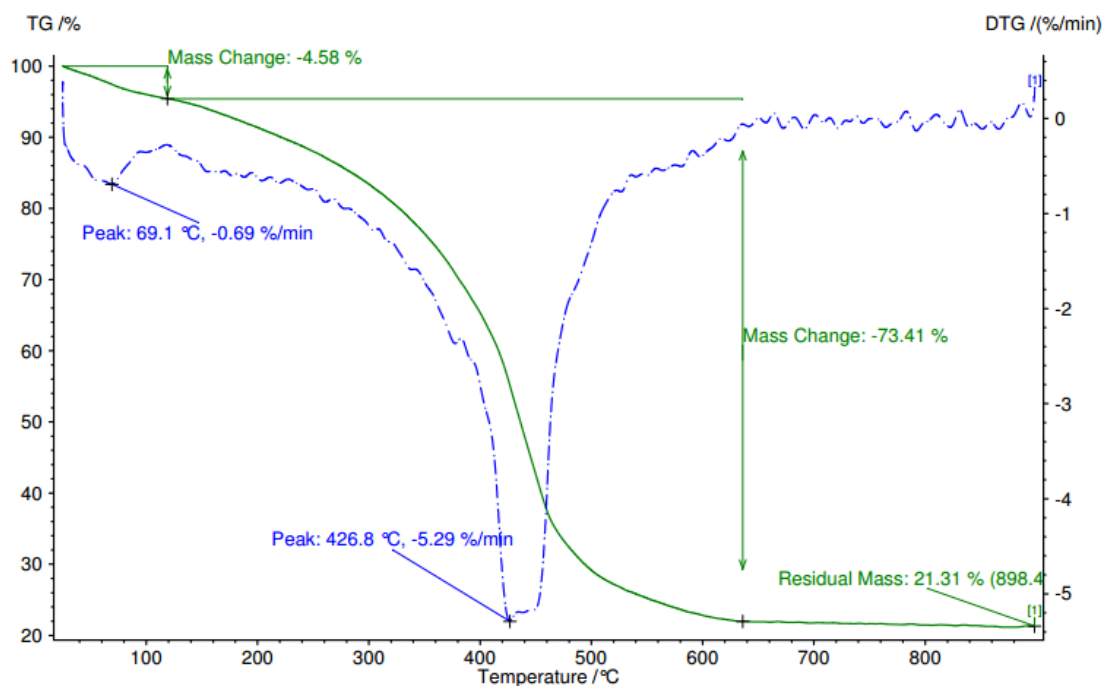
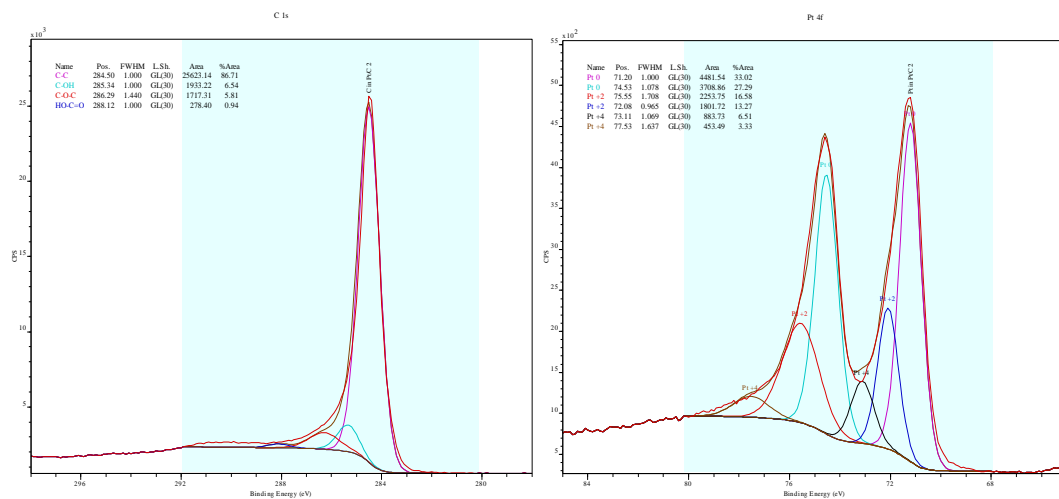


Figure.3.2. TGA of Pt-80%RGO-20%C sample

3.2. XPS

Pt/C



Pt/RGO

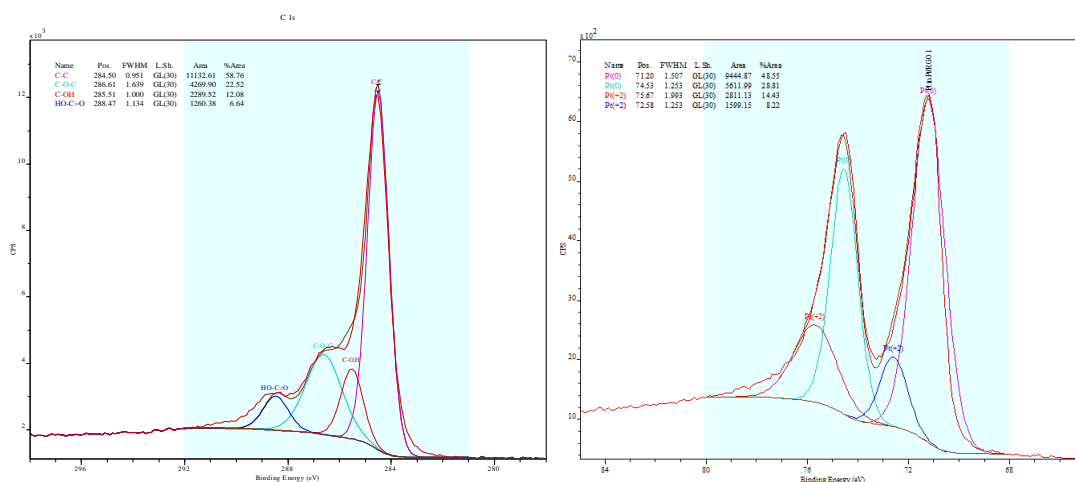


Figure.3.3. XPS spectra of Pt/C and Pt/RGO

As we know, the peak at 284.5 eV is the characteristic of the C sp^2 hybridisation, and the peaks at 286.5 and 289 eV are attributed to the C-O bonds. Specifically, 285.9, 286.6 and 289.0 eV correspond to hydroxyl (C-OH), ketone (C=O) and carboxylic groups (HO-C=O) respectively (Moulder, Stickle, Sobol, & Bomben, 1992; Sharma et al., 2010). In the XPS spectra of the Pt/C and Pt/RGO (Fig.3.3), there is one main peak in the C 1s band of C at 284.5 eV and other three peaks are tiny. While the C 1s band of GO illustrates three peaks evidently at almost 284.5, 286.5 and 289 eV. The differences

are clearly revealed between C and GO used as support materials. The presence of Pt 4f spectra, which appears as doublets of Pt 4f^{7/2} (71.2 eV) and Pt 4f^{5/2} (74.5 eV) confirmed the existence of Pt at different oxidation states (Pt⁰, Pt²⁺ and Pt⁴⁺) in the catalyst. Overall, the XPS spectra clearly suggest that Pt particles have been placed on the reduced graphene oxide sheets successfully.

3.3. FT-IR

Fig.3.4 shows the FT-IR spectrum curves of Pt/RGO catalysts synthesized at the pH of 8 and 12 and that of Pt-60%RGO-40%C catalyst respectively. For GO, it shows evidence of hydroxyl groups (O-H stretch) on the surface at ~3356 cm⁻¹ (a broad band) and ~1360 cm⁻¹, a C=O stretch at 1725 cm⁻¹, a C-O stretch at 1044 cm⁻¹, as well as a C-O-C stretch at 1220 cm⁻¹. The peak at 1620 cm⁻¹ is ascribed to the aromatic C=C bonds. Obviously, the FT-IR spectrum curves of Pt/GO suspension for 40 s microwave duration with synthesis pH at 8 is only a little different to that of commercial GO. This illustrated that, at the lower pH (less OH⁻) of Pt and GO suspension before the MWAPP, GO could not be reduced efficiently. However, there are many differences when examining the spectrum curve for pH=12. We can see the peak at 1220 cm⁻¹ and 1360 cm⁻¹ disappears completely and the peak around 1044, 1725 and 3356 cm⁻¹ attenuated obviously, which suggests that the oxygen functional groups of GO have been reduced successfully in Pt/RGO catalyst (He et al., 2012; Song, Zhang, Sun, Cui, & Lin, 2012; Zhou, Liu, Jiang, Yang, & Chen, 2010). Meanwhile, a new peak at 1566 cm⁻¹, representing the restoration of highly C=C conjugated structure, emerged after reduction. As for the Pt-60%RGO-40%C catalyst, nearly all the peaks of oxygen functional disappeared completely.

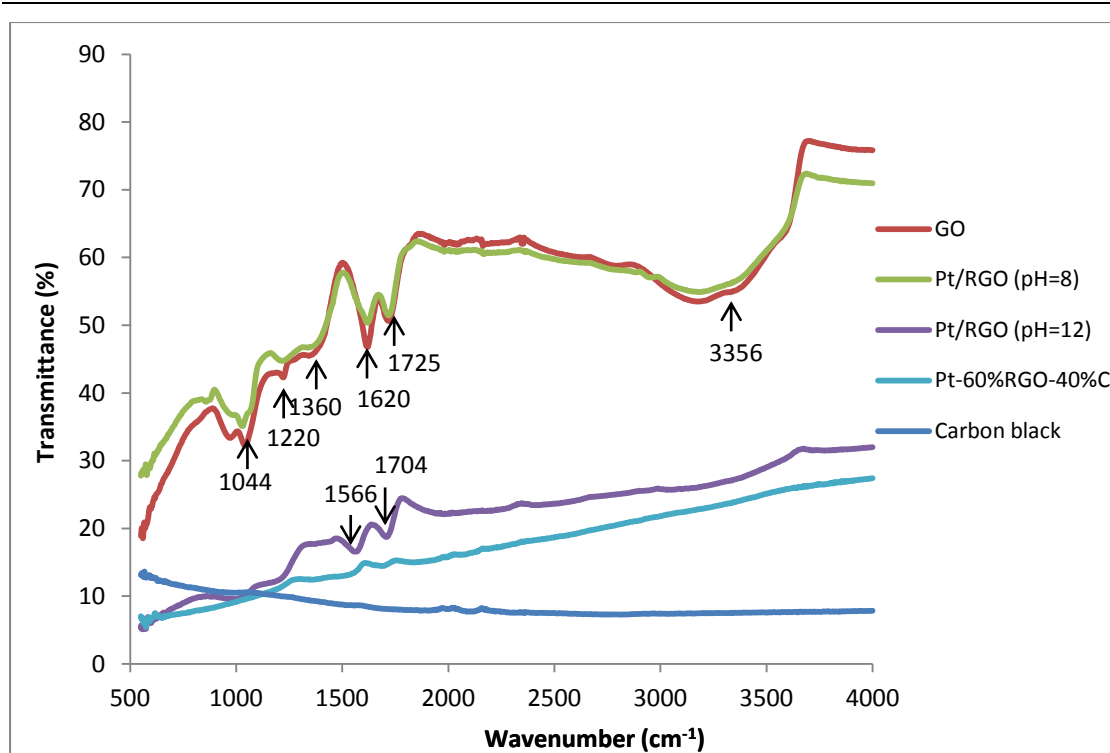


Fig.3.4.FT-IR of GO, C, Pt/RGO made in different pH (8 and 12) and Pt-60%RGO-40%C

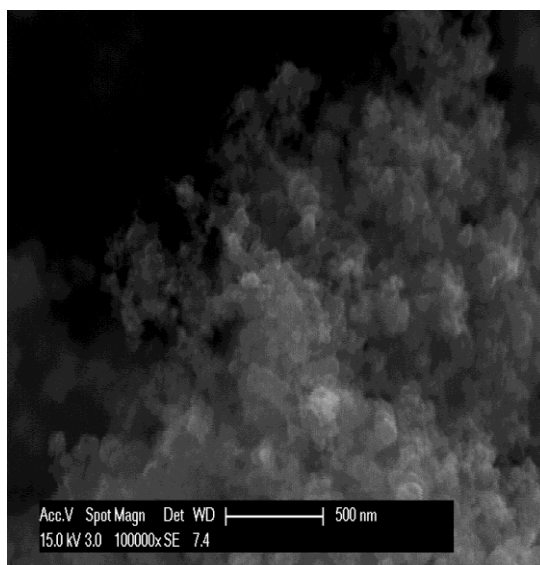
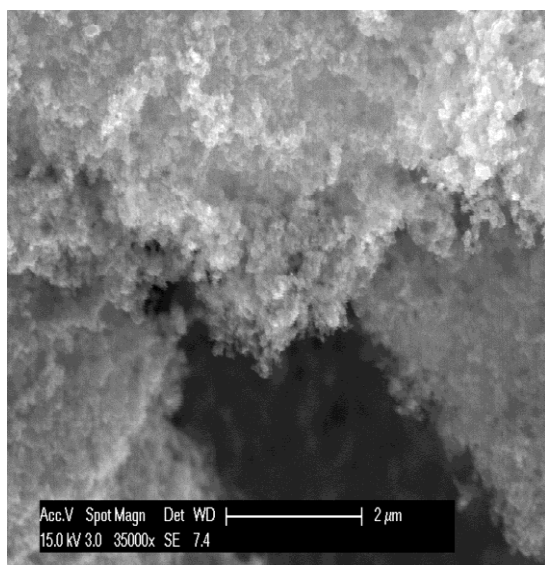
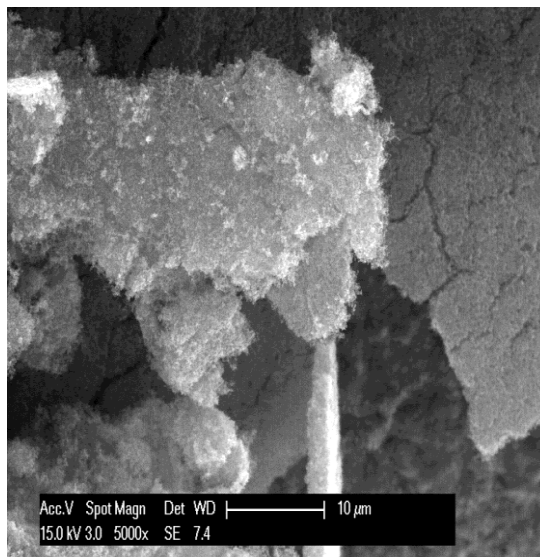
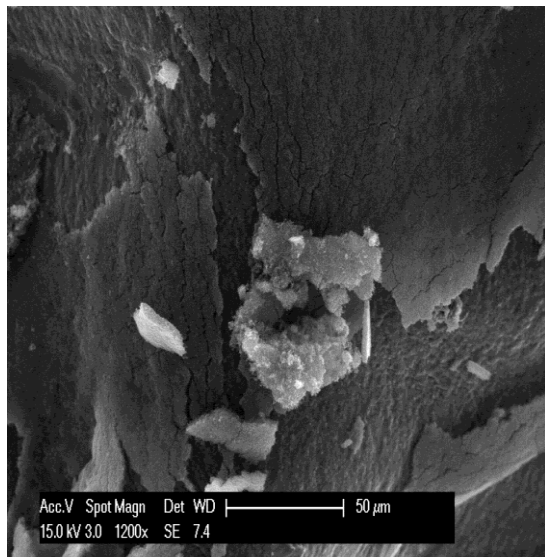
These results confirmed the reduction mechanism of GO in MWAPP requiring numerous hydroxide ion in the system. Moreover, Pt salt could be more stable existing at Pt^{4+} form in alkaline solution (Mohamed A., et al., 2001). According to the mechanism (Kundu et al., 2011), without adding enough OH^- into the Pt/GO suspension, the absence of enough Pt^{4+} would cause the $-COOH$ of GO to not take off $C=O$ groups to form into RGO. Meanwhile, it provides a good explanation to the corresponding ex-situ CV results, which mentioned the Pt/RGO catalyst made at pH 8 did not show any electrical activity. In addition, the difference transmittance of the FT-IR of sample was varied as their layer thickness and the mass tested samples on the FT-IR testing stage.

3.4. SEM

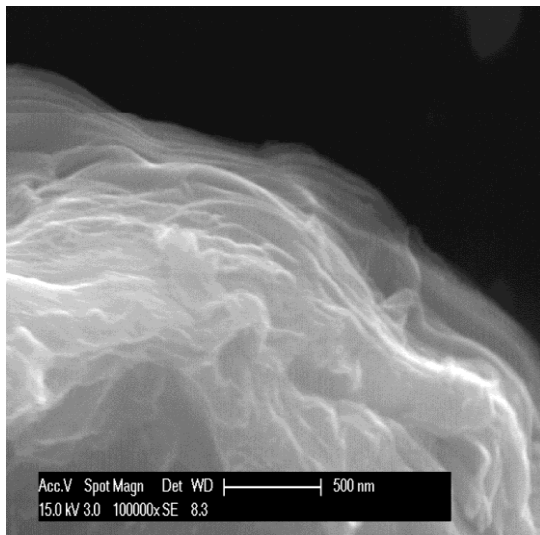
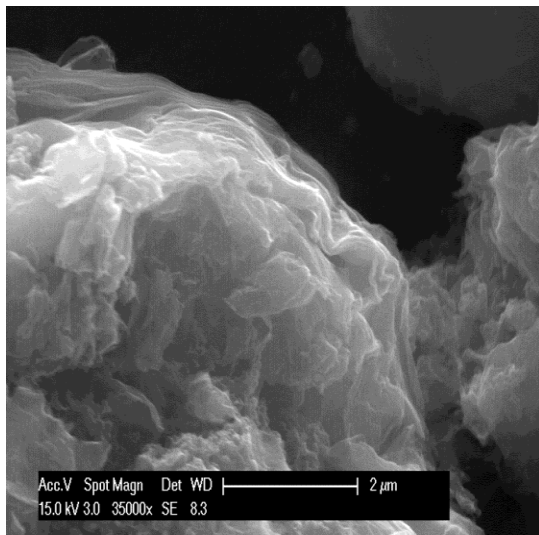
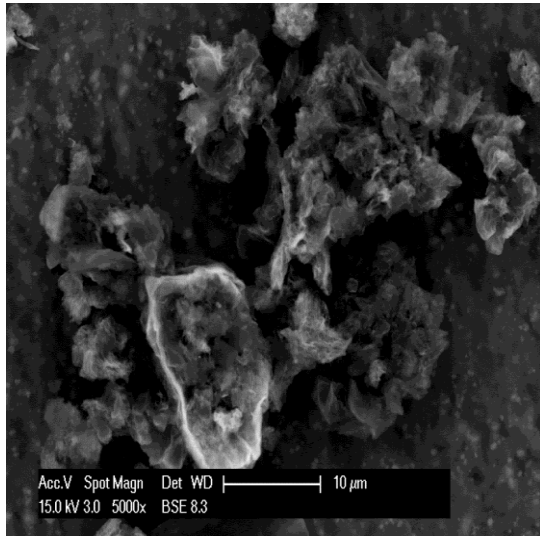
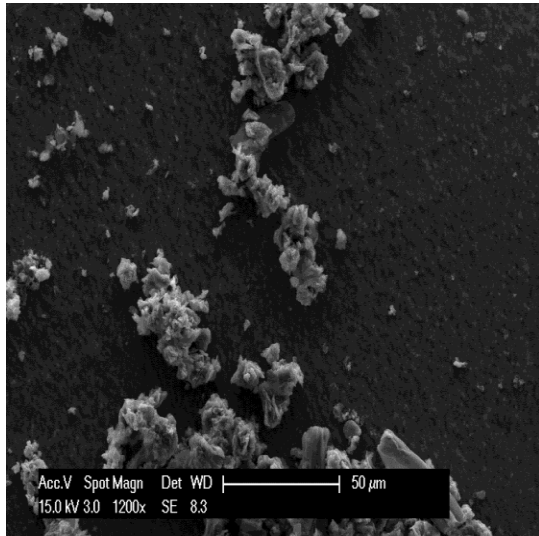
The sample for ESEM test is fabricated by drop casting catalyst ink, in which catalyst is dispersed into IPA by sonication, onto the aluminum foil. As shown in Fig.3.5, the morphologies of different samples were analysed using 15 kV acceleration voltages at different magnifications of 1200, 5000, 35000 and 100000. In the ESEM images, the structure and dispersion of support materials can be observed, while Pt nanoparticles are too small to be seen. Through the comparison among the samples at low magnification, we can see that Pt/C catalyst tends to unfold on the surface of aluminum foil. However, the Pt/RGO catalyst prefers to agglomerate together. As to the Pt/(RGO+C) catalyst, RGO and C exist together as the support materials and illustrate more uniform dispersion than Pt/RGO catalyst. For more details, we focus on the morphologies at the magnification of 35000 and 100000. The carbon black looks like small particles and the RGO has a typical sheet structure. The serious stacking of RGO sheets is observed in the SEM image of Pt/RGO. The thickness of RGO existing in Pt/RGO almost reaches the micron level. Meanwhile, the strong ultrasonic treatment aided in reducing the size of RGO sheets. However, the small RGO pieces still tend to cluster together in the Pt/RGO samples. According to the SEM images of our Pt/(RGO+C) catalysts, the addition of carbon black has solved this problem very well. The carbon black particles encircle the RGO sheets to prevent them from stacking. Specifically, in Pt/(60%RGO+40%C) catalyst, the thickness of RGO sheets was only about 20 nm. As it is shown in Fig.3.6, the SEM images of different Pt/(RGO+C) samples with various carbon content at the magnification of 35000 are compared to each other. As the C content increase, the amount of carbon particles is clearly growing and the agglomeration of RGO is releasing further. More SEM images of Pt/(RGO+C) with different carbon contents

(10%, 20% and 30%) can be seen in the appendix chapter.

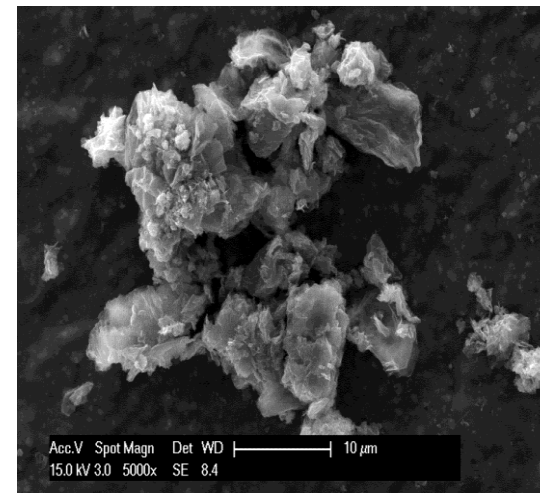
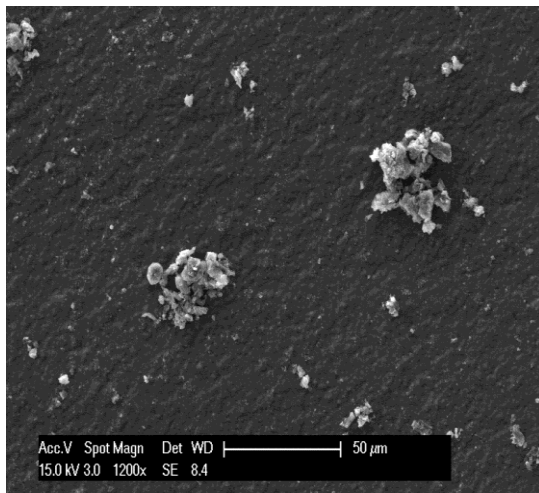
Pt/C

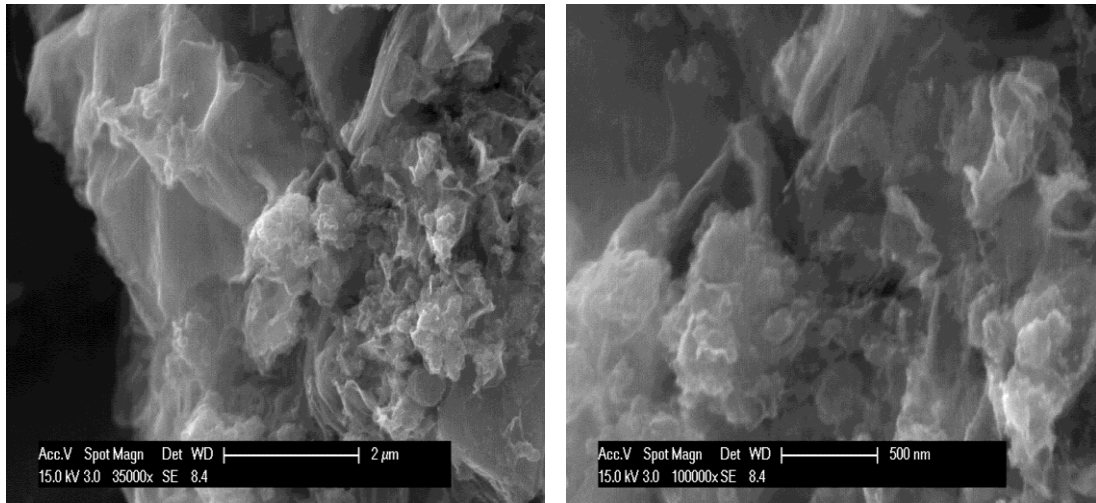


Pt/RGO



Pt/RGO with strong sonication





Pt/(60%RGO+40%C)

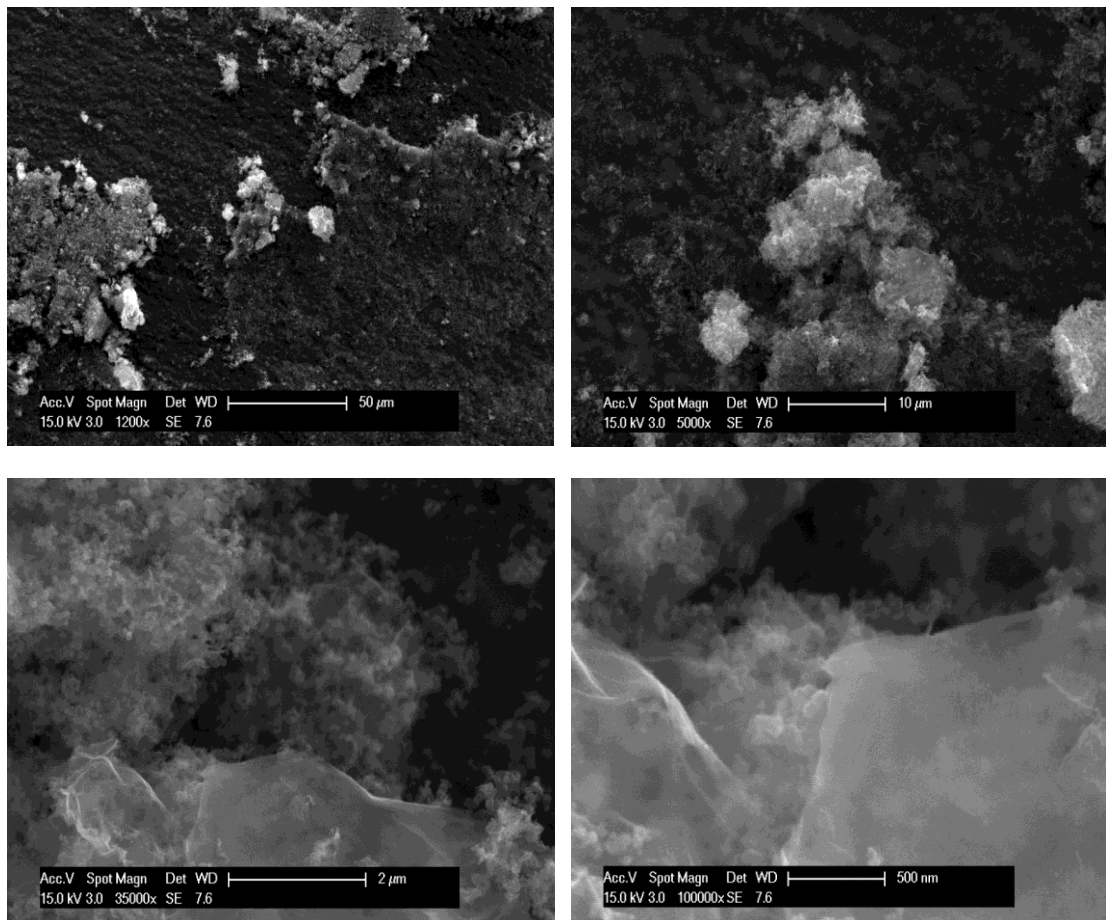


Figure.3.5. SEM images of Pt catalysts (Pt/C, Pt/RGO, Pt/RGO with sonication and Pt-60%RGO-40%)

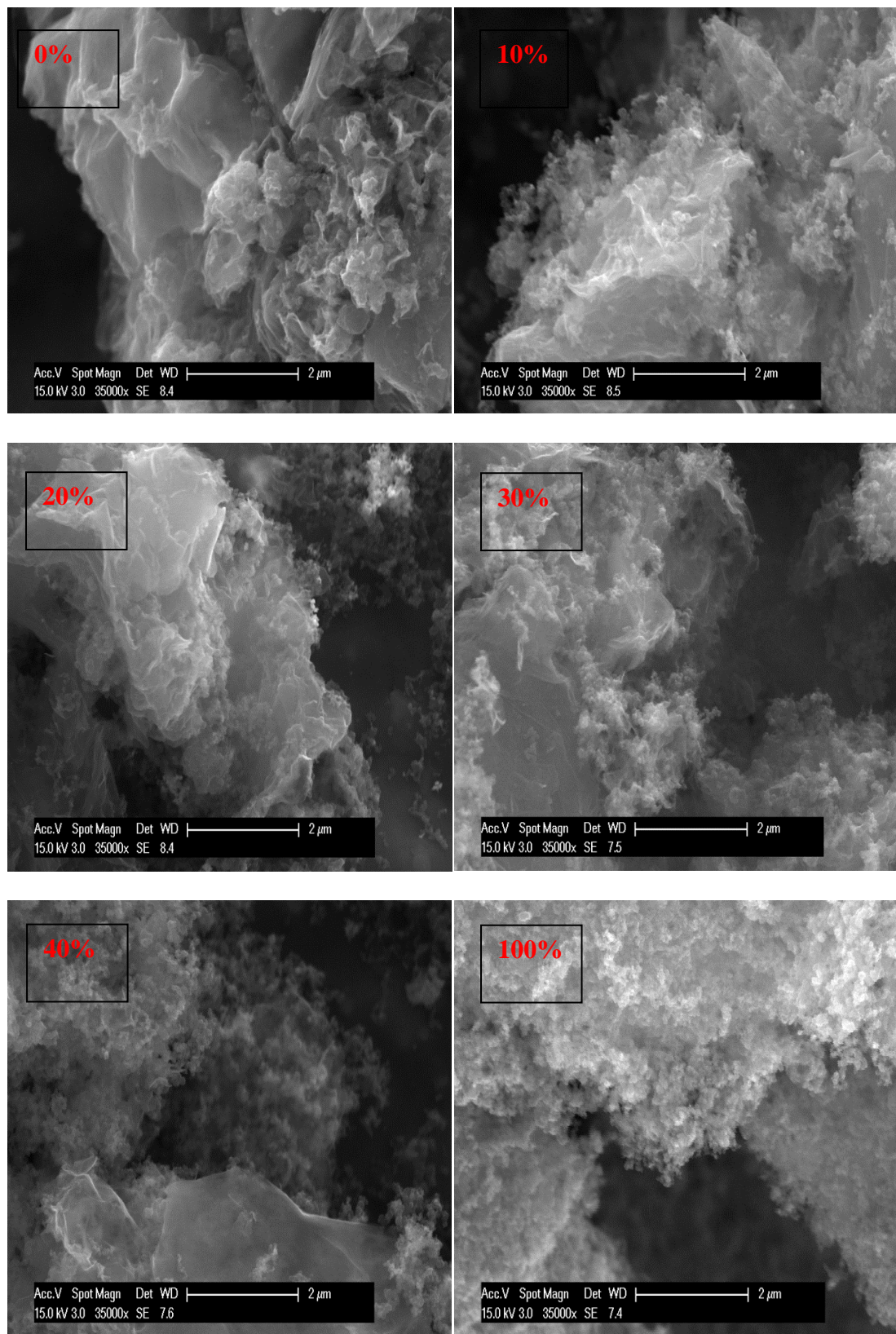
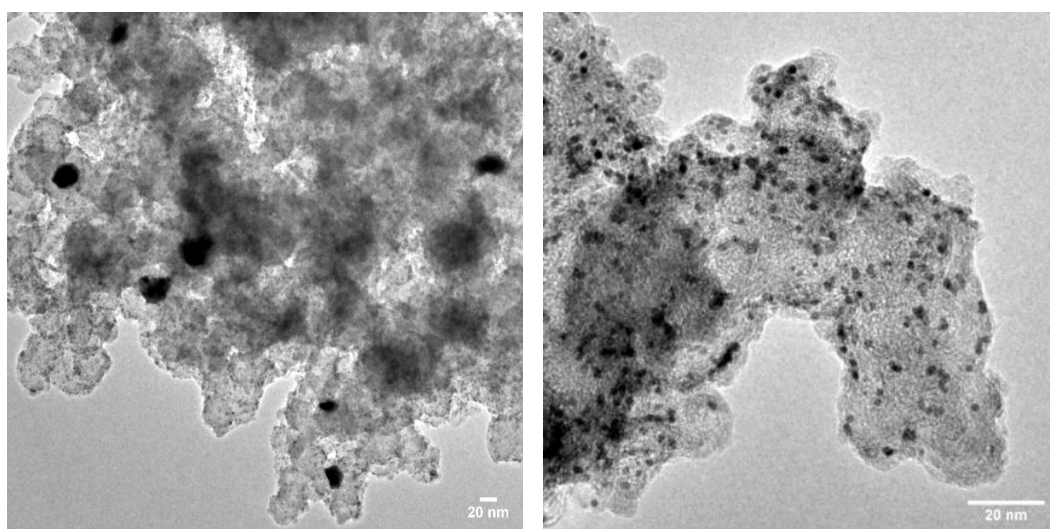


Figure.3.6.SEM images of different Pt/(RGO+C) samples with various carbon content (0%,10%,20%,30%,40% and 100%) at the magnification of 35000

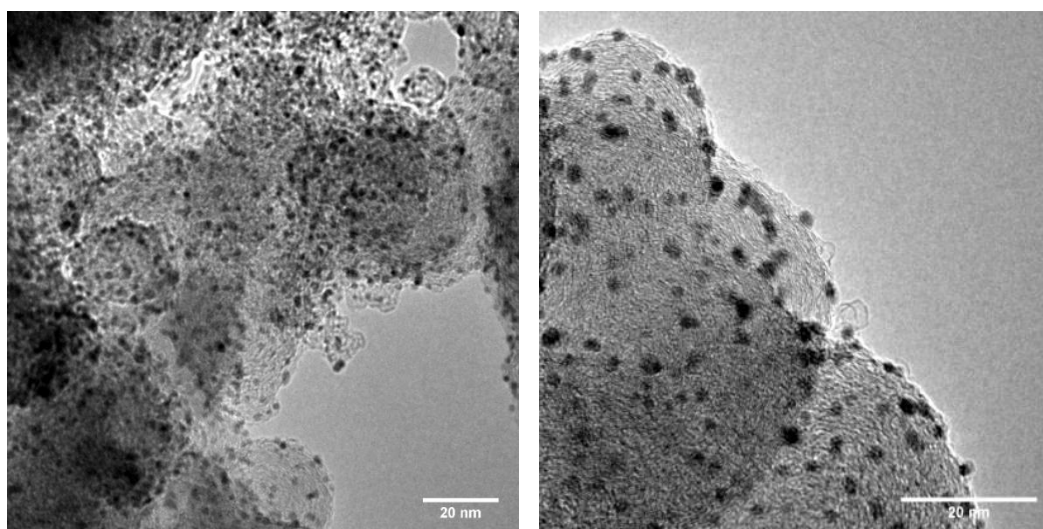
3.5. TEM

TEM images of Pt catalysts made in-house are shown in Fig.3.7. The average diameters of the samples illustrated in table.3.1 are according to the TEM images and analyzed using imageJ. The average diameters of Pt/C sample 2, 3, Pt/RGO, Pt/(60%RGO+40%C) and TKK are 2.1, 1.6, 1.8, 3.2 and 2.8 nm separately.

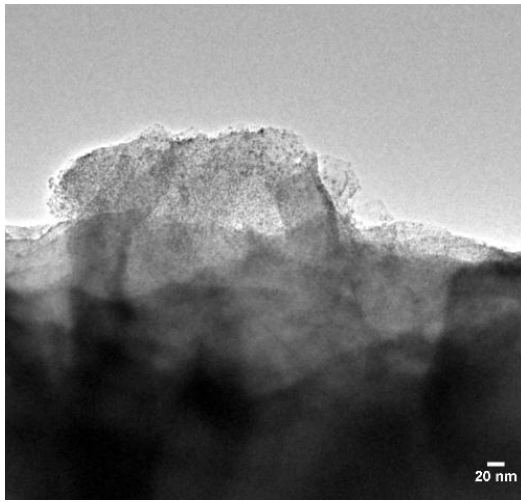
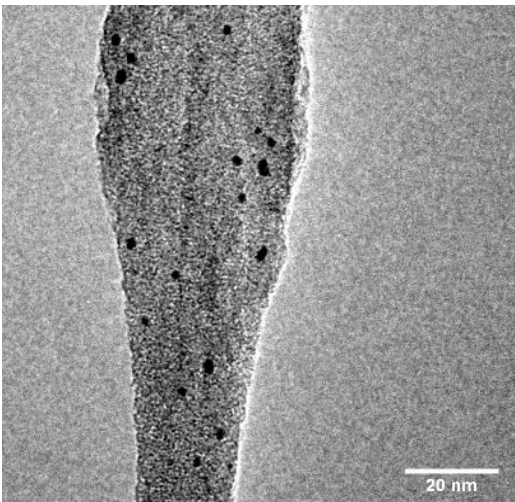
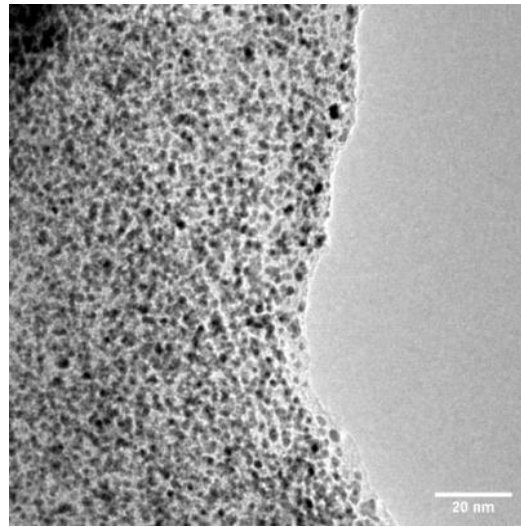
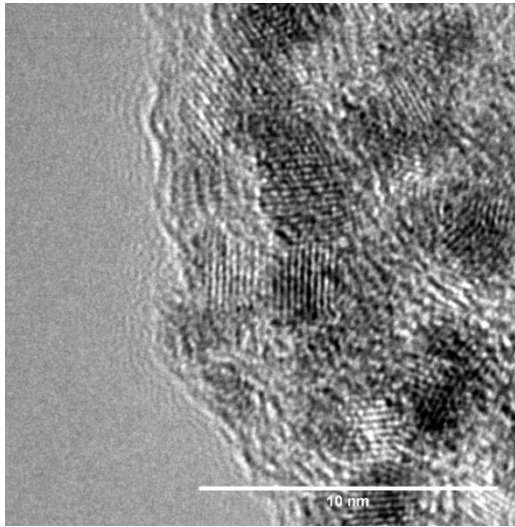
Pt/C 2



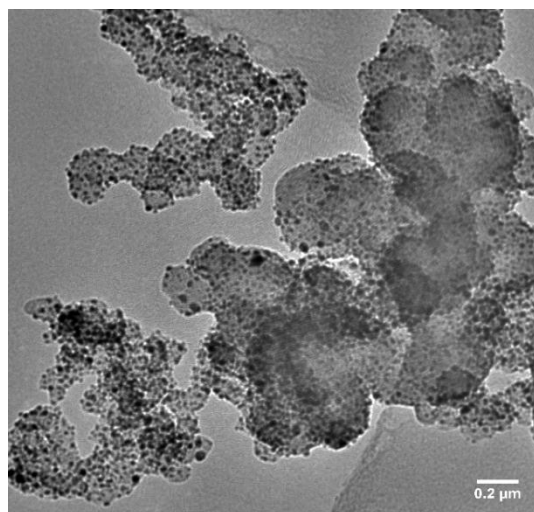
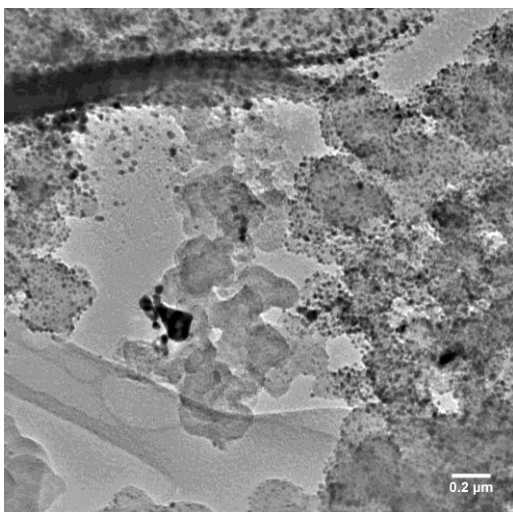
Pt/C 3

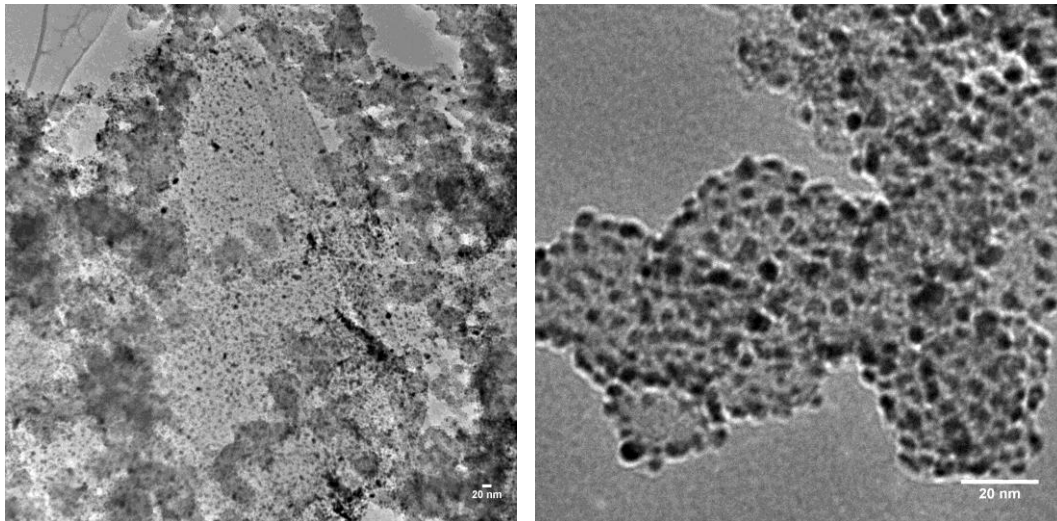


Pt/RGO



Pt/(60%RGO+40%C)





TKK

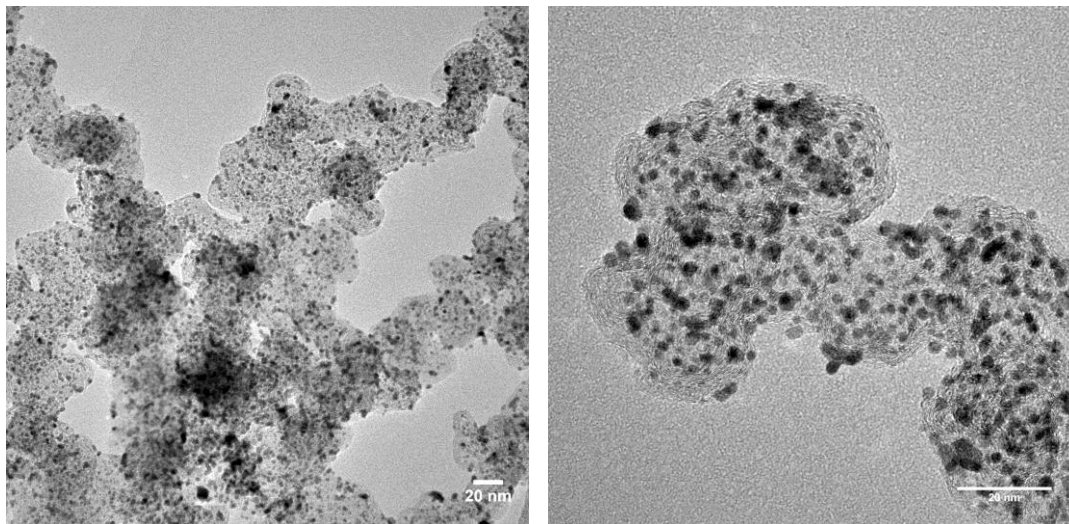


Figure.3.7. TEM images of Pt catalysts (Pt/C sample 2, 3, Pt/RGO, Pt/(60%RGO+40%C) and TKK)

Table.3.1. The average diameters of Pt catalysts based on TEM

Sample	Average diameter (nm)
Pt/C sample 2	2.1
Pt/C sample 3	1.6
Pt/RGO	1.8
Pt/(60%RGO+40%C)	3.2
TKK	2.8

From the TEM of Pt/C samples, it can be seen that the Pt nanoparticles are successfully distributed on the surface of carbon black. When compared to the TEM of the Pt/C sample 2 (Pt content ca. 30wt %) and sample 3 (Pt content ca. 20%), we can find that sample3 has a lower Pt content percentage but has a better distribution, less Pt clusters and smaller Pt nanoparticles. When combined with the ECSA of the tested samples (sample 2 ($49 \text{ m}^2\text{g}^{-1}$) and sample 3 ($60 \text{ m}^2\text{g}^{-1}$)), the results of the ex-situ test is confirmed by this result very well. Meanwhile, considering the stability of Pt nanoparticles, the Pt content property cannot be too small. Therefore, based on this, in our research, the Pt content percentage is designed at 20 wt%.

When looking at the TEM of Pt/RGO, Pt distribution on RGO is more uniform and compact than that on carbon black. This can be explained for the existence of the oxygen functional groups on the GO, which forms defects during microwave process to help Pt distribute better and prevent Pt nanoparticles agglomeration at the same time. As it is enlarged, the Pt lattice fringes of a single Pt nanoparticle can be found, which reveals the presence of the fcc structures. Meanwhile, the images of Pt/RGO have also reflected the main problems: the Pt agglomeration still exists in the catalyst; and there is a serious accumulation of GO sheets during the synthesis of Pt/RGO. The stacking of

GO sheet enfolds various Pt nanoparticles inside and directly reduces the ECSA of catalyst. Thus, the strategy of Pt/(RGO+C) is designed to solve these problems. According to the TEM images of Pt/(60%RGO+40%C), it is clear that, the Pt nanoparticles only grew on the surface of RGO. That is to say, the addition of C after MWAPP did not act as the support materials of Pt nanoparticles. Moreover, a majority GO sheets have been changed into little pieces by strong ultrasonic treatment. The rare remaining RGO sheets are much thinner than the RGO sheets in Pt/RGO. Compared to the commercial Pt/C catalyst, our catalysts with the mixture support material of RGO and C have similar nanoparticle sizes and are more uniform with stable Pt distribution. These aspects provides good evidence for the excellent performance in both ex-situ and in-situ test of our Pt/(RGO+C) made in-house. The average diameter of Pt/(60%RGO+40%C) catalyst (3.2 nm) is larger than Pt/RGO, because we control the same mass of Pt and support materials during the manufacture process. As the C addition increase, the ratio of Pt to RGO is growing.

3.6 CV and LSV

3.6.1 Pt/C

As the first fabrication of Pt catalysts, the synthesis of Pt/C was carried out to find the best conditions for producing Pt nanocatalysts. As shown in table 3.2 and Fig.3.8, we can find that the lower weight percentage of Pt causes an increase in the ECSA, as well as an increase in produced current. This situation can be explained by the lower weight percentage resulting in smaller size of nanoparticles. Through the calculation of the ideal surface area of the nanoparticle spheres in different sizes, it is obvious that ECSA will be larger when there is a decrease in their size. As the density of Pt is 21.4

g/cm^3 , the ideal surface area of the nanoparticles is shown below in table 3.3. Meanwhile, it was also found that, when the sample Pt/C 3 was heated at 150°C for 2 hrs to get sample Pt/C 4, there was an increase ($18 \text{ m}^2\text{g}^{-1}$) of the ECSA. Overall, the ECSA of the Pt/C catalysts that we can reproducibly fabricate is ca. $80 \text{ m}^2\text{g}^{-1}$. When compared with TKK, it illustrates that the ECSA of our Pt/C catalyst is higher than that of TKK in the ex-situ test. Moreover, it is can be seen that, in the same MWAPP power and duration, the electric double layers of different samples are similar.

Table.3.2. Experimental parameters comparison for the production of Pt/C catalysts

Variable	Species	MWAPP	TGA	ECSA (m^2g^{-1})
Beginning	Pt/C 1	650W, 140s	39%	25
Carbon Black	Pt/C 2	650W, 140s	27%	49
MWAPP	Pt/C 3	800W, 40s	17%	60
Heat treatment	Pt/C 4	800W, 40s	Ca. 20%	78
Commercial catalyst	TKK		47%	73

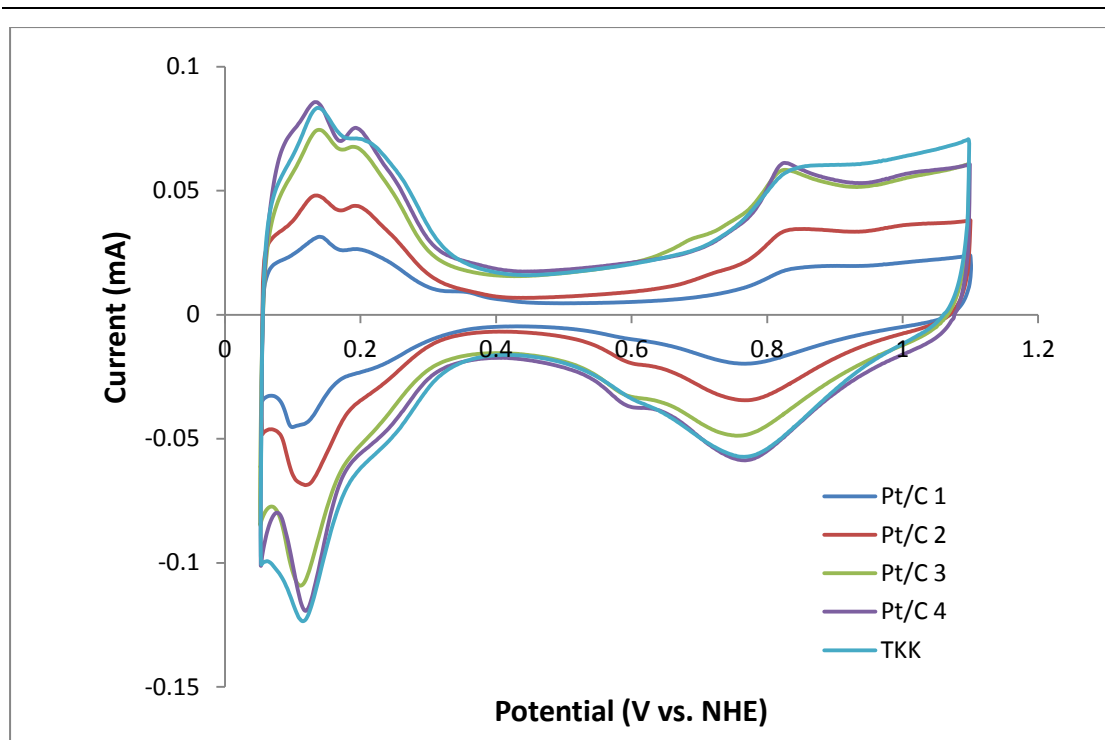


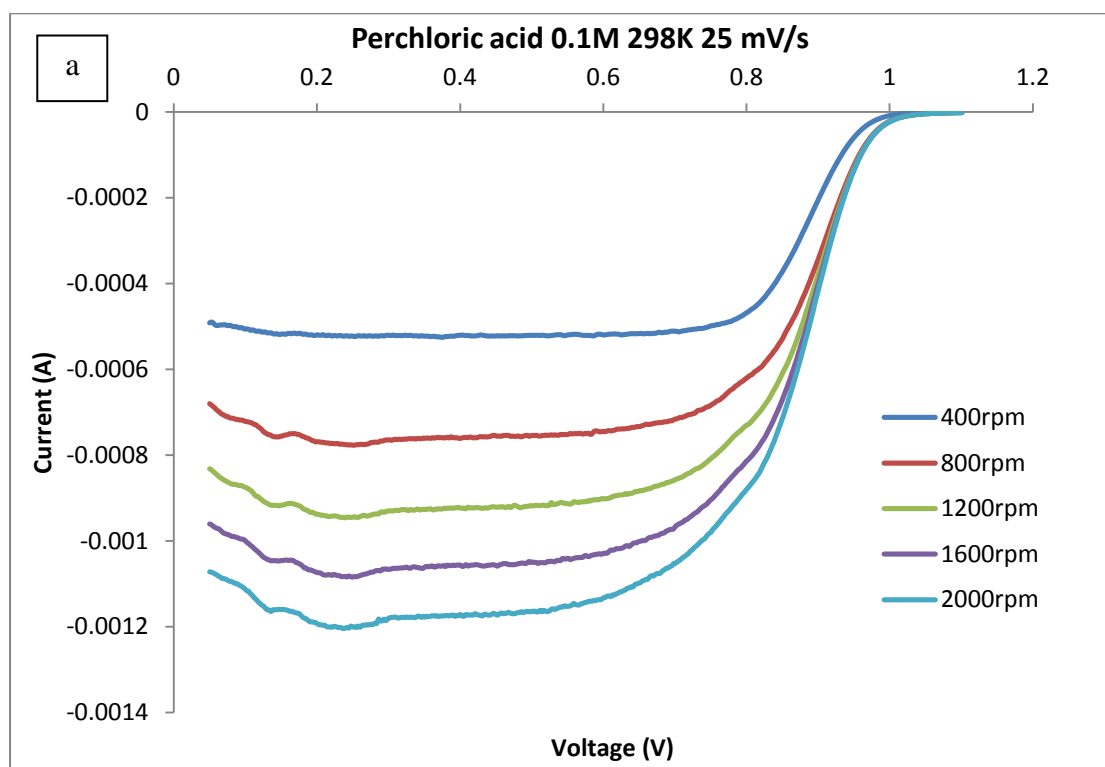
Figure.3.8. CVs of Pt/C catalysts in N_2 -saturated 0.1M $HClO_4$ solution at 20 mVs^{-1}

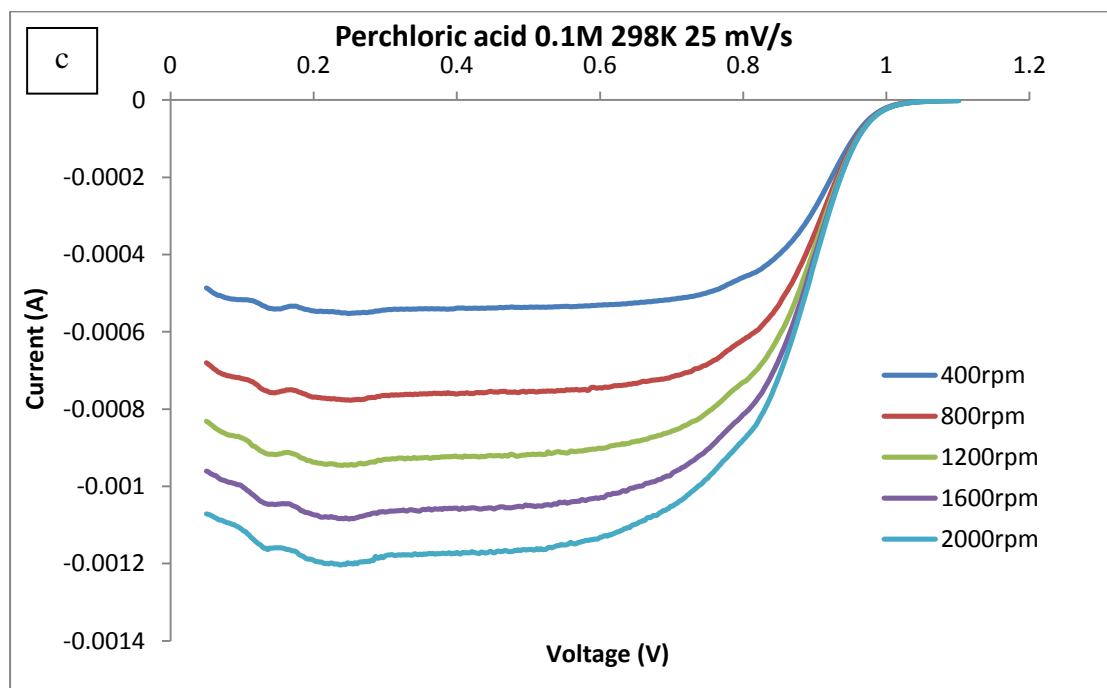
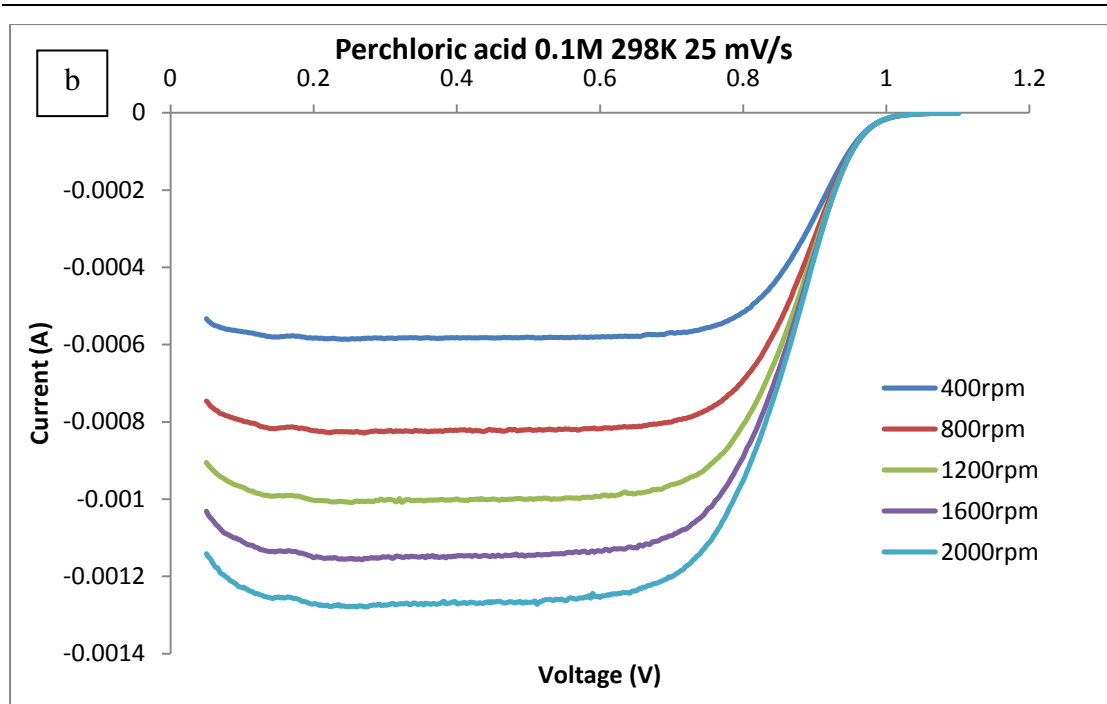
Table.3.3. The ideal ECSA of different diameter in nanoparticles

Nanoparticles Sphere Diameter (nm)	Calculated ECSA (m^2/g)
2	140
3	93.5
4	70.2

As for the oxygen reduction reaction (ORR) data from ex-situ testing, the LSV results of different Pt/C samples are illustrated in Fig.3.9 (a, b, c, d and e responding to sample 1,2, 3, 4 and TTK respectively). The currents at different voltages (0.82, 0.84, 0.86, 0.88, 0.90, 0.92, 0.94, 0.96 and 0.98V) were collected for the Koutecky-Levich plot. Furthermore, based on this, we can obtain the Tafel plot. Various information of the catalyst can be shown in Koutecky-Levich plots and Tafel plots. However, as we are interested in a catalyst that performs well for the ORR

characteristic, we chose the electron transfer number as the key property of our catalysts. That is to say, the electron transfer number of the better catalyst is much closer to four, which shows preference for the four electrons ORR production of water rather than the two electrons ORR production of hydrogen peroxide. The Koutechy-Levich plots of Pt/C 3, 4 and TKK are illustrated in Fig.3.10. The electron transfer numbers (shown in table.3.4) are calculated to be 2.96, 3.77 and 3.75. From this, it is certified that the heat treatment at 150°C is useful to improve the property in the LSV as well. Moreover, the Pt/C sample made in-house has the similar results with the commercial TKK.





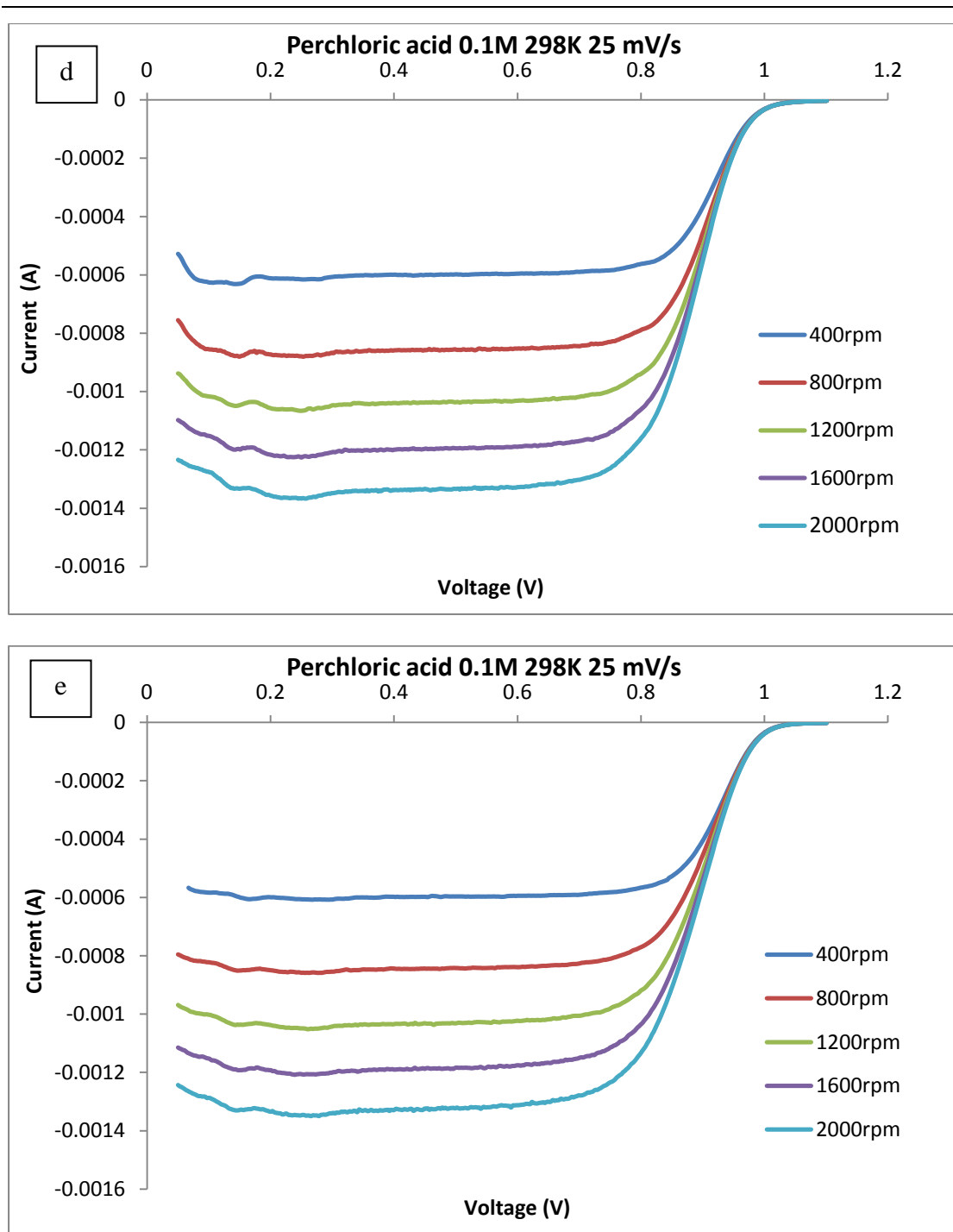
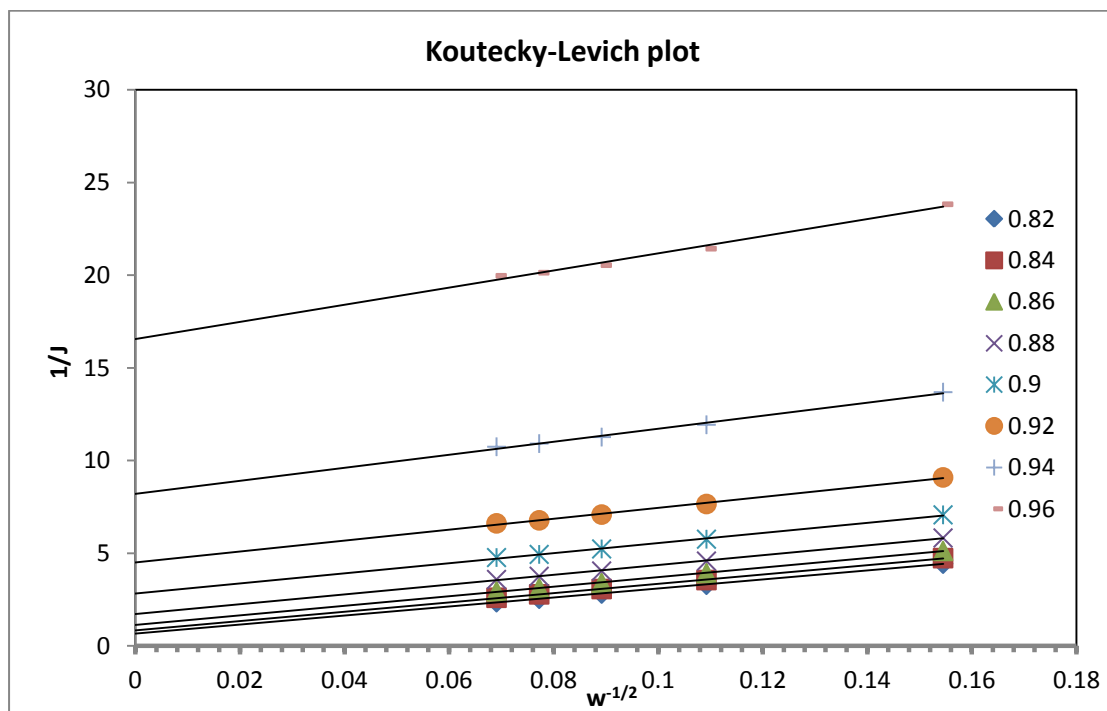
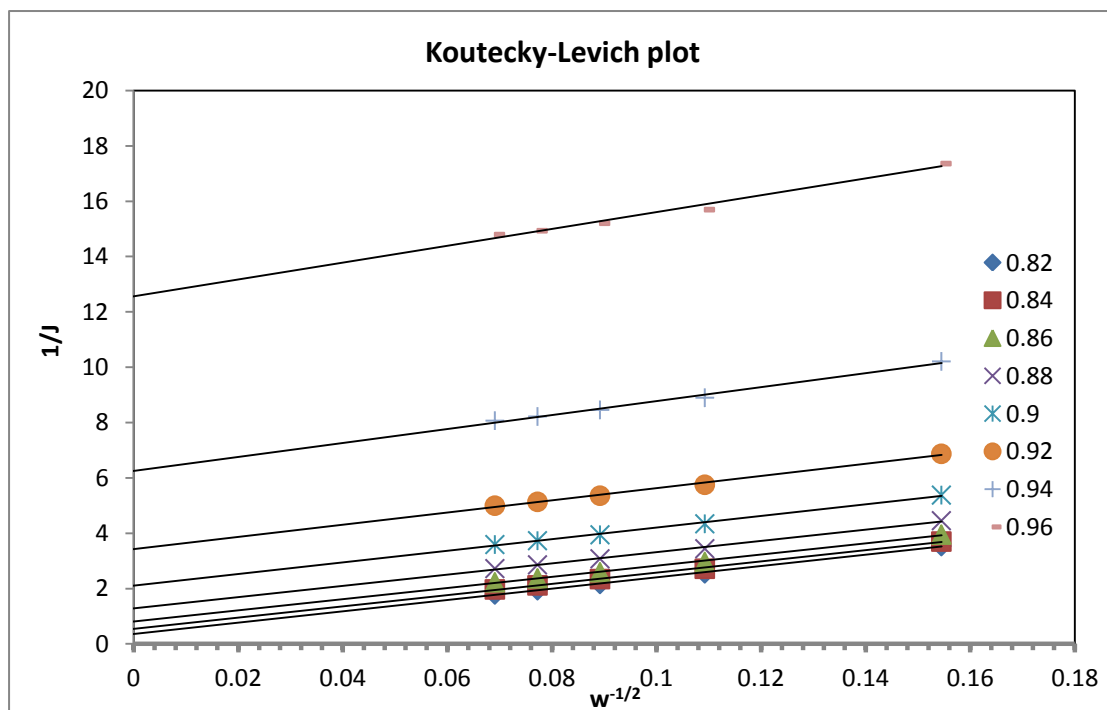


Figure.3.9. LSV of Pt/C catalysts in 0.1M HClO₄ solution at 298K and 25 mVs⁻¹ (a, b, c, d and e responding to sample 1, 2, 3, 4 and TTK respectively)

Pt/C 3



Pt/C 4



TKK

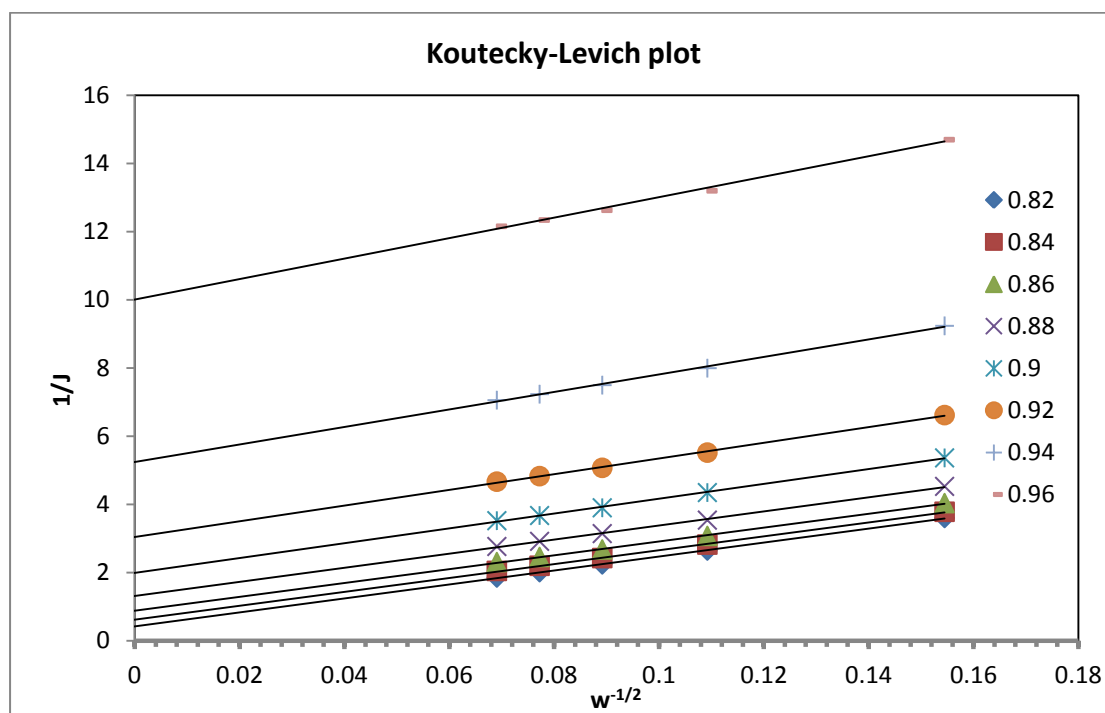


Figure.3.10. Koutecky-Levich plot of Pt/C catalysts (Pt/C 3, 4 and TKK)

Table.3.4. ECSA and Electron transfer number of different catalysts

Sample	ECSA (m^2g^{-1})	Electron transfer number
Pt/C sample 3	60	2.96
Pt/C sample 4	78	3.77
Pt/RGO	30	1.83
Pt/RGO after heat treatment	44	2.91
TKK	73	3.75

3.6.2. Pt/RGO

The same synthesis procedure was used to produce the Pt/RGO catalyst as well. We successfully produced the Pt/RGO with ECSA of $30.3 \text{ m}^2\text{g}^{-1}$ and electron transfer number of 1.84. During the MWAPP process, the Pt precursor (K_2PtCl_6), GO, ethylene

glycol (EG) and IPA were mixed thoroughly and then heated rapidly to grow Pt nanoparticles on GO sheets. When EG was heated, it decomposes into in-situ reducing species that can reduce K_2PtCl_6 and removes some oxygen group on the GO surface. Based on this principle, it formed defects on the GO sheet surface. These defects serve as nucleation centers to attach Pt element, thereby forming Pt nanoparticles on RGO. Through the MWAPP process, the colour of mixtures has an obvious change from a brown solution to a black precipitate.

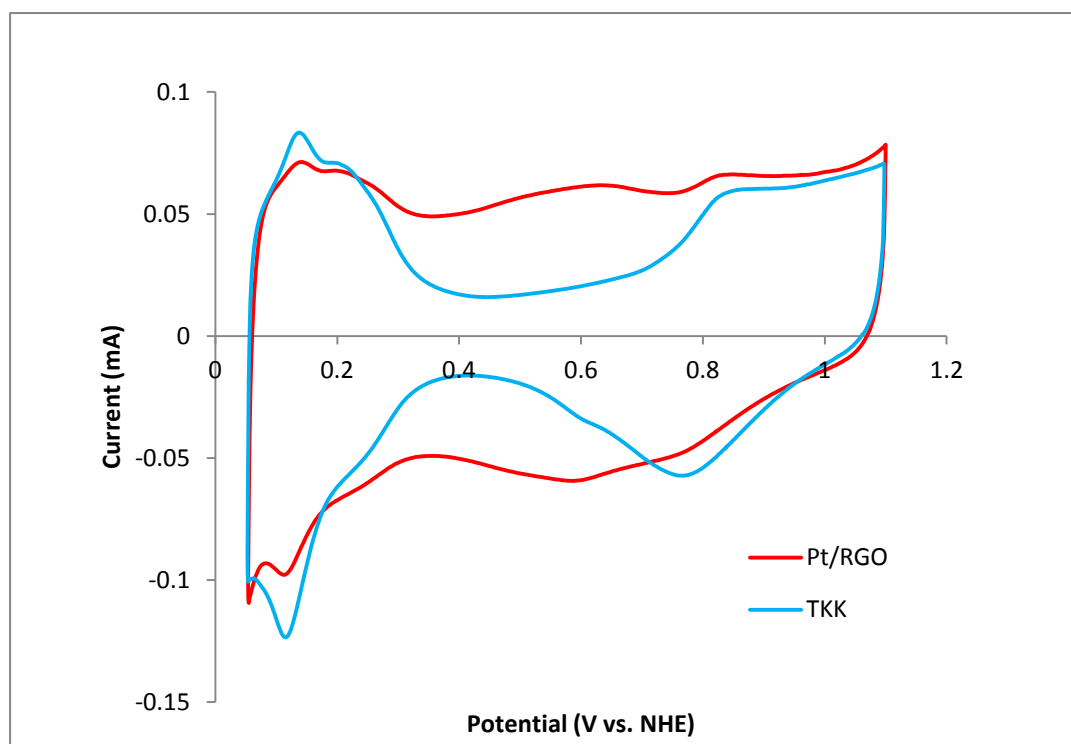


Figure. 3.11. CV of Pt/RGO (40 s) and TKK

When focused on the CV curves of Pt/C (Fig.3.8) and Pt/RGO (Fig.3.11), though the ECSA of Pt/RGO is significantly lower than that of Pt/C that we made in-house, we still could find that the 110 and the 111 catalytically active faces existed in the catalyst (from the expected two peaks found at 0.15 and 0.2 V). Compared to Pt/C, the current value of RGO is high enough, while the double layer capacitance region of Pt/RGO is much larger than it is for Pt/C. It's also worth noting that there is a characteristic peak of

the RGO at ca 0.65V in the CV. However, it is not currently known what causes this peak to be present.

As an ideal support material with large available surface area, good electrical conductivity and good adhesion between the support and Pt particles, the Pt/RGO should be much more than 30.3 m²g⁻¹. Focusing on this problem, numerous optimizations have been carried out to find out the best reproducible methods for fabricating Pt/RGO catalyst. The experimental parameter comparisons of Pt/RGO preparation conditions, such as pH adjustment before MWAPP, MWAPP power and durations and further reduced by NaBH₄, were illustrated in table.3.5. When the ECSA shows 0, it means the CV curves of catalysts don't have the hydrogen desorption peaks and reflects the catalyst performance is poor. In order to facilitate comparison, in the following experiment, we used 1.4 mg catalyst (ca. 20 wt% Pt) to prepare the ink.

Table.3.5. Experimental parameters comparison for optimizing production of Pt/RGO

Variable	Specific description	MWAPP	ECSA (m ² g ⁻¹)
Baseline	12	800W, 40s	30.3
pH value before	8	800W, 40s	0
MWAPP	The same total	300W, 110s	10.5
MWAPP	energy		
conditions	Heat	800W, 50s	37.1
	continuously	800W, 60s	29.6
		800W, 70s	26.0
	Break heating	800W, 80s	25.6

NaBH ₄ reduction	40s on-10s off	800W, 120s	0
		800W, 160s	0
	2 hrs in ultrasonic bath	800W, 40s	36.0
	2 hrs at 60 °C stirring	800W, 40s	21.1

Based on the ECSA data calculated from CV results, it can be seen that before the microwave process, adjusting the pH value to 12 is a necessary condition for the Pt/RGO fabrication. Meanwhile, when keeping the same energy in MWAPP, the condition with high power and short duration is beneficial to the catalyst. Furthermore, too much duration in procedure will make the Pt/RGO lose its catalytic activity. The best reaction duration should be between 40 s and 80 s. Meanwhile, as we know, the longer duration commonly results in the larger size of the Pt nanoparticles.

In order to get the best duration for Pt/RGO fabrication, the samples of different durations with 50, 60 and 70 s are produced as well. The CVs of them and the relationship between duration and ECSA are shown in the Fig.3.12 and Fig.3.13 respectively, which clearly illustrate that the best duration in our experiment comes to be 50 s. Meanwhile, the difference among the ECSA of these samples is not too large. We also find the ECSA of Pt/RGO made at 70s is similar to that made at 80s. The reason for this is because they used different heating profiles; continuous and intermittent heating process. Generally, with the same duration, continuous heating provides more energy to the sample compared with intermittent heating. Therefore, we can suppose that, if we keep using intermittent heating process, the best duration for Pt/RGO may come to be 60 seconds.

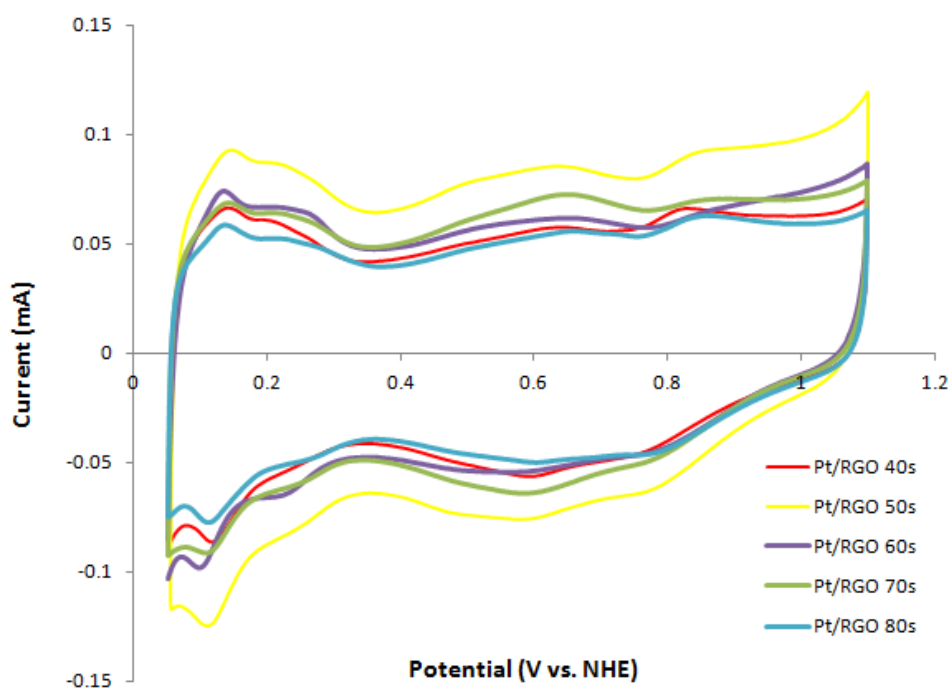


Figure.3.12. CVs of Pt/RGO samples made at different MWAPP durations

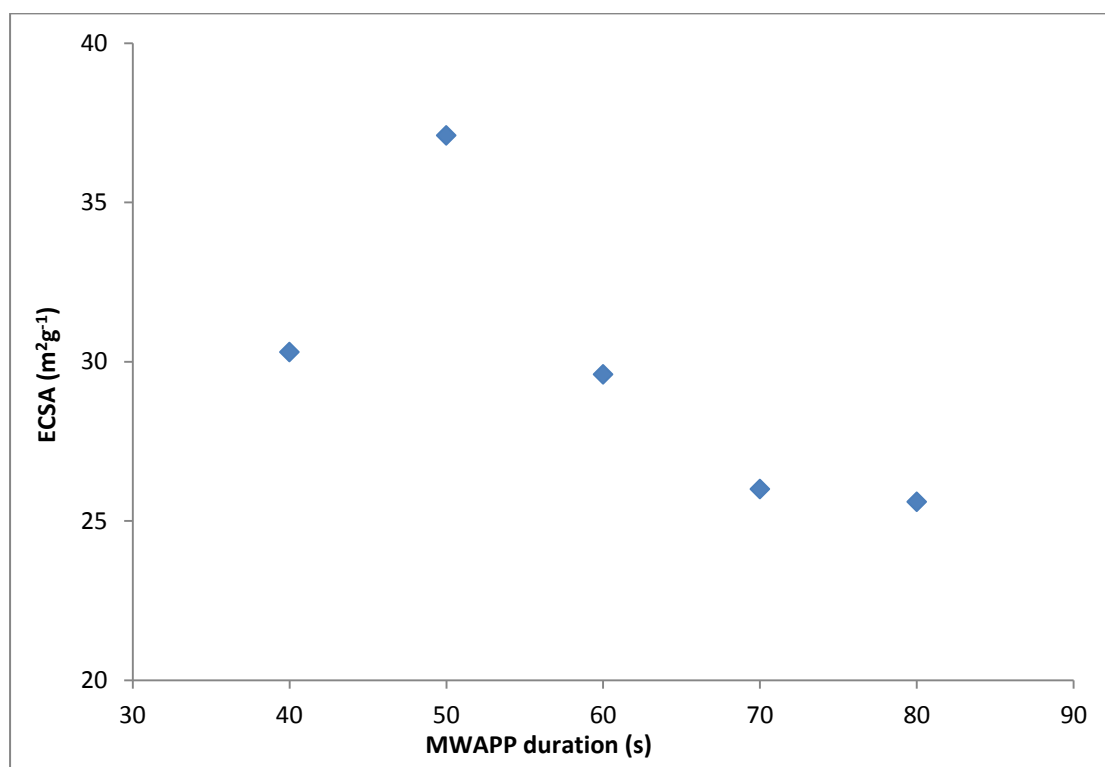


Figure.3.13. The relationship between ECSA and MWAPP durations of Pt/RGO

The further reduction was designed and utilized to the Pt/RGO catalysts by using NaBH_4 , which acted as the reducing agent in this process. From the Fig.3.14, when the reduction was operated in the ultrasonic bath for 2 hours, it achieved to improve the current and the ECSA of Pt/RGO from 30 to $36 \text{ m}^2\text{g}^{-1}$. However, it was found that when the NaBH_4 was added and stirred at 60°C for 2 hrs, the ECSA decreased to $21 \text{ m}^2\text{g}^{-1}$. The reason why the ECSA decreased may be the Pt particles clustered in the reduction process. Meanwhile, it is also possible that the temperature at 60°C cannot provide enough energy to reduce the RGO.

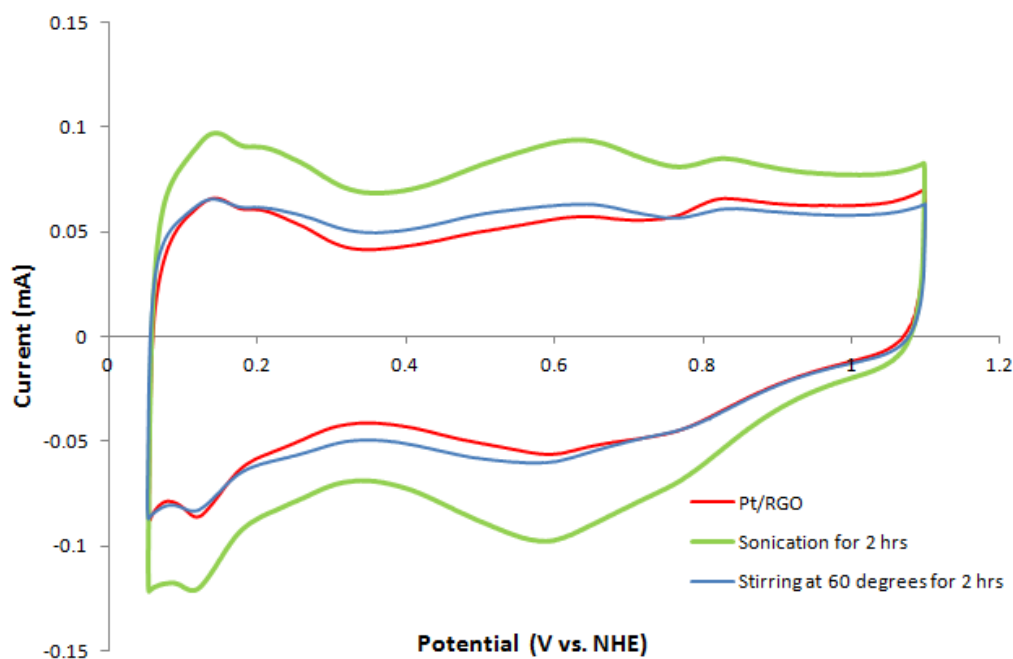


Figure. 3.14. CVs of Pt/RGO reduced by NaBH_4 in different methods (sonication/stirring)

As the heat treatment to the Pt/C catalyst worked in improving the performance, we also heated the Pt/RGO in the oven at different temperatures for 2 hrs in order to improve the catalysts. Generally, ECSA is not only related to the rate of surface area, but also influenced by many other effects, such as atom arrangement, morphology and structure. There are three common low index surface ((111) (110) (100)) in face-centered cubic structure (fcc) of Platinum (J. Chen, Lim, Lee, & Xia, 2009). In

the oxygen reduction reaction, these surface structures illustrate different performances. It is verified by previous researchers that in adsorbing electrolyte like sulfuric acid (H_2SO_4), the activity of ORR grows as $(111) < (100) < (110)$. While, in the non-activity electrolyte like perchloric acid (HClO_4), the ORR activity increase as $(100) < (111) < (110)$. The principles of these can be explained in two aspects. One is the strength of selective interaction between oxygen and exposed facets. Another one is the promoting or inhibiting effect of oxygen containing function group to the adsorption on the Pt surfaces. The surface (110) also has more strong connection to hydrogen than other surface structures (111) and (100) (Garcia-Araez, Climent, & Feliu, 2010).

Various attempts of the heat treatment at different temperatures (60, 100, 150, 180, 200, 250, 300 °C) were tried in our experiment. The ECSAs of the samples after heat treatment were calculated based on the CV results. The CV results of them are shown in the Fig.3.15. Moreover, the relationship between ECSA and heat temperature is illustrated in the table.3.6 and Fig.3.16. Specifically, we can see the current data of 150 °C is much larger than others and the current of 300 °C is the least. There is an increase trend of ECSA from $30.3 \text{ m}^2\text{g}^{-1}$ (60 °C) to $44.1 \text{ m}^2\text{g}^{-1}$ (150 °C). This increase may be caused by the decrease of water content in the catalysts after heat treatment. In addition, the active sites for edges, corners or porous on the RGO sheets were grown gradually along with the temperature ascending below 150 °C

When the temperature is over 150 °C, the linear decrease is demonstrated in the graph, with the ECSA of $11.3 \text{ m}^2\text{g}^{-1}$ at 300 °C. It can be speculated that, the forces of the growing/collapsing of the active sites and the potential of Pt particles clustering to larger sizes are balanced at around 150 °C. Thus, the performance decreased dramatically from 150 °C to 300 °C. This reducing trend illustrates that the Pt catalysts

will lose the activity in high temperature, due to the active sites damaged by high temperature. Overall, these results clearly illustrate that the best temperature of the heat treatment to the Pt/RGO catalysts comes to be about 140 °C.

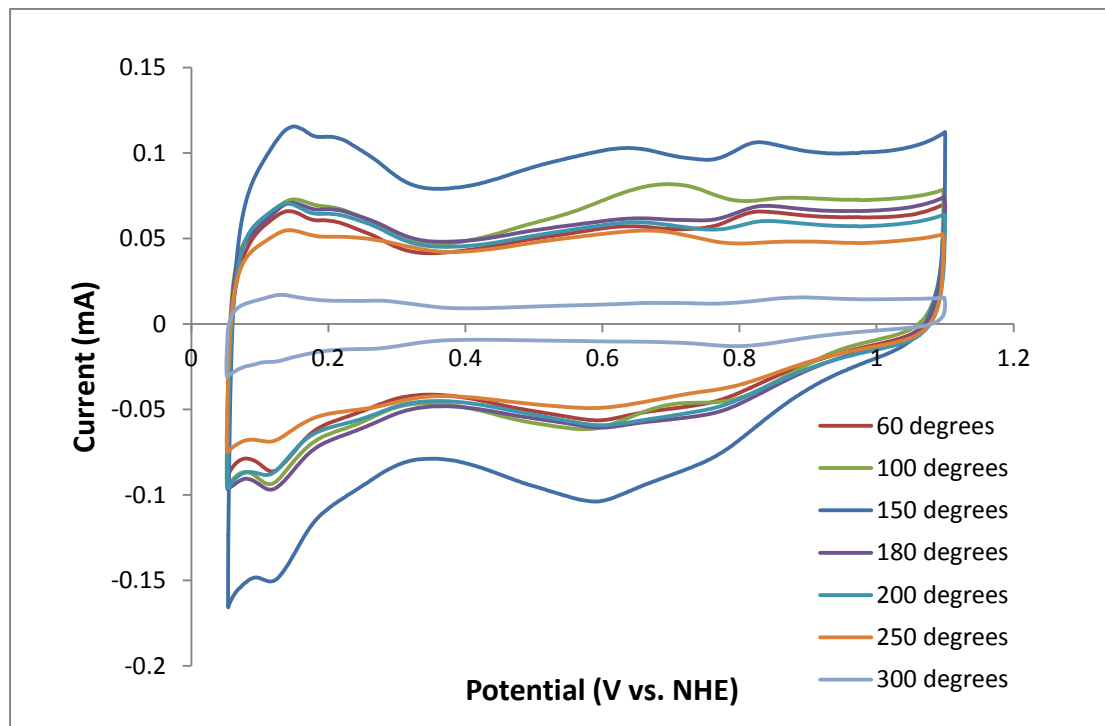


Figure. 3.15. CV of Pt/RGO heated at different temperatures for 2 hrs

Table.3.6. ECSA change of Pt/RGO after heat treatment at different temperature

Heat temperature (°C)	ECSA (m ² g ⁻¹)
60	30.3
100	33.9
150	44.1
180	31.4
200	30.5
250	15.3
300	11.3

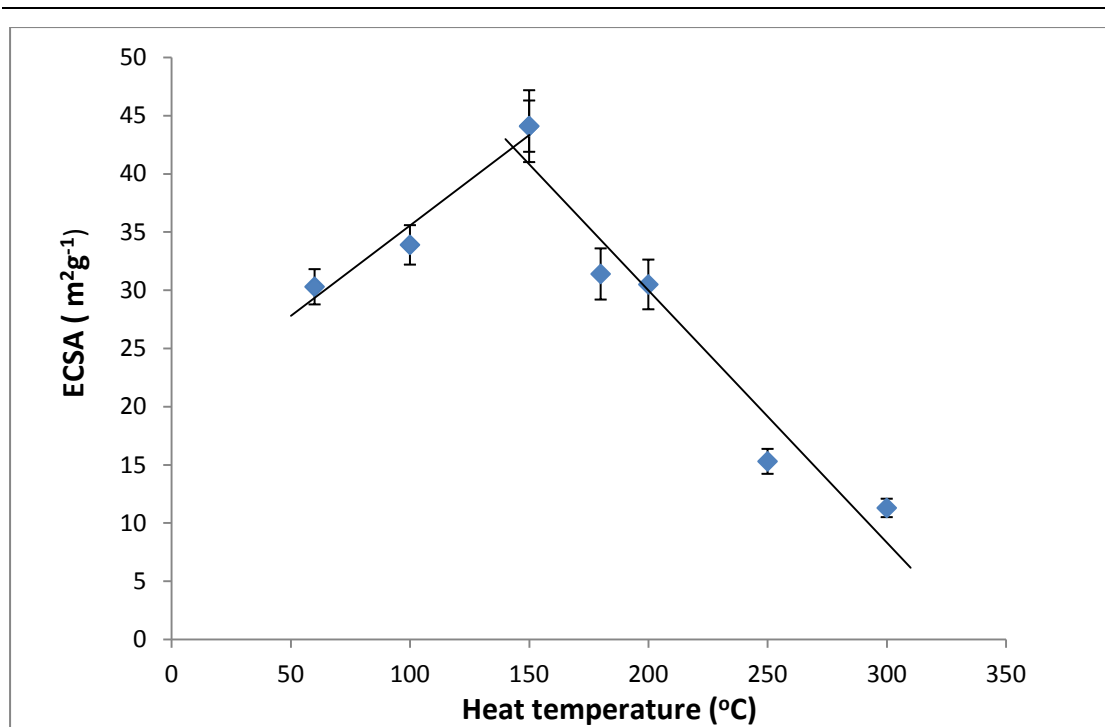


Figure.3.16. ECSA change of Pt/RGO after heat treatment at different temperature

As to the LSV curve we tested of Pt/RGO (Fig.3.17), through Kouttecky-Levich analysis (Fig.3.18), the electron transfer number of Pt/RGO is 1.83 at the beginning. It is much lower than that of Pt/C catalyst we made. This reflects the issue that, in the Pt/RGO catalyst, the oxygen tends to be reduced to peroxide ions (O_2^{2-}) instead of oxygen ions (O^{2-}). After the heat treatment at 150 °C for 2 hrs, not only is there an improvement at ECSA, but also a significant increase at electron transfer number from 1.83 to 2.91 (shown in table.3.4). The reason for this improvement may be that, during the heat process, the surface (100) and (111) were transferred into more stable surface structure (110).

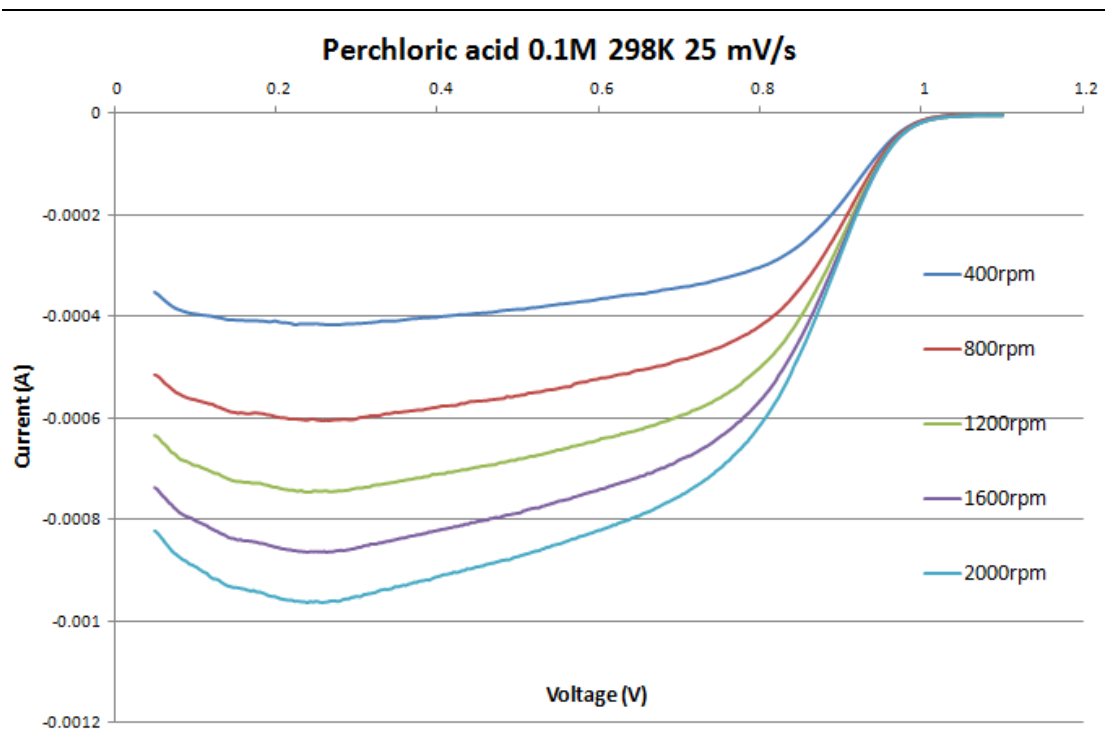


Figure.3.17. LSV of Pt/RGO catalyst in 0.1M HClO₄ solution at 298K and 25 mVs⁻¹

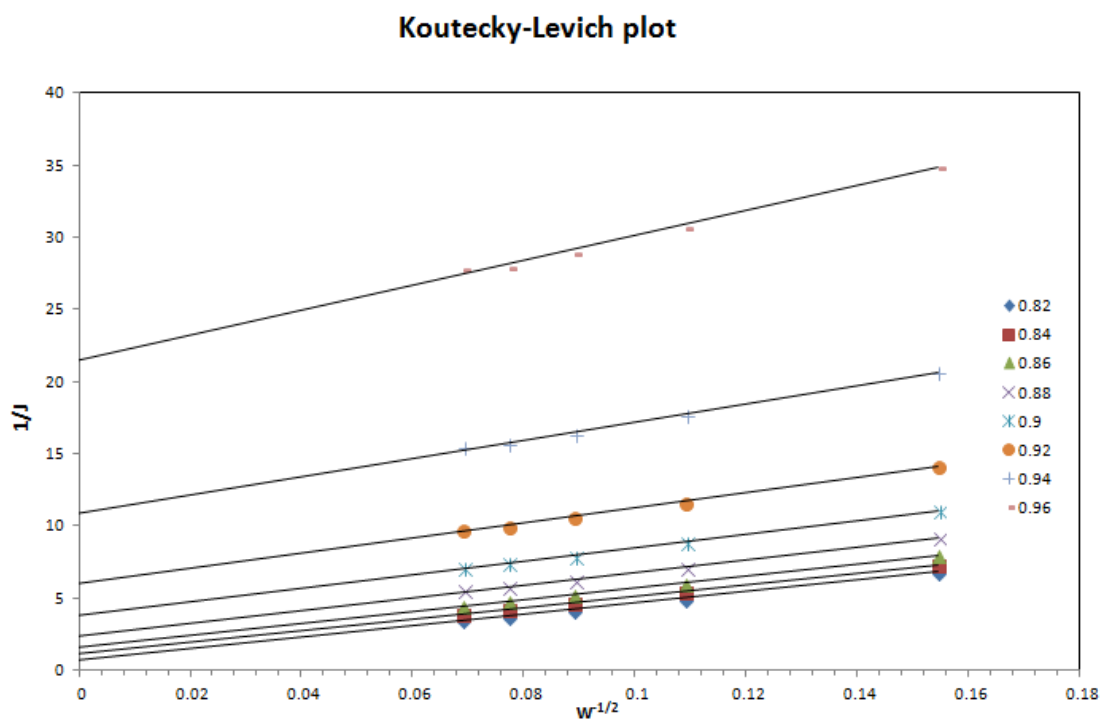


Figure.3.18. Koutecky-Levich plot of Pt/RGO catalyst

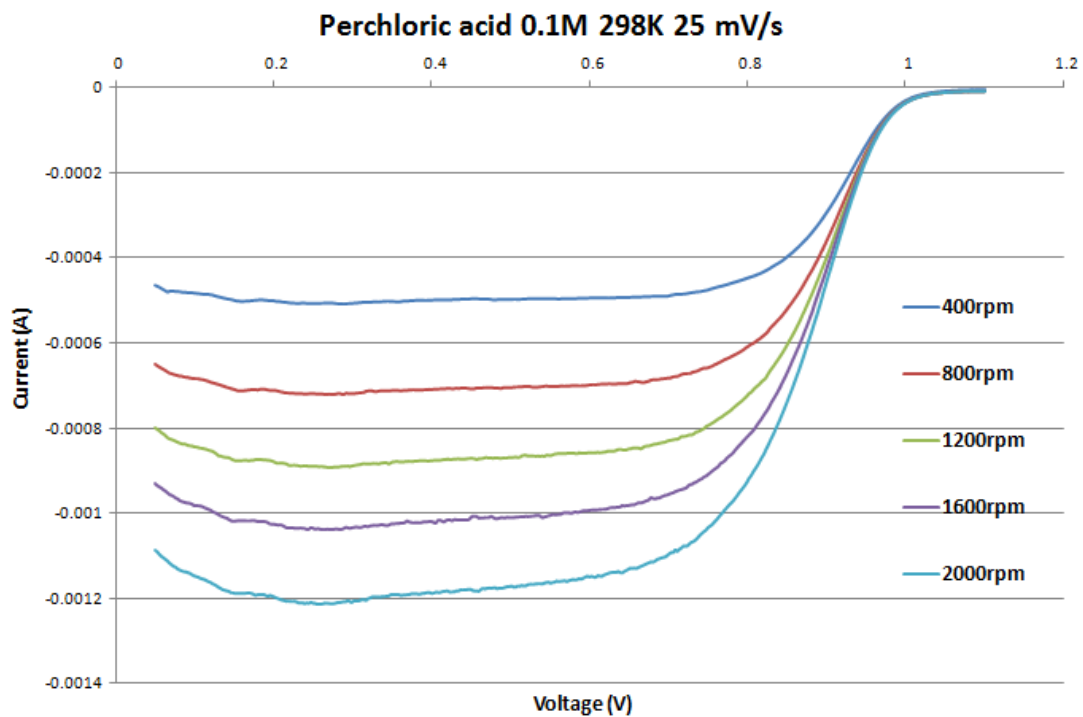


Figure. 3.19. LSV of Pt/RGO after heat treatment at 150 degrees in 0.1M HClO₄ solution at 298K and 25 mVs⁻¹

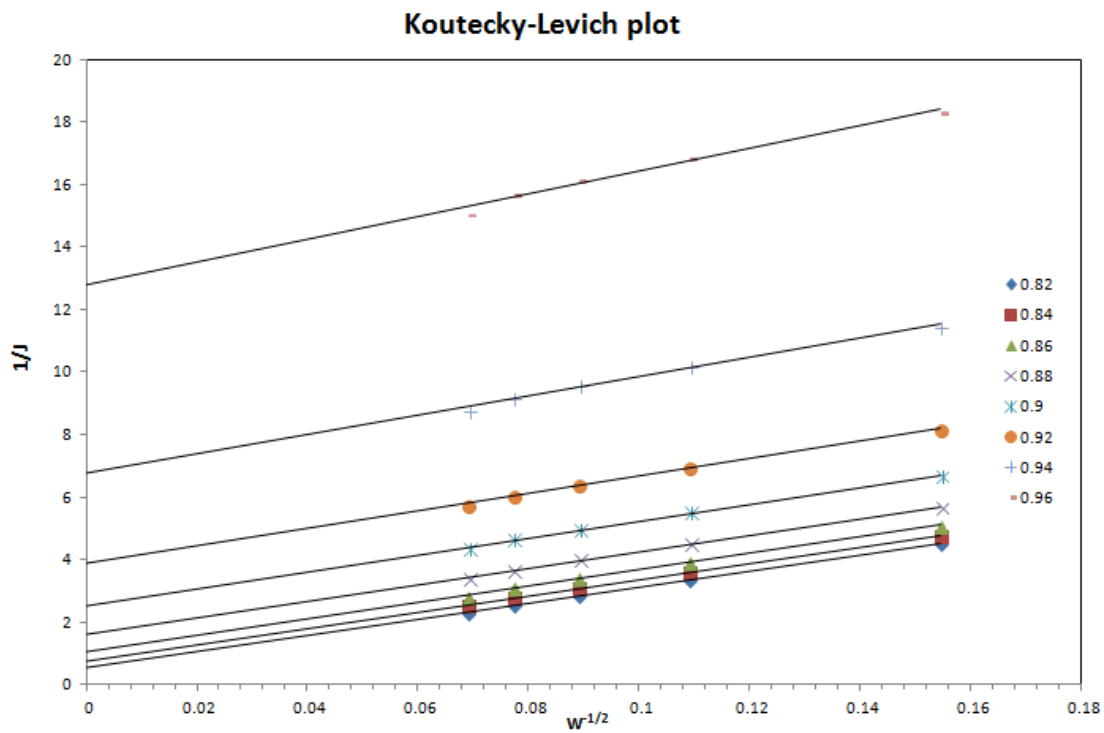


Figure. 3.20. Koutecky-Levich plot of Pt/RGO catalyst after heat treatment at 150 degrees

The Fig.3.19 and Fig.3.20 have shown us the LSV information about Pt/RGO catalyst after heat treatment. Meanwhile, though the improvement of catalyst property is obvious, the electron transfer number is still less than 3. That is to say, there are still more than 50% O₂ reduced to peroxide ions (O₂²⁻) in the ORR.

3.6.3 Pt/(RGO+C)

Though heat treatment to the Pt/RGO catalyst really works at improving the performance, it still hasn't reached our goal of high ECSA. We designed two strategies to improve the property of Pt/RGO catalyst further. One was using ultrasonic probe at a strong power (100W) and a suitable duration (30 mins) to reduce the size of commercial GO sheet for relieving the Pt agglomeration. Specifically, before the commercial GO were used as support material, a strong ultrasonic treatment (100W, 30 mins) was attempted, working as 30s on – 10s off, in order to reduce its size and make it disperse better in solution. Another method was adding C after MWAPP process to prevent the RGO from stacking in the drying process. At the same time, carbon black is an excellent electricity conductor as well. Meanwhile, when the mixture support materials of RGO and C are used in the in-situ test, it may have some advantages to water managements.

In order to get high ECSA, two strategies were utilized together to fabricate the Pt/(RGO+C). As to the support materials, adding C into the RGO before or after the MWAPP process will have different influence. In other words, if carbon black is added into the solution before MWAPP, the Pt/(RGO+C) catalyst produced would have Pt nanoparticles on the carbon black as well. On the other hand, if the calculated C is added after MWAPP, Pt nanoparticles would only grow on the surface of RGO. Different samples of Pt/(80wt%RGO+20wt%C) have been fabricated and characterized to see the performance of the catalysts. In Fig.3.21, the ECSA of the

sample adding C after MWAPP ($59.2 \text{ m}^2\text{g}^{-1}$) is similar to that of the sample where C was added before MWAPP ($58.9 \text{ m}^2\text{g}^{-1}$). The peak at 0.6 V of the sample adding C before MWAPP is small because the Pt nanoparticles grow on carbon black as well. Based on this and the in-situ results illustrated in the following section, we make the conclusion that adding C after MWAPP is a much improved method of fabricating the Pt/(RGO+C) catalysts. Therefore, we use this procedure to produce Pt/(RGO+C) catalysts with different carbon content.

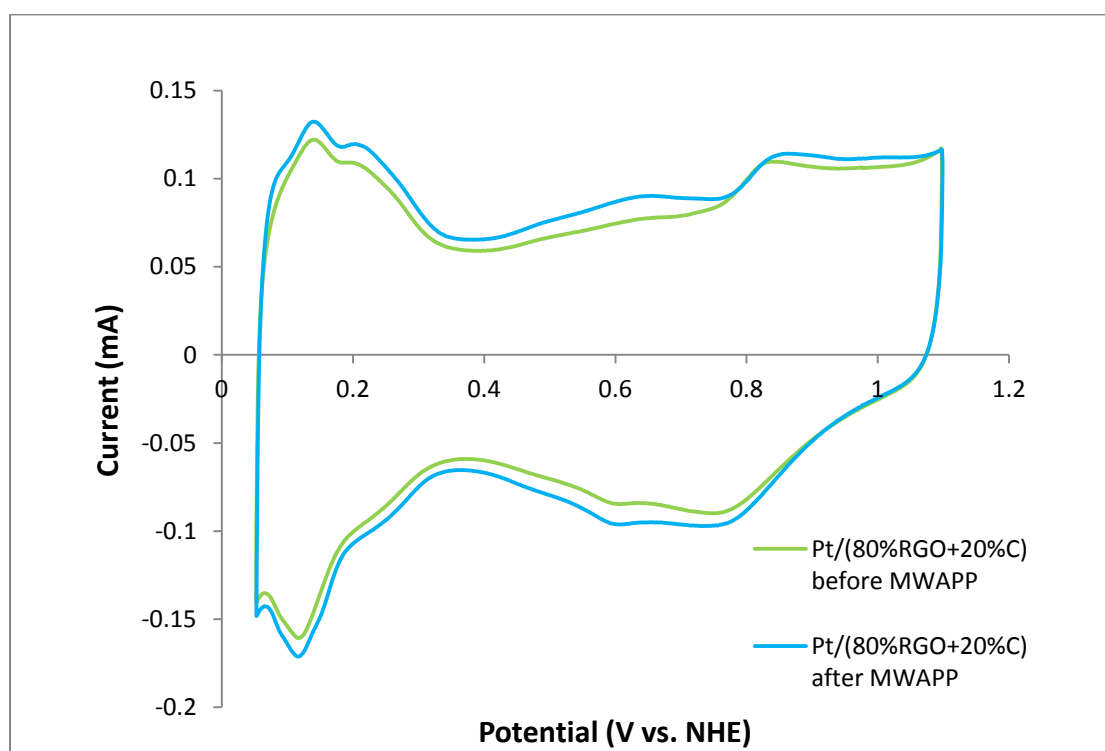


Figure.3.21. CVs of Pt/(80%RGO+20%C) in different C adding order

When the ECSA of Pt/(80%RGO+20%C) catalyst is compared to the original Pt/RGO catalyst, it shows a significant improvement from $30.3 \text{ m}^2\text{g}^{-1}$ to $59.2 \text{ m}^2\text{g}^{-1}$. This improvement evidently confirms that, strong ultrasonic treatment and the addition of C are a good way to enhance the performance of Pt catalyst. However, the effect of each of them separately is still not clear. Therefore, two methods were separately tried and characterized in our experiment. From the CVs of samples (shown as Fig.3.22), the ECSAs of the Pt/RGO sample after strong ultrasonic

treatment and the Pt/(RGO+C) without strong ultrasonic are calculated to be $35.3 \text{ m}^2\text{g}^{-1}$ and $29.7 \text{ m}^2\text{g}^{-1}$ respectively. It is clearly illustrated that, compared to the original Pt/RGO (ECSA= $30.3 \text{ m}^2\text{g}^{-1}$), there is an increase in ECSA of the sample after the strong ultrasonic treatment. But the improvement is not very much, only $5 \text{ m}^2\text{g}^{-1}$. This illustrates that the decrease of the size of GO sheet is really beneficial to the catalyst. While, small pieces of GO sheet still tend to stack during the drying process. Meanwhile, if the GO sheet hasn't been reduced by strong ultrasonic treatment, the addition of C doesn't have the ability to forbid the GO sheet from stacking. This may be because that the size of carbon black is much less than that of GO sheet. During the drying process, the carbon black would be enfolded by the GO sheet. Thus, carbon black cannot work as intended to support the GO layers. Overall, in order to get excellent Pt catalysts, the two strategies need to be used together. After the GO sheet is changed into small pieces by strong ultrasonic treatment, the C addition can aid in the prevention of the GO aggregation problem.

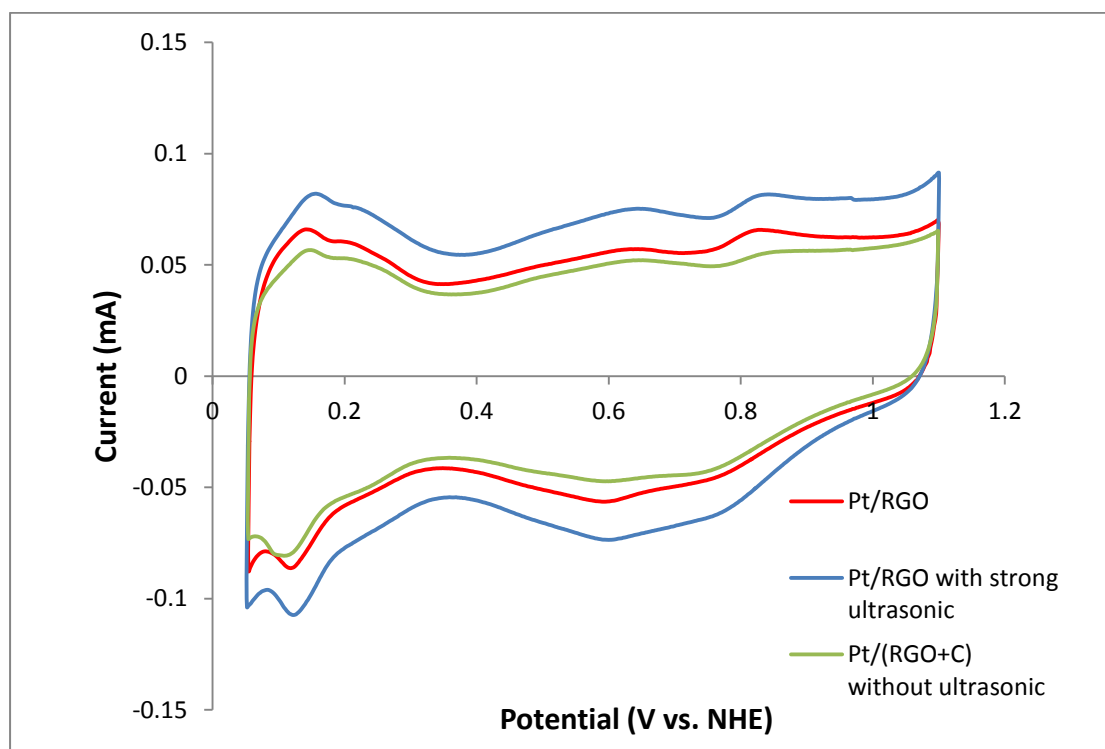


Figure.3.22. CVs of the samples by different design strategies

As previously described, the Pt/(RGO+C) catalyst made in-house shows the potential to be an excellent catalyst. So we did various experiments to find the best carbon black content in support materials. During our research, different C content samples (10wt%, 20wt%, 30wt%, 40wt% and 50wt%) were fabricated and tested. From the CV graphs of different C content samples (Fig.3.23), it can be found that, as the carbon content increasing, there is a significant drop of the electric double layers and the peak at about 0.6 V. Combined with table.3.7 and Fig.3.24, we can summarize the trend between ECSA and the carbon black content of the support materials as below. When the C content is less than 30%, the ECSA rises as the carbon content increases. On the other hand, when the C content is larger than 40%, the ECSA decreases as the carbon content increases. This trend is because of two main reasons. One is the increase of carbon content will decrease the GO content in the catalyst. That is to say, the ratio of Pt to GO will increase as the carbon content rises. The diameter of Pt nanoparticle will become larger. As we analyzed in table.3.3, the larger diameter means the less ECSA. Thus, in this aspect, the rise of C content is bad for getting a high ECSA. The carbon black can prevent GO from stacking. In this aspect, more carbon black means more available Pt nanoparticles on the RGO sheet. Overall, because of these two effects, the ECSA trend in the ex-situ test shows as increasing with carbon content, remaining stable and decreasing. The optimum carbon content of Pt/(RGO+C) catalyst can be predicted at the range of 35% and 40%, with ECSA of about $70 \text{ m}^2\text{g}^{-1}$, which reached the same level of TKK.

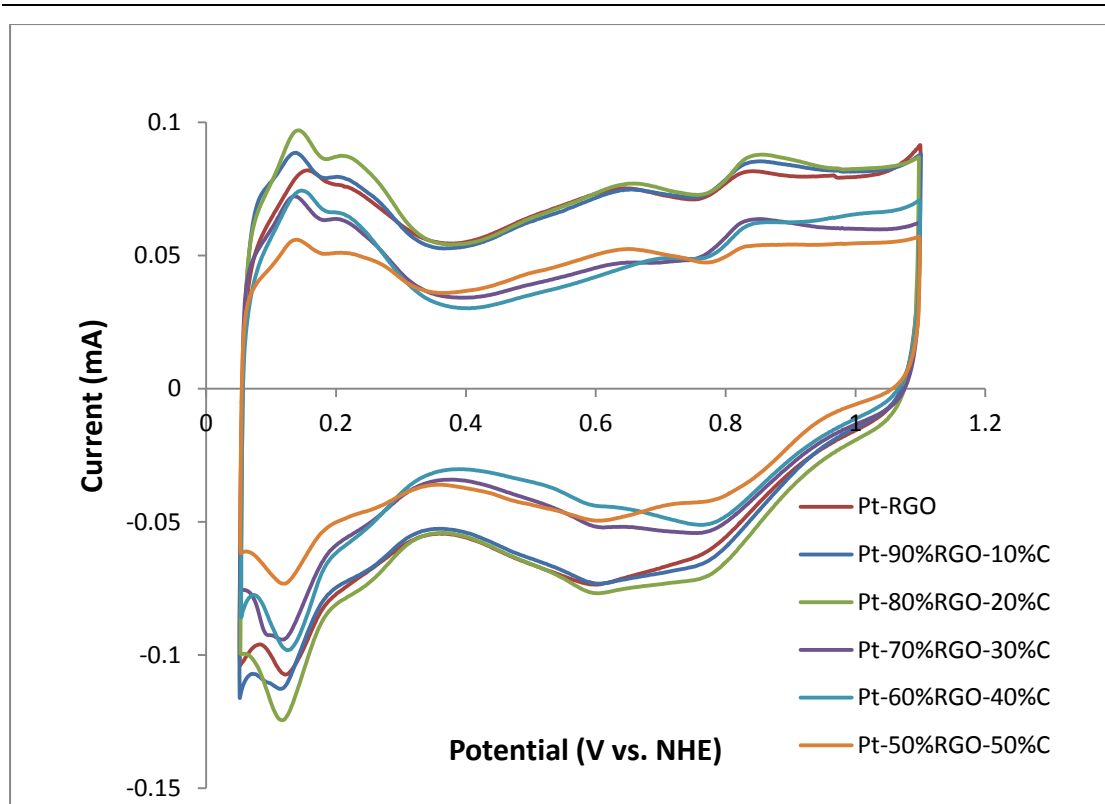


Figure.3.23. CVs of the Pt/(RGO+C) catalysts in different carbon content

Table.3.7. ECSA of different catalysts with various carbon content in the ex-situ test

Carbon content	ECSA (m^2g^{-1})
0	33.8
10%	47.1
20%	56.2
30%	66.3
40%	64.3
50%	25

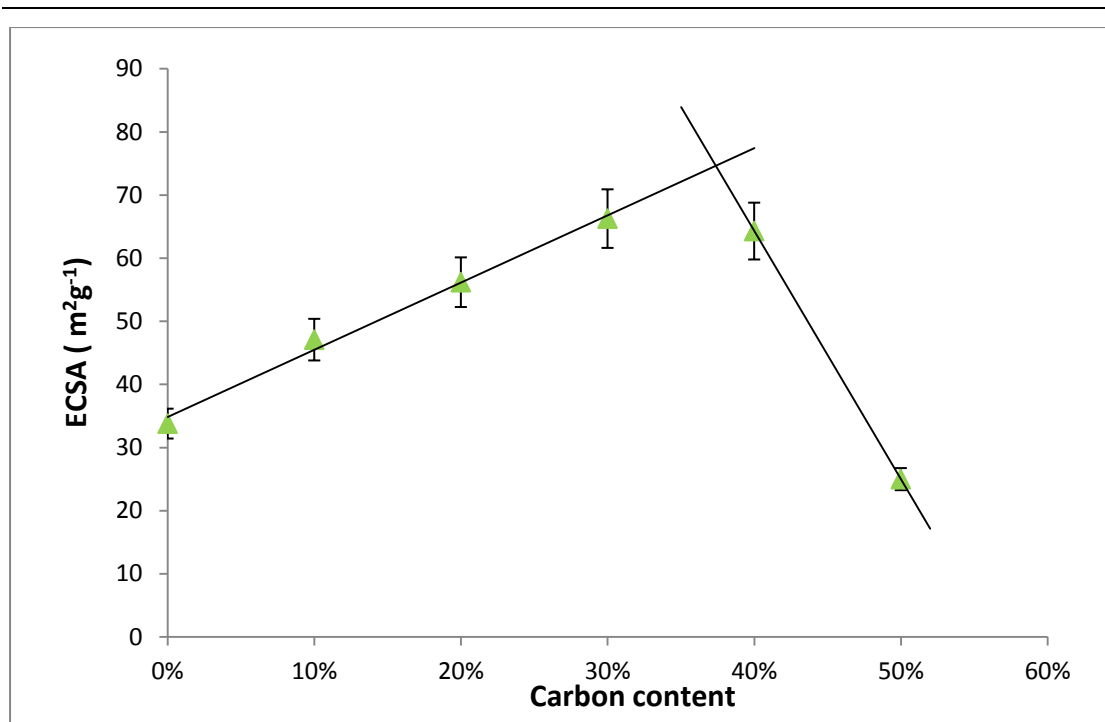


Figure.3.24. The relationship between different carbon-content catalysts and corresponding ECSA in the ex-situ test

3.7. MEA testing (in-situ testing)

As described in the experimental work section before, the MEA testing was carried on after the ex-situ electrochemical testing to see how the catalysts perform in the fuel cell. The Pt catalyst powder was mixed to get a colloidal ink, sonicated and then hand-painted onto the commercial GDL. The catalyst samples used as cathodes in the MEA were measured to assess their viability for the ORR.

As it is shown in Fig.3.25, the polarisation curves of Pt/C sample 2 and 3 in the MEA were performed at 80 and 120 °C for the comparison. Obviously, the performance of sample 2 (ECSA= 49 m²g⁻¹) is much better than sample 3 (ECSA= 60 m²g⁻¹). This result demonstrates that the ECSA is not the only influencing factor to in-situ performance. The tendency to agglomerate of the small-size nanoparticles also

results in quick decrease of the current density in polarization curves. On the other hand, as to an excellent catalyst, high ECSA is necessary.

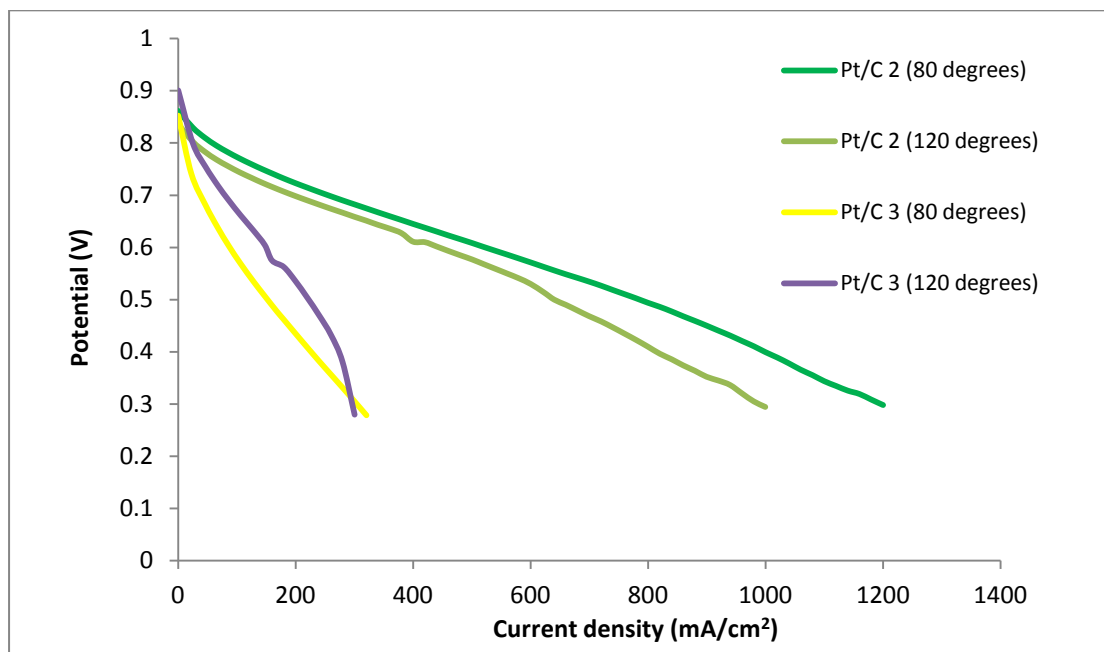


Figure.3.25. Polarization curves of Pt/C catalysts (Pt loading 0.4 mg/cm²)

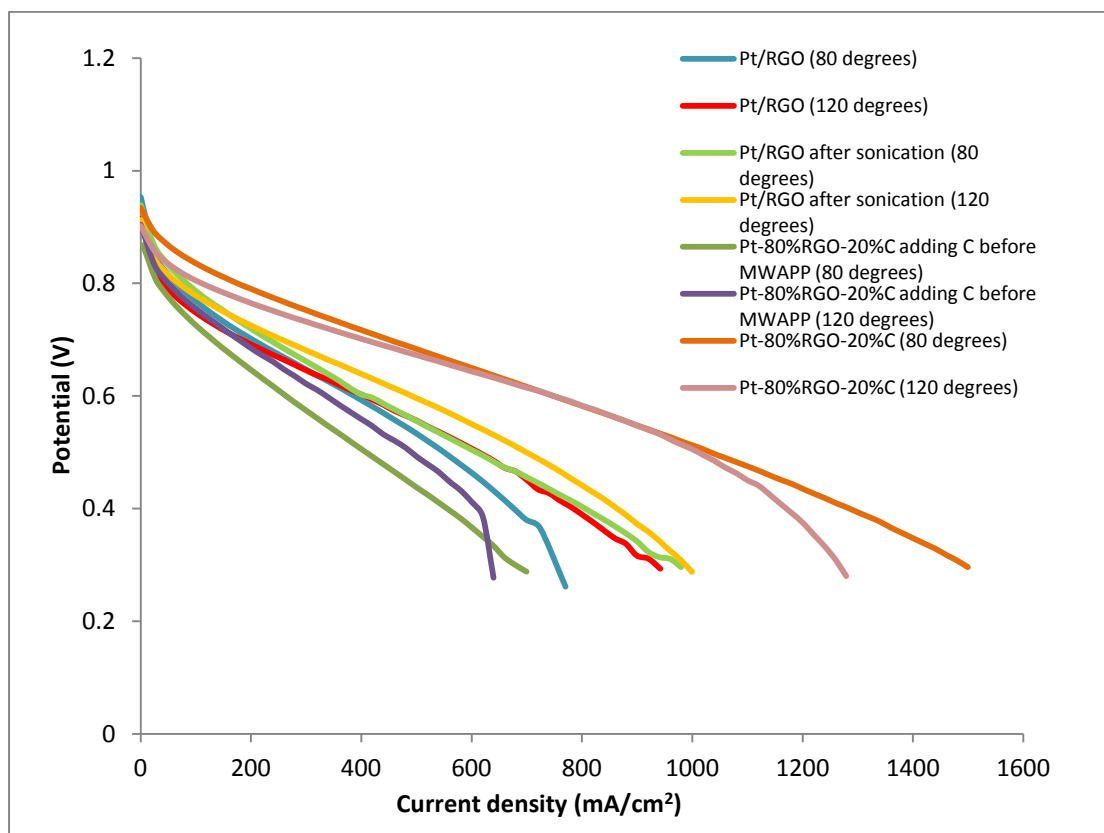


Figure.3.26. Polarization curves for cathodes catalysts made in-house

Table.3.8. Current densities at 0.6 V at different temperatures of various Pt catalysts

Sample	Temperature (°C)	Current density at 0.6 V (mA/cm²)
Pt/RGO	80	380
	120	400
Pt/RGO after sonication	80	400
	120	480
Pt-80%RGO-20%C (C before MWAPP)	80	260
	120	340
Pt-80%RGO-20%C	80	740
	120	750
Pt-80%C-20%C	80	380
	120	560

During the hand-painting process, it was obvious that the drying speed of the top layer of Pt/RGO is much quicker than that of Pt/C. Compared to Pt/C catalyst; the colour of Pt/RGO layer is much lighter. As we described before, the samples of two strategies (strong sonication to the GO and C addition) have been researched in the in-situ test as well. According to Fig.3.26 and table.3.8, compared to the polarization curves of Pt/RGO, it is confirmed that, there is an increase when the strong ultrasonic treatment was used to GO before MWAPP. As the sample that only adds carbon black into the catalyst showed worse ECSA in the ex-situ test, therefore we didn't test it in the in-situ test. The order of adding carbon black into the catalyst before MWAPP and after MWAPP was then tested, even though they illustrated similar results in the ex-situ test. There was an obvious drop of performance of the sample adding C before

MWAPP in the in-situ. Meanwhile, it is worth noting that, when these strategies were utilized at the same time, the current density of Pt-80%RGO-20%C sample is nearly as two times as that of Pt/RGO sample. This result has given us a new method to improve the performance of Pt catalysts vastly. Based on this discovery, the MEA of catalysts with different addition amounts of carbon black have been fabricated to find out the best ratio of C to RGO with highest current density at 0.6V and largest ECSA in the in-situ test.

In order to certify the advantages of RGO as support material, the same process was used to produce Pt/C catalyst. As it is shown in Fig.3.27, the polarization curves of Pt-80%RGO-20%C are much higher than that of Pt/C catalyst. This clearly illustrated that, when RGO was utilized as support material instead of carbon black, the shortages of carbon black, such as poor durability and low stability, have been solved substantially. RGO has better performance because of its excellent electrical conductivity, large surface area and good adhesion to the Pt nanoparticles. Meanwhile, the remaining oxygen functional group on the RGO surface will also influence the property of catalyst in MEA.

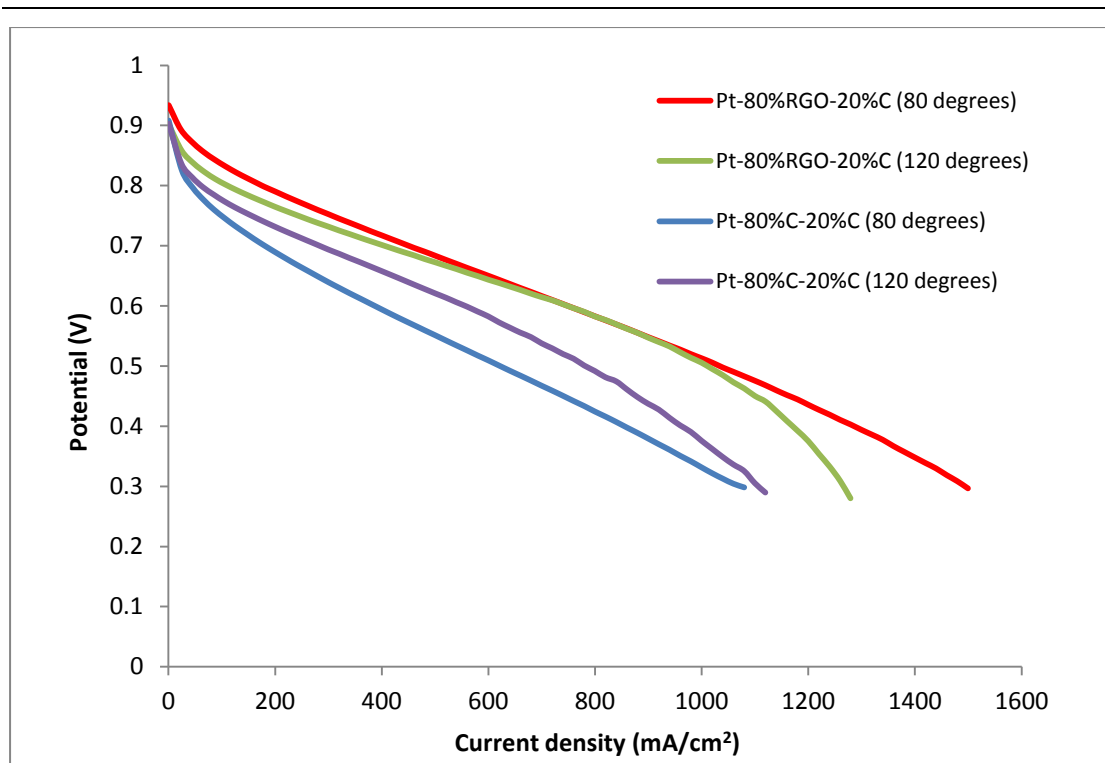


Figure.3.27. Polarization curves of Pt-RGO-C and Pt-C in the same fabrication process

Numerous experiments have been done for the best performing Pt-RGO-C catalyst. Each sample with different C content was made into MEA and measured at various temperatures (80, 90, 100, 110 and 120 °C) at 1.8 bar gas back pressure with a relative humidity of 100%. As shown in table.3.9, current densities at 0.6 V which got from the polarization curves of different sample under various conditions were collected.

Table.3.9. Current densities at 0.6 V at different temperatures of various Pt-RGO-C catalysts in different carbon content

Sample	Temperature (°C)	Current density at 0.6 V (mA/cm ²)
Pt-100%RGO	80	400
	120	480
Pt-90%RGO-10% C	80	279

Pt-80%RGO-20% C	90	540
	100	720
	110	740
	120	480
	80	750
Pt-70%RGO-30% C	90	920
	100	920
	110	870
	120	750
	80	760
Pt-60%RGO-40% C	90	940
	100	1130
	110	1100
	120	900
	80	1100
Pt-50%RGO-50% C	90	1160
	100	1100
	110	1040
	120	930
	80	770
Johnson Matthey 0165	90	900
	100	960
	110	940
	120	790
	80	653

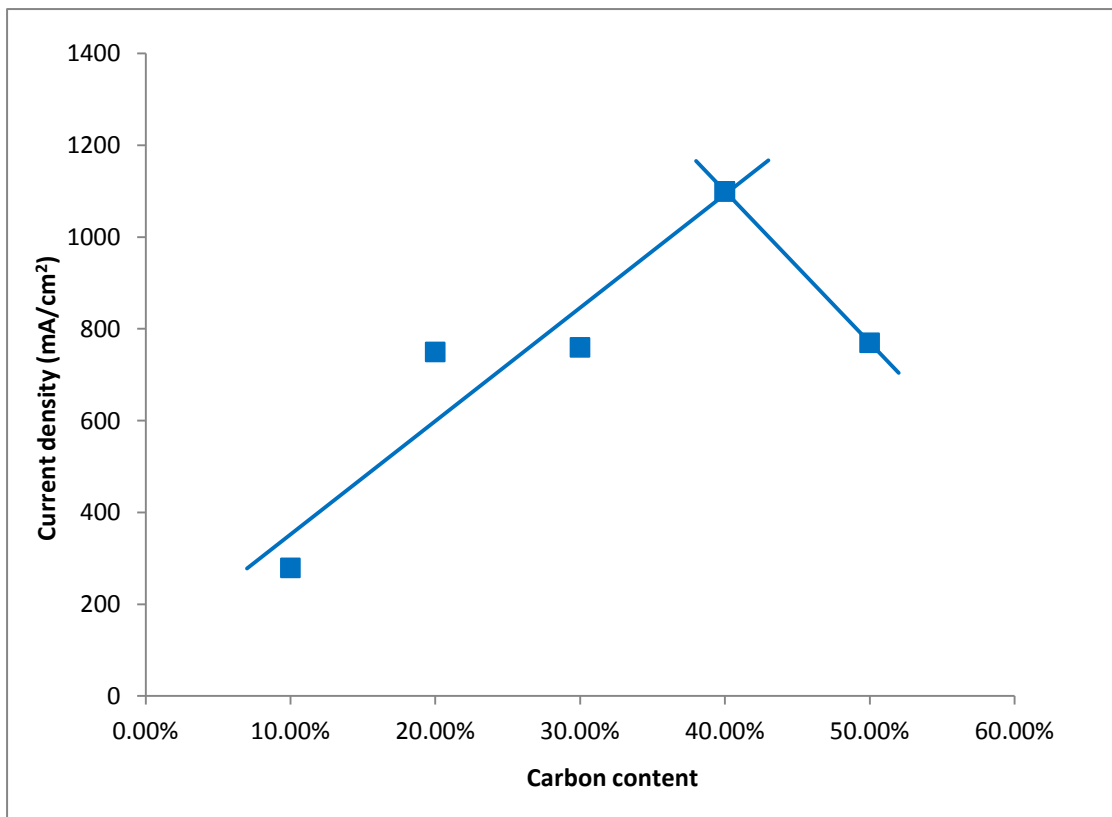
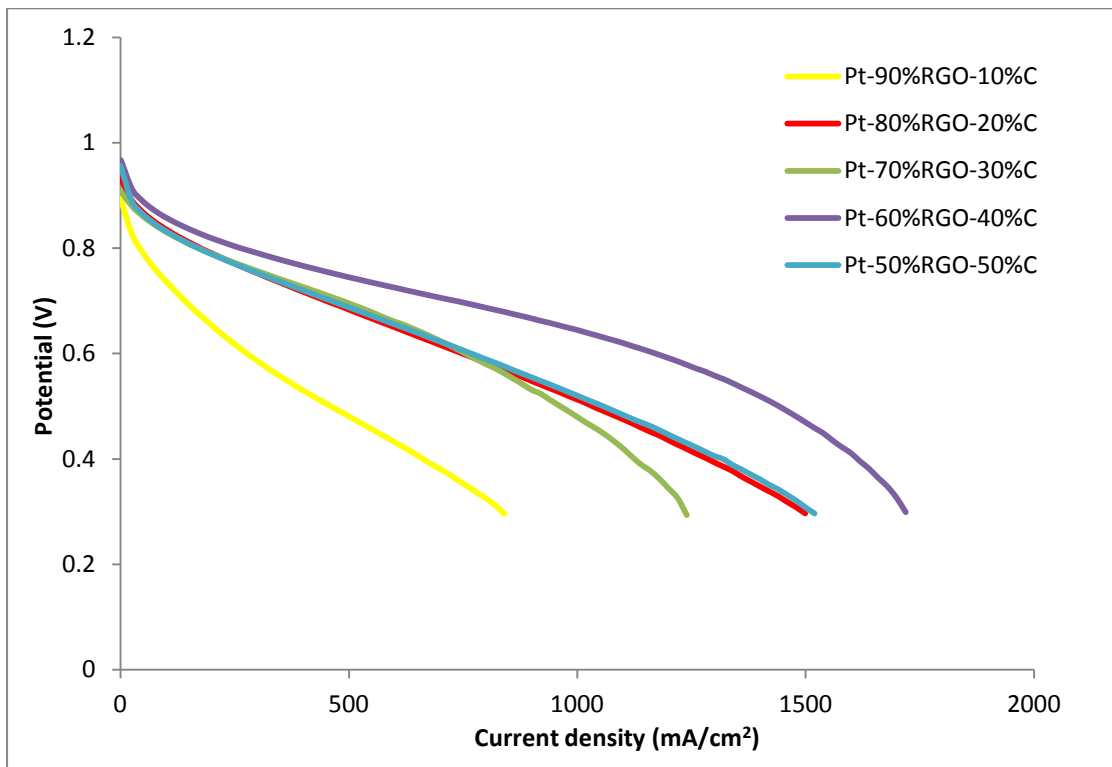
TKK	120	787
	80	560
	120	621

In order to observe the relationship more obviously, the polarization curves and the relationship between current densities at 0.6 V and the carbon content at 80, 90, 100, 110 and 120 °C are drawn in Fig.3.28 respectively. According to the data, as the amount of carbon added increases, the performance increased from 10% to 30%, while reduced when it is over 40%. Compared with commercial GDE (Johnson Matthey 0165) and commercial catalyst (TKK), our Pt-RGO-C catalysts have much higher current densities. Specifically, the current density of Pt-60%RGO-40%C catalyst at 80 °C is about 1.5 times to that of commercial GDE, even higher to that of TKK (Fig.3.29). Meanwhile, based on this data, the best percentage of carbon black is speculated to be in the range of 30% to 40%.

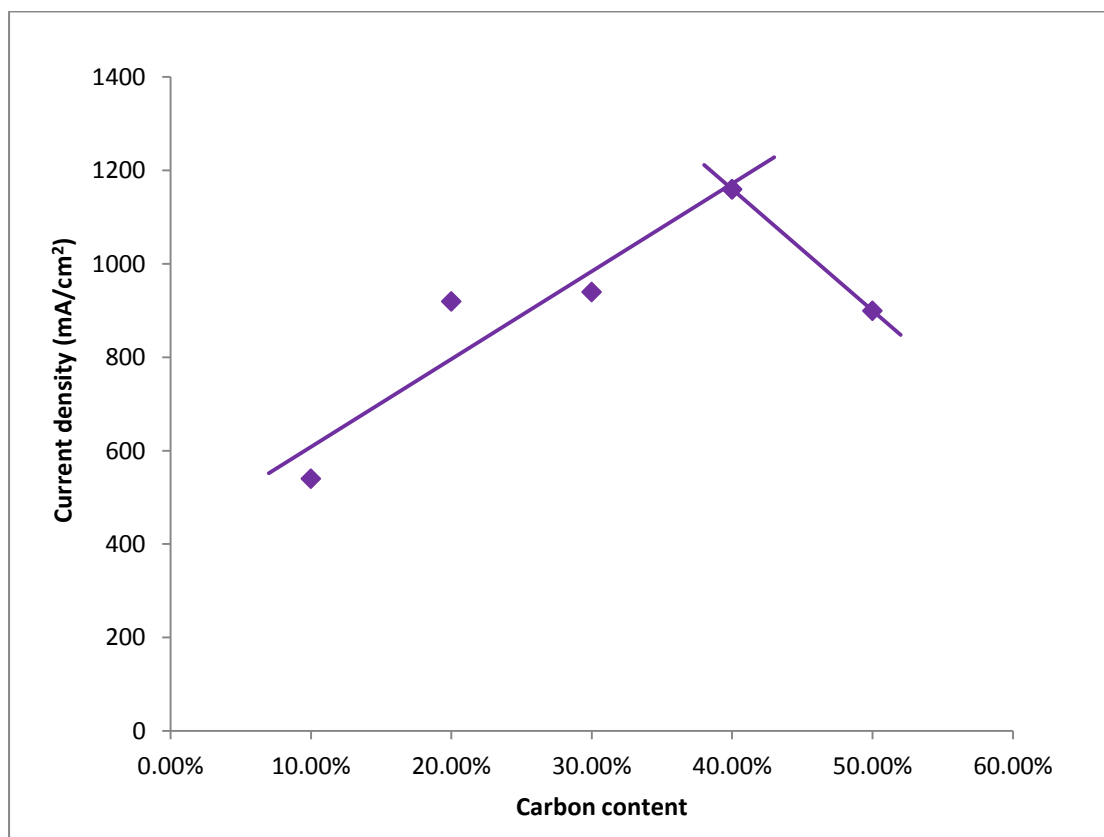
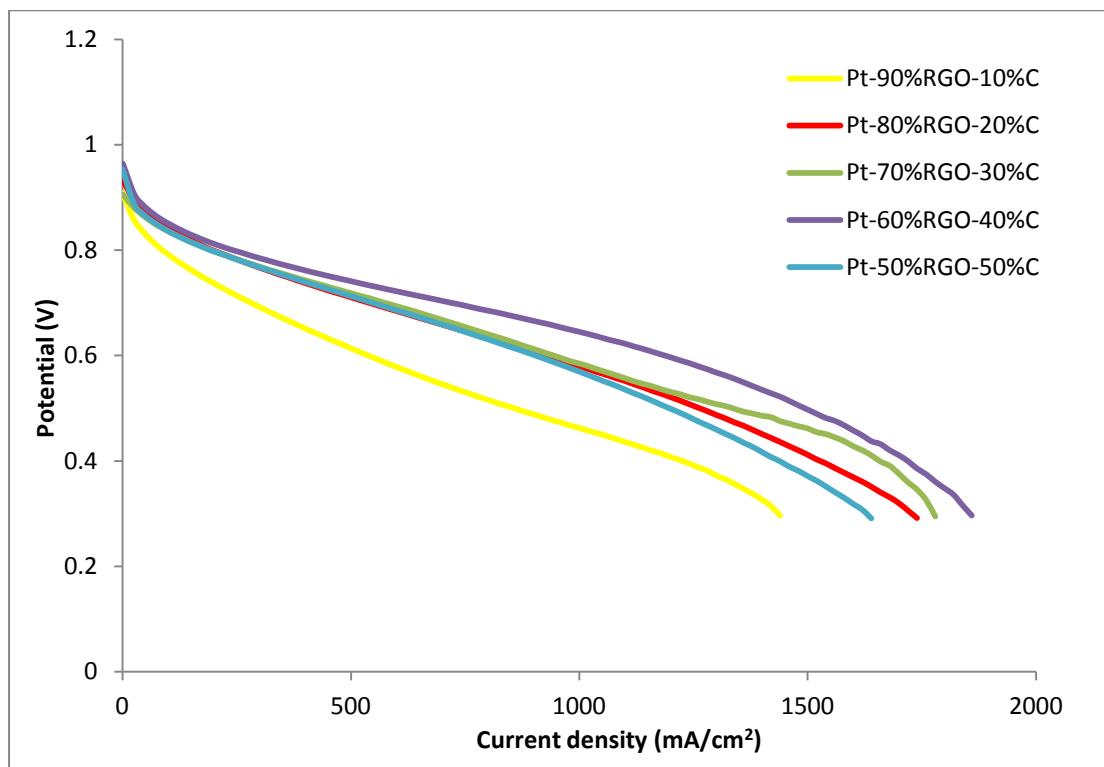
The principle of linear fit in this analysis process was according to the in-situ ECSAs, which were calculated by CVs obtained at 25 °C with gas relative humidity of 100% in the MEA at the scanning rate of 40 mV s⁻¹. As it is illustrated in table.3.10 and Fig.3.30, the results of in-situ ECSAs have demonstrated good linear relationship to the carbon content from 10% to 40%. While, though the polarization curves are actually influenced by many effects, such as water management, membrane capability and others, the property of catalyst (ECSA) is still the main factor. Therefore, it is acceptable to do the linear fit to get the best carbon content of the catalyst. Moreover, the existence of other effects also explains the reason for the deviation between actual data and ideal linear fit point. The effects are also related to the operating temperature of MEA, so there are some varies of the best ratio of carbon content under different

testing temperature. Moreover, more details can be found out when focus on the change of current density along with the temperatures during the in-situ test. For instance, the polarization curves and the corresponding current densities at 0.6 V of Pt-RGO-C catalysts at various temperature (80, 90, 100, 110 and 120 °C) are shown in Fig.3.31. Generally, it is accepted that, the catalyst usually performs better at higher test temperature. While, in our Pt-RGO-C MEA, there is an evident drop of performance at 120 °C. We think this situation is caused by the activity loss of membrane at high temperature. Specifically, more results and figures in the in-situ test about CV of different catalysts at various scanning rates.

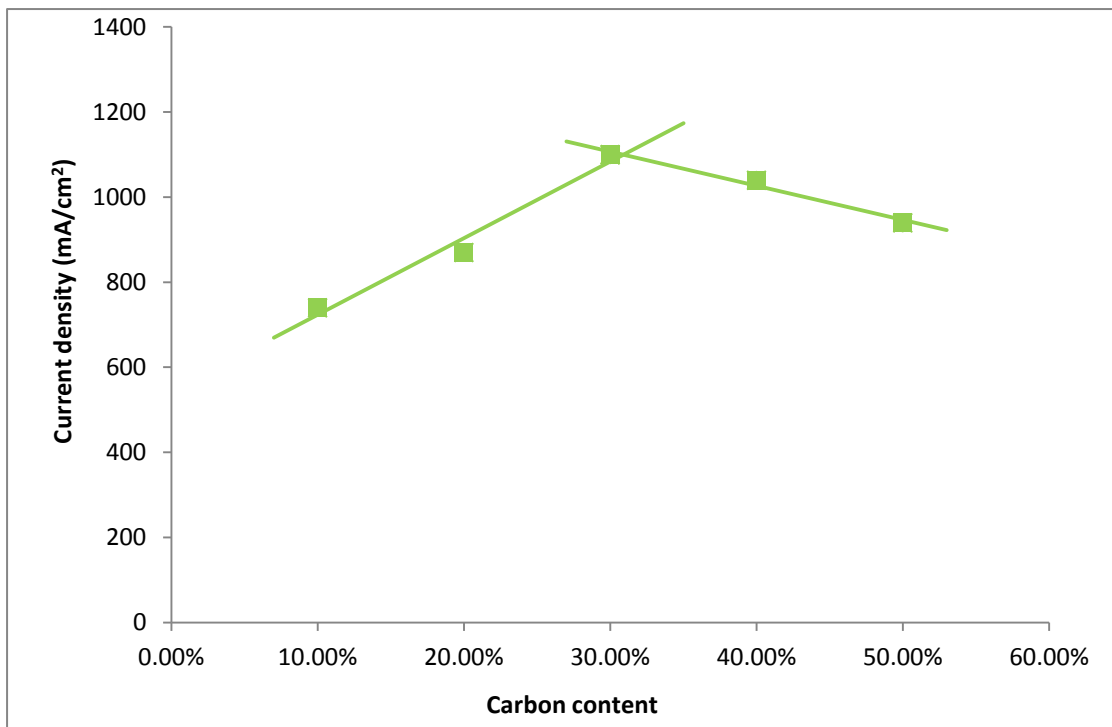
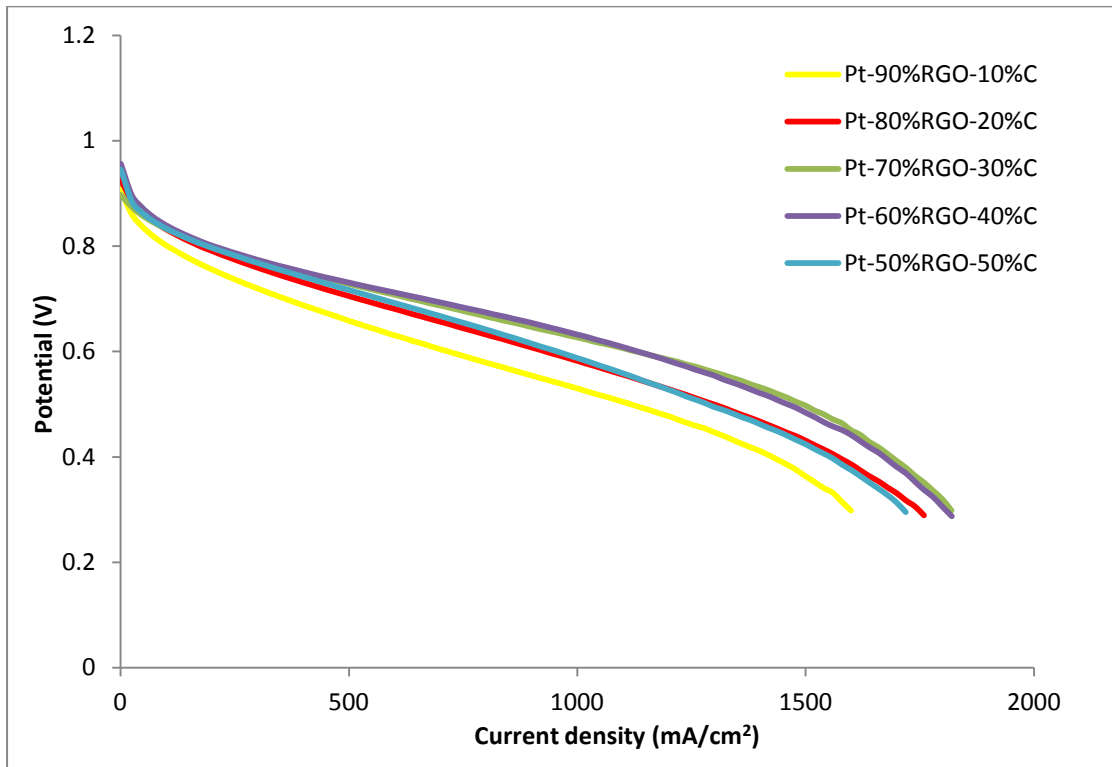
80 °C



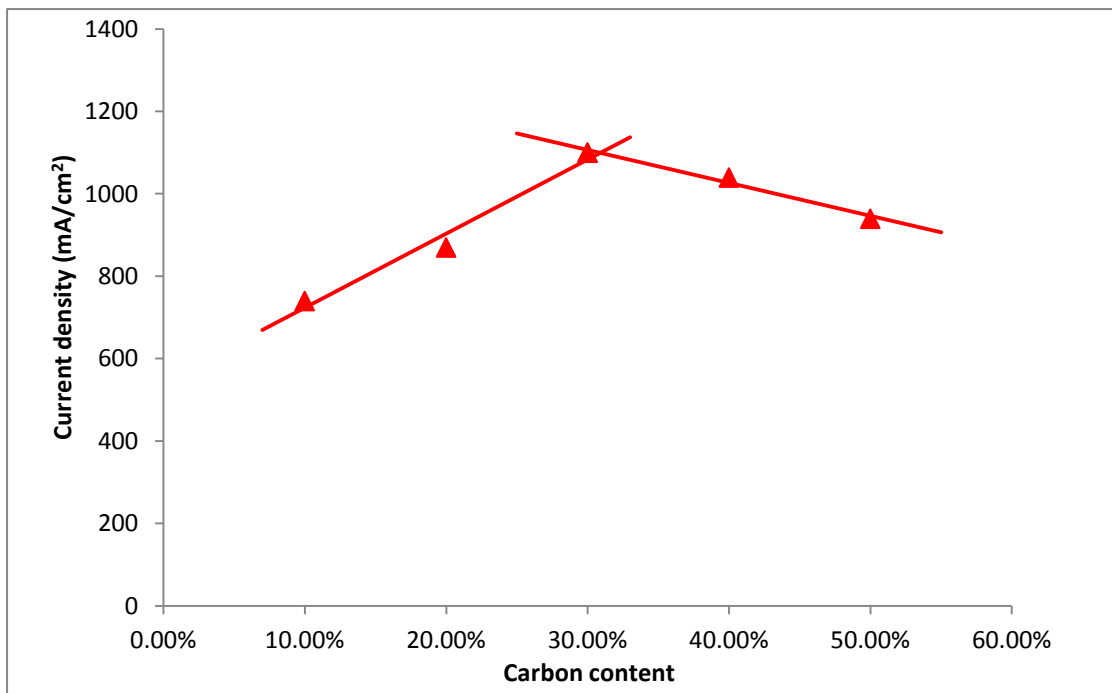
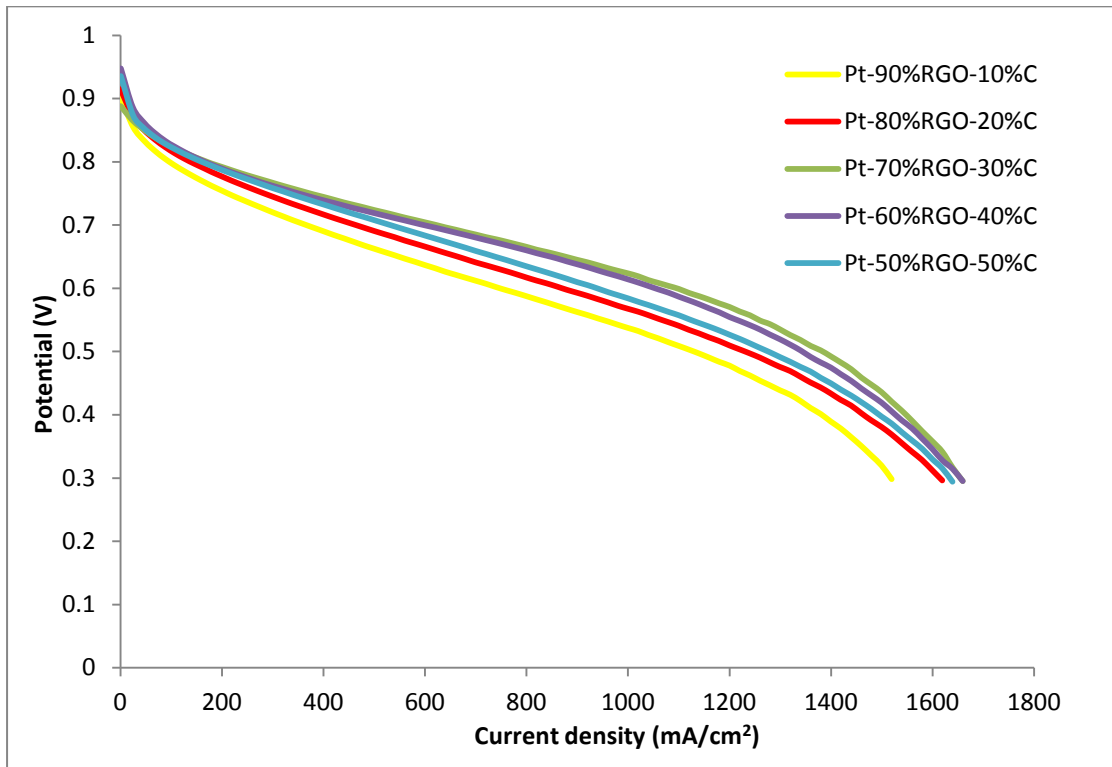
90 °C



100 °C



110 °C



120 °C

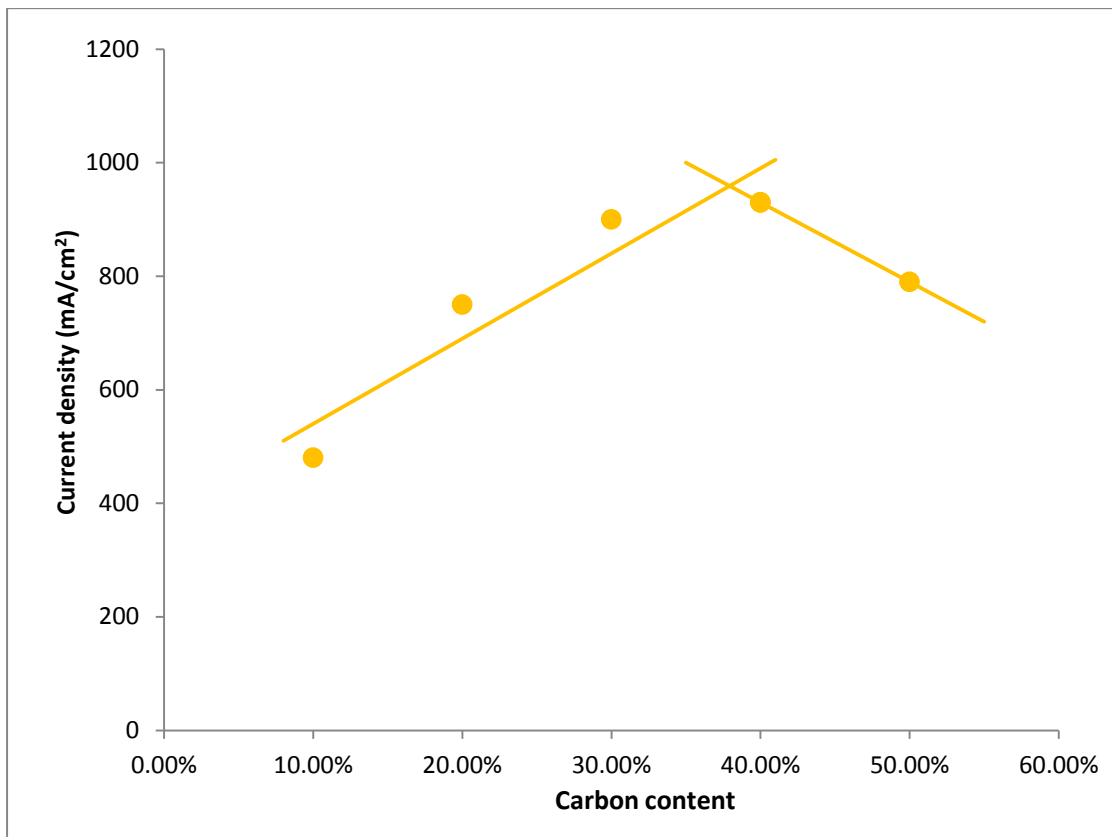
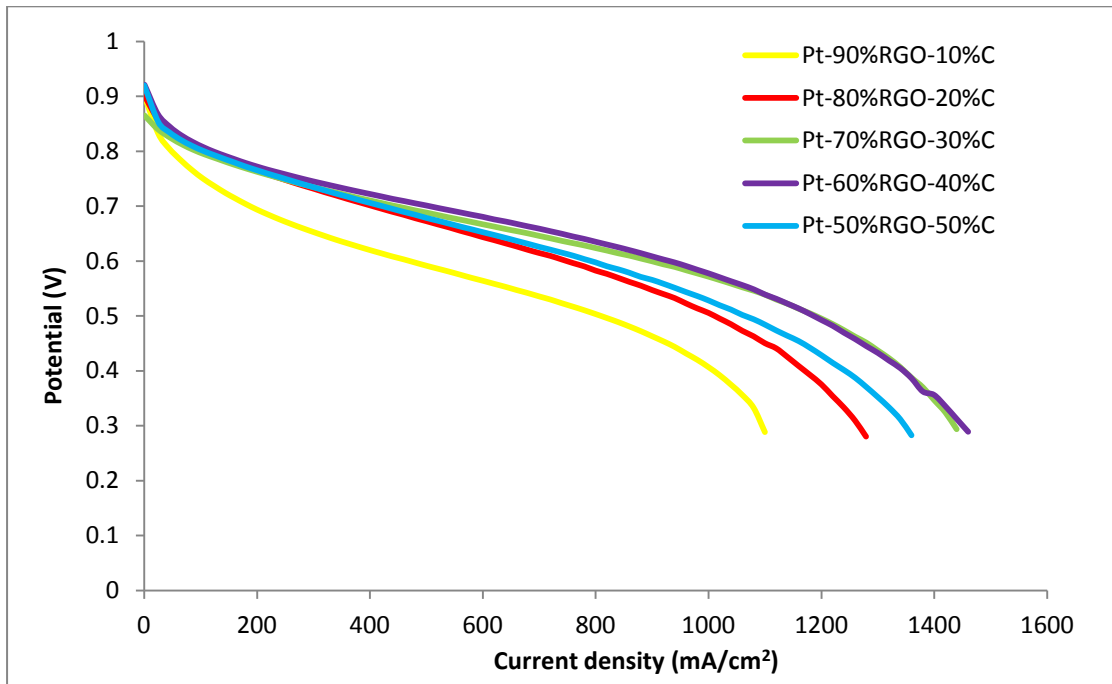


Figure.3.28. Polarization curves and the relationship between current densities at 0.6 V and the carbon content of different Pt catalysts at 80, 90, 100, 110 and 120 °C

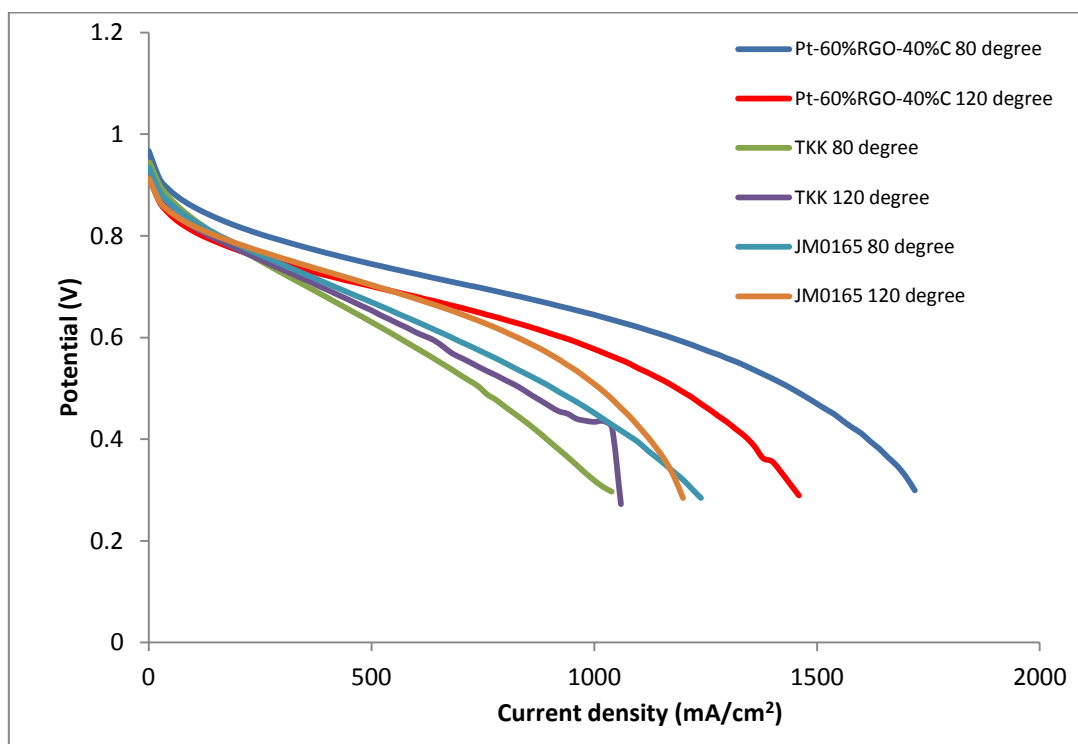


Figure.3.29. Polarization curves of Pt catalysts (Pt/(60%RGO+40%C), TKK and JM0165)

Table.3.10. ECSA of different catalysts with various carbon content in the in-situ test

Carbon content	ECSA (m^2g^{-1})
10%	45
20%	57
30%	75
40%	90
50%	19
Johnson Matthey 0165	60
TKK	72

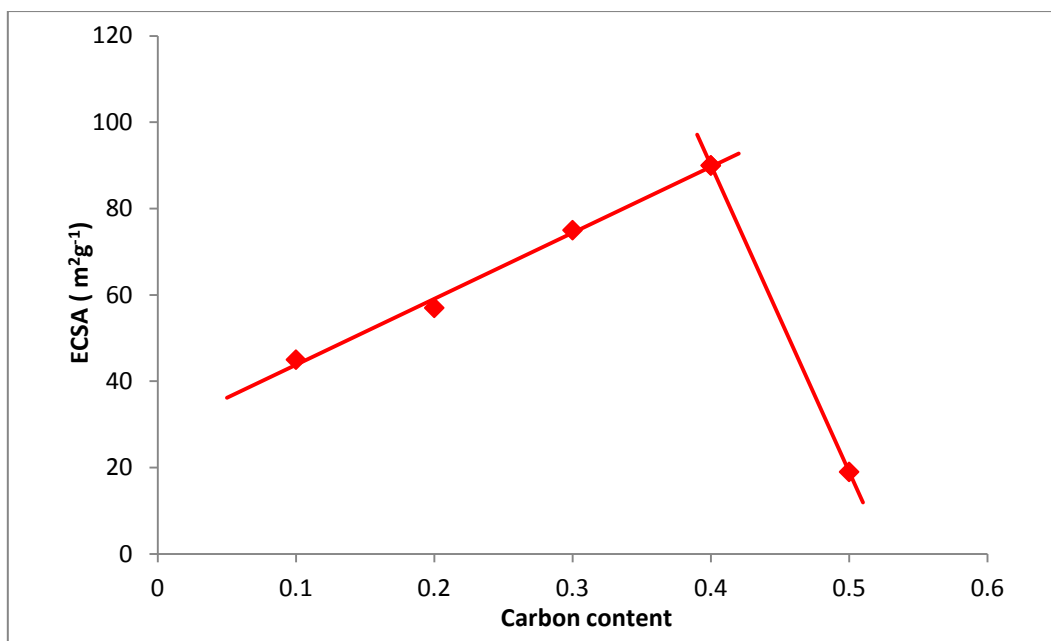


Figure.3.29.The relationship between different carbon-content catalysts and corresponding ECSA in the in-situ test

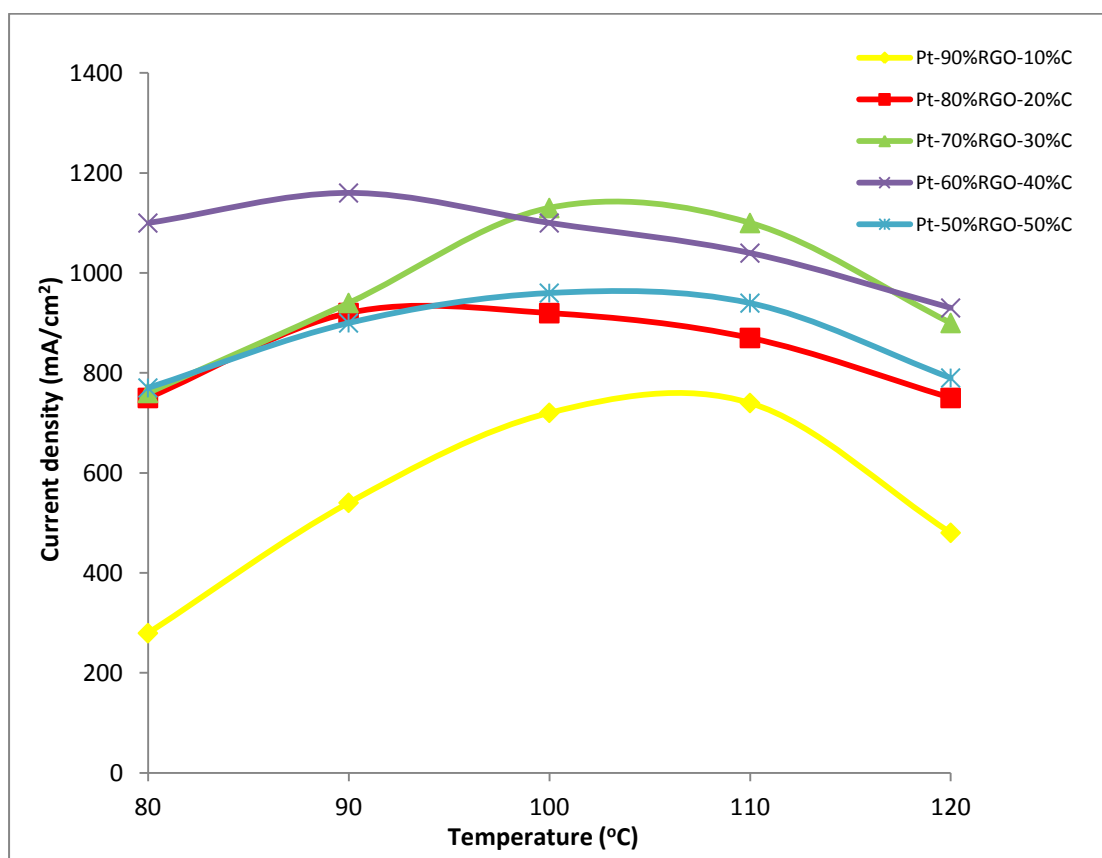


Fig.3.30. The effect of temperature to the current density at 0.6 V of Pt-RGO-C catalysts

4. Conclusions and Further Work

According to the state-of-art researches, Polymer Electrolyte Fuel Cells (PEFCs) have attracted a lot of interest due to their good response to load change, quick start up times and high efficiency value. During its operation process, hydrogen is oxidized at the anode and oxygen is reduced at the cathode. As the most significant problem, the cost of platinum catalyst is an obstacle in the commercial application of PEFC. In the cathode catalyst, available three phases (proton, electron and gas) boundary and transport are the essential determinants to the electrical efficiency.

The degradation of electrical property in the catalyst is due to three aspects: the agglomeration of Pt, the dissolution of Pt into the polymer electrolyte and the detachment of Pt nanoparticles from the support materials. Specifically, the diameter of Pt nanoparticles on the support materials is generally distributed as several nanometers. The high specific surface energy of Pt nanoparticles lets them tend to agglomerate during the operation, especially under the harsh conditions in PEFC operation. Based on the challenges outlined for PEFC catalysts, ideal support materials are usually required to own the following advantages: excellent electrical conductivity, large available surface area, mesoporous structure and good adhesion between catalyst particles and the support.

During our research, in order to reduce the platinum amount used in electrodes and get better electrochemical performance in both ex-situ and in-situ tests, we have broadened the utilization of electrode support materials (Carbon black, RGO and the mixed material of them) and achieved the fabrication and optimization of catalysts. The composition and structure of the catalysts we synthesized were characterized via TGA, XPS, FT-IR, SEM and TEM. The electrochemical characterizations were performed in both ex-situ and in-situ system.

TGA results have provided the evidence that the actual Pt contents of our Pt/RGO and Pt/(RGO+C) samples are approximative to our design data, ca. 20 wt%. In the XPS spectra, the different peaks illustrate that there are more oxygen functional group in Pt/RGO than Pt/C, as well as Pt particles have been successfully located on the support materials after MWAPP. FT-IR results illustrated the reduction reaction of GO in MWAPP requiring numerous hydroxide ion in the system, with pH at about 12.

The structure and dispersion of different support materials were observed in the ESEM images. The carbon black looks like small particles and the RGO has a typical sheet structure. The serious stacking of RGO sheets is observed in the SEM image of Pt/RGO. The stacking of GO sheet enfolds various Pt nanoparticles inside and directly reduces the ECSA of catalyst. The thickness of RGO existing in Pt/RGO almost reaches the micron level. Meanwhile, the strong ultrasonic treatment aided in reducing the size of RGO sheets. However, the small RGO pieces still tend to cluster together in the Pt/RGO samples. As to our Pt/(RGO+C) catalysts, the addition of carbon black has solved this problem very well. The carbon black particles encircle the RGO sheets to prevent them from stacking. As the C content increase, the amount of carbon particles is clearly growing and the agglomeration of RGO is releasing further. Specifically, in Pt/(60%RGO+40%C) catalyst, the thickness of RGO sheets was only about 20 nm. According to the TEM images of Pt/(60%RGO+40%C), it is clear that, the Pt nanoparticles only grew on the surface of RGO. That is to say, the addition of C after MWAPP did not act as the support materials of Pt nanoparticles. Moreover, a majority GO sheets have been changed into little pieces by strong ultrasonic treatment. The rare remaining RGO sheets are much thinner than the RGO sheets in Pt/RGO. Compared to the commercial Pt/C catalyst, our catalysts with the mixture support material of RGO and C have similar nanoparticle sizes and are more

uniform with stable Pt distribution. These aspects provides good evidence for the excellent performance in both ex-situ and in-situ test of our Pt/(RGO+C) made in-house.

As to the ex-situ test, the ECSA of the Pt/C catalysts that we can reproducibly fabricate is ca. $80 \text{ m}^2\text{g}^{-1}$. When compared with TKK, it illustrates that the ECSA of our Pt/C catalyst is higher than that of TKK. Moreover, the Pt/C sample made in-house has the similar electron transfer number with the commercial TKK. Meanwhile, we successfully produced the Pt/RGO with ECSA of $30.3 \text{ m}^2\text{g}^{-1}$ and electron transfer number of 1.84. Compared to Pt/C, the current value of RGO is high enough, while the double layer capacitance region of Pt/RGO is much larger than it is for Pt/C.

As to the fabrication process, the microwave-assisted polyol process (MWAPP) was used to fabricate catalysts in a quick way, involving only Pt precursor, support materials and polyol solution. Numerous results have been shown and analyzed to achieve the improvement of the Pt catalyst properties. In conclusion, when keeping the same energy, the condition with high power and short duration is beneficial to the catalyst. Furthermore, too much duration in procedure will make the Pt/RGO lose its catalytic activity. By our research, at 800W, the best reaction duration is clearly illustrated to be 50 s. Through various attempts of the heat treatment at different temperatures, the best temperature of the heat treatment to the Pt/RGO catalysts comes to be about 140°C .

The performance of the PEFC is influenced by many properties of the catalyst, such as electrical and ionic conductivity, hydrophobicity and reactant diffusivity. Thus a good balance among these aspects should be researched to optimize the catalyst layer. For reducing the losses in the transport processes, the volume amount of each phase among the transport media in catalyst is well distributed to achieve the electrode

optimization. Through our research, promising mixtures of support materials of C and RGO were proven to be efficient to improving the performance of Pt catalyst in both ex-situ and in-situ test, by reducing the agglomeration of Pt nanoparticles on RGO and increasing the stability of catalyst. The largest ex-situ ECSAs of the Pt/C catalyst and Pt/RGO catalyst were ca. $80 \text{ m}^2\text{g}^{-1}$ and ca. $45 \text{ m}^2\text{g}^{-1}$ respectively. As to the promising Pt-RGO-C catalysts, the Pt-60%RGO-40%C catalyst had an ex-situ ECSA at ca. $65 \text{ m}^2\text{g}^{-1}$, in-situ ECSA at ca. $90 \text{ m}^2\text{g}^{-1}$. At $80 \text{ }^\circ\text{C}$ and $120 \text{ }^\circ\text{C}$ it showed about 68% and 18 % higher current density (1100 and 930 mA/cm^2 , respectively), at 0.6 V , than the commercial GDE (JM0165) and commercial catalyst (TKK) in the polarization curve. Therefore, in our Pt-RGO-C catalysts, RGO has been utilized as support material instead of carbon black. The shortages of carbon black, such as poor durability and low stability, have been solved substantially. RGO has better performance because of its excellent electrical conductivity, large surface area and good adhesion to the Pt nanoparticles. Meanwhile, the remaining oxygen functional group on the RGO surface will also influence the property of catalyst in MEA. The different ratio between C and RGO has been optimized to find the best balance, which is in the range of 30 wt% to 40 wt% C in the support materials.

In future work, further test and characterization of catalyst is needed, such as utilizing the XRD analysis as to get more details of Pt lattice variety in the Pt/RGO after heat treatment, as well as more clear images under high resolution TEM. Moreover, attempts should be made to combine the optimization of the catalyst together to fabricate a new generation Pt catalyst with better performance. That is to say, we can create a fabrication process that produces Pt-65%RGO-35%C catalyst with MWAPP duration at 50 s, and then heat it at $140 \text{ }^\circ\text{C}$ for 2 hrs. Meanwhile, we will use the GO made in-house instead of the commercial GO. The GO produced

in-house is much easier for us to design, adjust and replace the oxygen functional groups on the surface. It is credible that the suitable modification to GO will bring about further progress to the Pt catalyst.

On the other hand, as it is introduced that a PEFC consists of five components, the overall performance of PEFCs is related to the property of each part. According to our results, there is an evident decrease of performance in MEA at 120 °C because of the activity loss of polymer electrolyte membrane at high temperature. Therefore, the type of membrane used in MEA, the system pressure, the relative humidity of gases as well as the ratio of Nafion to catalyst, will be further researched. In order to get an excellent PEFC, every component needs to be well designed and matching to each other.

5. References

- Antolini, E., & Giorgi, L. (1999). Influence of Nafion loading in the catalyst layer of gas-diffusion electrodes for PEFC, 136–142.
- Biyikoglu, a. (2005). Review of proton exchange membrane fuel cell models. *International Journal of Hydrogen Energy*, 30(11), 1181–1212. doi:10.1016/j.ijhydene.2005.05.010
- Carrassi, a, & Abati, S. (n.d.). [Introduction to scanning electron microscopy]. *Mondo Odontostomatologico*, 29(2), 29–36.
- Chandan, A., Hattenberger, M., El-kharouf, A., Du, S., Dhir, A., Self, V., Bujalski, W. (2013). High temperature (HT) polymer electrolyte membrane fuel cells (PEMFC) – A review. *Journal of Power Sources*, 231, 264–278. doi:10.1016/j.jpowsour.2012.11.126
- Chang, C. H., Yuen, T. S., Nagao, Y., & Yugami, H. (2011). Catalytic activity of carbon-supported iridium oxide for oxygen reduction reaction as a Pt-free catalyst in polymer electrolyte fuel cell. *Solid State Ionics*, 197(1), 49–51. doi:10.1016/j.ssi.2011.06.015
- Chang, Z., Pu, H., Zhao, Z., Pan, H., Li, B., & Wan, D. (2013). Preparation and Characterization of Semi-IPN Fluorine Containing Polybenzimidazole/Nafion Composite Membrane for Fuel Cells. *Fuel Cells*, 13(6), 1186–1195. doi:10.1002/face.201300177
- Chen, D., Li, L., & Guo, L. (2011). An environment-friendly preparation of reduced graphene oxide nanosheets via amino acid. *Nanotechnology*, 22(32), 325601. doi:10.1088/0957-4484/22/32/325601
- Chen, J., Lim, B., Lee, E. P., & Xia, Y. (2009). Shape-controlled synthesis of platinum nanocrystals for catalytic and electrocatalytic applications. *Nano Today*, 4(1), 81–95. doi:10.1016/j.nantod.2008.09.002
- Chen, W. X., Lee, J. Y., & Liu, Z. (2002). Microwave-assisted synthesis of carbon supported Pt nanoparticles for fuel cell applications. *Chemical Communications*, (21), 2588–2589. doi:10.1039/b208600j
- Chen, W., Zhao, J., Lee, J. Y., & Liu, Z. (2005). Microwave heated polyol synthesis of carbon nanotubes supported Pt nanoparticles for methanol electrooxidation. *Materials Chemistry and Physics*, 91(1), 124–129. doi:10.1016/j.matchemphys.2004.11.003
- Chen, W.-X., Lee, J. Y., & Liu, Z. (2004). Preparation of Pt and PtRu nanoparticles supported on carbon nanotubes by microwave-assisted heating polyol process. *Materials Letters*, 58(25), 3166–3169. doi:10.1016/j.matlet.2004.06.008

Chu, Y.-Y., Wang, Z.-B., Gu, D.-M., & Yin, G.-P. (2010a). Performance of Pt/C catalysts prepared by microwave-assisted polyol process for methanol electrooxidation. *Journal of Power Sources*, 195(7), 1799–1804. doi:10.1016/j.jpowsour.2009.10.039

Curnick, O. J., Mendes, P. M., & Pollet, B. G. (2010). Enhanced durability of a Pt/C electrocatalyst derived from Nafion-stabilised colloidal platinum nanoparticles. *Electrochemistry Communications*, 12(8), 1017–1020. doi:10.1016/j.elecom.2010.05.013

Dadda, B., Abboudi, S., & Ghezal, A. (2013). Transient two-dimensional model of heat and mass transfer in a PEM fuel cell membrane. *International Journal of Hydrogen Energy*, 38(17), 7092–7101. doi:10.1016/j.ijhydene.2013.03.142

Dreyer, D. R., Park, S., Bielawski, C. W., & Ruoff, R. S. (2010). The chemistry of graphene oxide. *Chemical Society Reviews*, 39(1), 228–40. doi:10.1039/b917103g

Eda, G., Fanchini, G., & Chhowalla, M. (2008). Large-area ultrathin films of reduced graphene oxide as a transparent and flexible electronic material. *Nature Nanotechnology*, 3(5), 270–4. doi:10.1038/nnano.2008.83

Eikerling, M., & Kornyshev, a. . (1999). Electrochemical impedance of the cathode catalyst layer in polymer electrolyte fuel cells. *Journal of Electroanalytical Chemistry*, 475(2), 107–123. doi:10.1016/S0022-0728(99)00335-6

Ferreira, P. J., la O', G. J., Shao-Horn, Y., Morgan, D., Makharia, R., Kocha, S., & Gasteiger, H. A. (2005). Instability of Pt/C Electrocatalysts in Proton Exchange Membrane Fuel Cells. *Journal of The Electrochemical Society*, 152(11), A2256. doi:10.1149/1.2050347

Garcia-Araez, N., Climent, V., & Feliu, J. M. (2010). Analysis of temperature effects on hydrogen and OH adsorption on Pt(111), Pt(100) and Pt(110) by means of Gibbs thermodynamics. *Journal of Electroanalytical Chemistry*, 649(1-2), 69–82. doi:10.1016/j.jelechem.2010.01.024

Hanawa, H., Kunimatsu, K., Watanabe, M., & Uchida, H. (2012). In Situ ATR-FTIR Analysis of the Structure of Nafion–Pt/C and Nafion–Pt₃Co/C Interfaces in Fuel Cell. *J. Phys. Chem. C*, 2012, 116 (40), pp 21401–21406 doi: 10.1021/jp306955q

Hasch é F. (2012a). Activity, stability, and degradation mechanisms of platinum and platinum alloy nanoparticle PEM fuel cell electrocatalysts. 2012.02.08

Hasch é F. (2012b). Activity, stability, and degradation mechanisms of platinum and platinum alloy nanoparticle PEM fuel cell electrocatalysts. 2012.02.08

He, W., Jiang, H., Zhou, Y., Yang, S., Xue, X., Zou, Z., Yang, H. (2012). An efficient reduction route for the production of Pd–Pt nanoparticles anchored on graphene nanosheets for use as durable oxygen reduction electrocatalysts. *Carbon*, 50(1), 265–274. doi:10.1016/j.carbon.2011.08.044

-
- Hirschenhofer, J., Stauffer, D., Engleman, R., & Klett, M. (1998). Fuel cell handbook, (November). Retrieved from [http://91.236.239.135/files/Survival/Energy and Fuel/Fuel Cell Handbook \(4th Ed, 1998\).pdf](http://91.236.239.135/files/Survival/Energy and Fuel/Fuel Cell Handbook (4th Ed, 1998).pdf)
- Kawatsu, S. (1998). Advanced PEFC development for fuel cell powered vehicles. *Journal of Power Sources*, *71*, 150–155.
- Komarneni, S., Li, D., Newalkar, B., Katsuki, H., & Bhalla, A. (2002). Microwave-polyol process for Pt and Ag nanoparticles. *Langmuir* *2002*, (30), 5959–5962.
- Kreuer, K.-D. (Ed.). (2013). *Fuel Cells*. New York, NY: Springer New York. doi:10.1007/978-1-4614-5785-5
- Kumar, R., Xu, C., & Scott, K. (2012). Graphite oxide/Nafion composite membranes for polymer electrolyte fuel cells. *RSC Advances*, *2*(23), 8777. doi:10.1039/c2ra20225e
- Kundu, P., Nethravathi, C., Deshpande, P. A., Rajamathi, M., Madras, G., & Ravishankar, N. Ultrafast Microwave-Assisted Route to Surfactant-Free Ultrafine Pt Nanoparticles on Graphene: Synergistic Co-reduction Mechanism and High Catalytic Activity. *Chemistry of Materials*, *23*(11), 2772–2780. doi:10.1021/cm200329a.2011.05.10
- Larminie, J., & Dicks, A. (2003a). *Fuel Cell Systems Explained*. West Sussex, England: John Wiley & Sons, Ltd., doi:10.1002/9781118878330
- Lebègue, E., Baranton, S., & Coutanceau, C. (2011). Polyol synthesis of nanosized Pt/C electrocatalysts assisted by pulse microwave activation. *Journal of Power Sources*, *196*(3), 920–927. doi:10.1016/j.jpowsour.2010.08.107
- Lee, D. C., Yang, H. N., Park, S. H., & Kim, W. J. (2014). Nafion/graphene oxide composite membranes for low humidifying polymer electrolyte membrane fuel cell. *Journal of Membrane Science*, *452*, 20–28. doi:10.1016/j.memsci.2013.10.018
- Lee, W.-D., Lim, D.-H., Chun, H.-J., & Lee, H.-I. (2012). Preparation of Pt nanoparticles on carbon support using modified polyol reduction for low-temperature fuel cells. *International Journal of Hydrogen Energy*, *37*(17), 12629–12638. doi:10.1016/j.ijhydene.2012.05.122
- Li, W., & Lane, A. M. (2011). Resolving the HUPD and HOPD by DEMS to determine the ECSA of Pt electrodes in PEM fuel cells. *Electrochemistry Communications*, *13*(9), 913–916. doi:10.1016/j.elecom.2011.05.028
- Liao, C.-S., Liao, C.-T., Tso, C.-Y., & Shy, H.-J. (2011). Microwave-polyol synthesis and electrocatalytic performance of Pt/graphene nanocomposites. *Materials Chemistry and Physics*, *130*(1-2), 270–274. doi:10.1016/j.matchemphys.2011.06.038
- Litster, S., & McLean, G. (2004). PEM fuel cell electrodes. *Journal of Power Sources*, *130*(1-2), 61–76. doi:10.1016/j.jpowsour.2003.12.055

-
- Liu, Z., Lee, J. Y., Chen, W., Han, M., & Gan, L. M. (2004). Physical and electrochemical characterizations of microwave-assisted polyol preparation of carbon-supported PtRu nanoparticles. *Langmuir : The ACS Journal of Surfaces and Colloids*, 20(1), 181–7.
- Makharia, R., Mathias, M., & Baker, D. (2005). Measurement of catalyst layer electrolyte resistance in PEFCs using electrochemical impedance spectroscopy. *Journal of The Electrochemical society*, vol. 970–977. doi:10.1149/1.1888367
- Mathew, P., Meyers, J. P., Srivastava, R., & Strasser, P. (2012). Analysis of Surface Oxidation on Pt and Pt Core-Shell Electrocatalysts for PEFCs. *Journal of The Electrochemical Society*, 159(5), B554. doi:10.1149/2.066205jes
- Mehta, V., & Cooper, J. S. (2003). Review and analysis of PEM fuel cell design and manufacturing. *Journal of Power Sources*, 114(1), 32–53. doi:10.1016/S0378-7753(02)00542-6
- Menéndez, J. a., Arenillas, a., Fidalgo, B., Fernández, Y., Zubizarreta, L., Calvo, E. G., & Bermúdez, J. M. (2010). Microwave heating processes involving carbon materials. *Fuel Processing Technology*, 91(1), 1–8. doi:10.1016/j.fuproc.2009.08.021
- Meng, H., & Wang, C.-Y. (2004). Electron Transport in PEFCs. *Journal of The Electrochemical Society*, 151(3), A358. doi:10.1149/1.1641036
- Millington, B., Du, S., & Pollet, B. G. (2011). The effect of materials on proton exchange membrane fuel cell electrode performance. *Journal of Power Sources*, 196(21), 9013–9017. doi:10.1016/j.jpowsour.2010.12.043
- Millington, B., Whipple, V., & Pollet, B. G. (2011). A novel method for preparing proton exchange membrane fuel cell electrodes by the ultrasonic-spray technique. *Journal of Power Sources*, 196(20), 8500–8508. doi:10.1016/j.jpowsour.2011.06.024
- Moulder, J., Stickle, W., Sobol, P., & Bomben, K. (1992). *Handbook of X-ray photoelectron spectroscopy*. Retrieved from [ftp://108-196-41-67.lightspeed.fyvlar.sbcglobal.net/Media/docs-archive/UARK/DMZ/XPS Handbook.pdf](ftp://108-196-41-67.lightspeed.fyvlar.sbcglobal.net/Media/docs-archive/UARK/DMZ/XPS%20Handbook.pdf)
- Murphy, O. J., Cisar, A., & Clarke, E. (1998). Low-cost light weight high power density PEM fuel cell stack. *Electrochimica Acta*, 43(24), 3829–3840. doi:10.1016/S0013-4686(98)00143-1
- Nicolet, T. (2001). Introduction to fourier transform infrared spectrometry. *Information Booklet*. Retrieved from <http://scholar.google.com/scholar?hl=en&btnG=Search&q=intitle:Introduction+to+Fourier+Transform+Infrared+Spectrometry#1>
- Optics, P. E. (n.d.). ENVIRONMENTAL SCANNING An Introduction to ESEM ®.

Pak, C., & Kang, S. (2010). Nanomaterials and structures for the fourth innovation of polymer electrolyte fuel cell. *Journal of Materials ...*, (May 2014), 2063–2071. doi:10.1557/JMR.2010.0280

Passalacqua, E., Lufrano, F., Squadrito, G., Patti, A., & Giorgi, L. (2001). Nafion content in the catalyst layer of polymer electrolyte fuel cells: effects on structure and performance. *Electrochimica Acta*, 46(6), 799–805. doi:10.1016/S0013-4686(00)00679-4

Ren, X., & Gottesfeld, S. (2001). Electro-osmotic Drag of Water in Poly(perfluorosulfonic acid) Membranes. *Journal of The Electrochemical Society*, 148(1), A87. doi:10.1149/1.1344521

Sasikumar, G., Ihm, J. W., & Ryu, H. (2004). Optimum Nafion content in PEM fuel cell electrodes. *Electrochimica Acta*, 50(2-3), 601–605. doi:10.1016/j.electacta.2004.01.126

Shao, Y., Yin, G., & Gao, Y. (2007). Understanding and approaches for the durability issues of Pt-based catalysts for PEM fuel cell. *Journal of Power Sources*, 171(2), 558–566. doi:10.1016/j.jpowsour.2007.07.004

Shao, Y., Zhang, S., Kou, R., Wang, X., Wang, C., Dai, S., ... Lin, Y. (2010). Noncovalently functionalized graphitic mesoporous carbon as a stable support of Pt nanoparticles for oxygen reduction. *Journal of Power Sources*, 195(7), 1805–1811. doi:10.1016/j.jpowsour.2009.10.036

Sharma, S., Ganguly, A., Papakonstantinou, P., Miao, X., Li, M., Hutchison, J. L., ... Ukleja, S. (2010). Rapid Microwave Synthesis of CO Tolerant Reduced Graphene Oxide-Supported Platinum Electrocatalysts for Oxidation of Methanol. *The Journal of Physical Chemistry C*, 114(45), 19459–19466. doi:10.1021/jp107872z

Shin, H.-J., Kim, K. K., Benayad, A., Yoon, S.-M., Park, H. K., Jung, I.-S., ... Lee, Y. H. (2009). Efficient Reduction of Graphite Oxide by Sodium Borohydride and Its Effect on Electrical Conductance. *Advanced Functional Materials*, 19(12), 1987–1992. doi:10.1002/adfm.200900167

Shin, S. I., Go, A., Kim, I. Y., Lee, J. M., Lee, Y., & Hwang, S.-J. (2013). A beneficial role of exfoliated layered metal oxide nanosheets in optimizing the electrocatalytic activity and pore structure of Pt-reduced graphene oxide nanocomposites. *Energy & Environmental Science*, 6(2), 608. doi:10.1039/c2ee22739h

SONE, Y. (2004). Fuel cell development for space applications: fuel cell system in a closed environment. *Journal of Power Sources*, 137(2), 269–276. doi:10.1016/j.jpowsour.2004.03.051

Song, P., Zhang, X., Sun, M., Cui, X., & Lin, Y. (2012). Synthesis of graphene nanosheets via oxalic acid-induced chemical reduction of exfoliated graphite oxide. *RSC Advances*, 2(3), 1168. doi:10.1039/c1ra00934f

Takahashi, I., & Kocha, S. (2010). Examination of the activity and durability of PEMFC catalysts in liquid electrolytes. *Journal of Power Sources*, 195(19), 6312–6322. doi:10.1016/j.jpowsour.2010.04.052

Tanuma, T., & Kinoshita, S. (2012). Impact of Gas Diffusion Layers (GDLs) on Water Transport in PEFCs. *Journal of The Electrochemical Society*, 159(2), B150. doi:10.1149/2.054202jes

Thostenson, E. T., & Chou, T.-W. (1999). Microwave processing: fundamentals and applications. *Composites Part A: Applied Science and Manufacturing*, 30(9), 1055–1071. doi:10.1016/S1359-835X(99)00020-2

Uchida, M., Aoyama, Y., Eda, N., & Ohta, A. (1995). Microstructure in the Catalyst Layer and Effects of Both Perfluorosulfonate Ionomer and PTFE - Loaded Carbon on the Catalyst Layer of Polymer Electrolyte Fuel Cells. *Journal of the Electrochemical ...*, 142(12). Retrieved from <http://jes.ecsdl.org/content/142/12/4143.short>

Vinodgopal, K., Neppolian, B., Salleh, N., Lightcap, I. V., Grieser, F., Ashokkumar, M., ... Kamat, P. V. (2012). Dual-frequency ultrasound for designing two dimensional catalyst surface: Reduced graphene oxide–Pt composite. *Colloids and Surfaces A: Physicochemical and Engineering Aspects*, 409, 81–87. doi:10.1016/j.colsurfa.2012.06.006

Watanabe, M., Igarashi, H., & Yosioka, K. (1995). An experimental prediction of the preparation condition of Nafion-coated catalyst layers for PEFCs. *Electrochimica Acta*, 40(3), 329–334.

Wee, J.-H., Lee, K.-Y., & Kim, S. H. (2007). Fabrication methods for low-Pt-loading electrocatalysts in proton exchange membrane fuel cell systems. *Journal of Power Sources*, 165(2), 667–677. doi:10.1016/j.jpowsour.2006.12.051

Xie, J., Wood, D. L., Wayne, D. M., Zawodzinski, T. a., Atanassov, P., & Borup, R. L. (2005). Durability of PEFCs at High Humidity Conditions. *Journal of The Electrochemical Society*, 152(1), A104. doi:10.1149/1.1830355

Zabihian, F., Davari, A., & Osei-Prempeh, G. (2013). Preliminary Results of Experiments on a Single Cell Polymer Electrolyte Fuel Cell Fueled With Carbon Monoxide. In *ASME 2013 11th International Conference on Fuel Cell Science, Engineering and Technology* (p. V001T01A012). ASME. doi:10.1115/FuelCell2013-18258

Zarrin, H., Higgins, D., Jun, Y., Chen, Z., & Fowler, M. (2011). Functionalized Graphene Oxide Nanocomposite Membrane for Low Humidity and High Temperature Proton Exchange Membrane Fuel Cells. *The Journal of Physical Chemistry C*, 115(42), 20774–20781. doi:10.1021/jp204610j

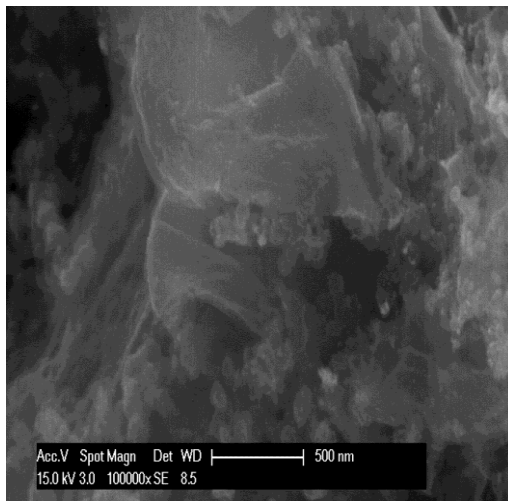
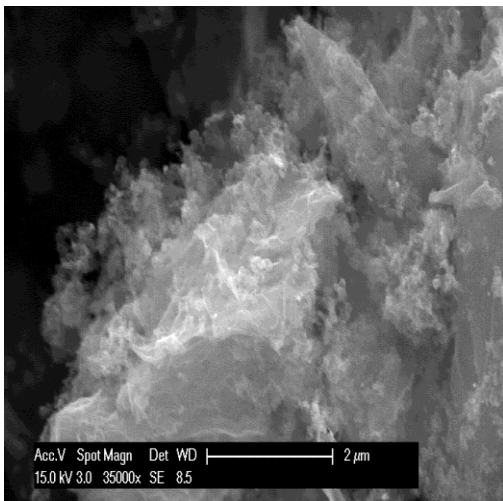
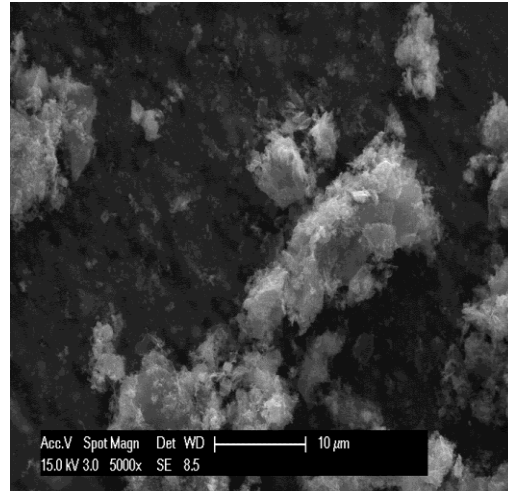
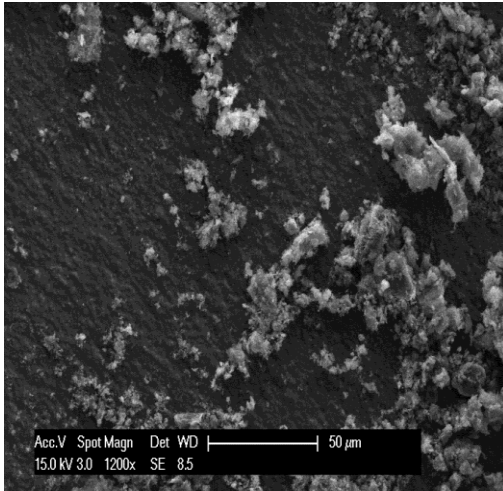
Zawodzinski, T. A. (1993). Water Uptake by and Transport Through Nafion® 117 Membranes. *Journal of The Electrochemical Society*, 140(4), 1041. doi:10.1149/1.2056194

Zhang, H., Xu, X., Gu, P., Li, C., Wu, P., & Cai, C. (2011). Microwave-assisted synthesis of graphene-supported Pd₁Pt₃ nanostructures and their electrocatalytic activity for methanol oxidation. *Electrochimica Acta*, 56(20), 7064–7070. doi:10.1016/j.electacta.2011.05.118

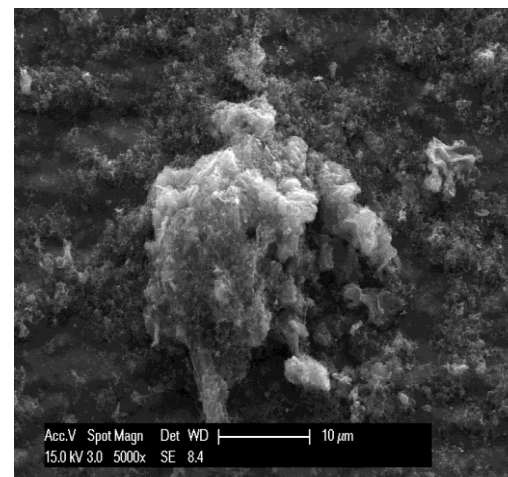
Zhou, Y., Liu, S., Jiang, H.-J., Yang, H., & Chen, H.-Y. (2010). Direct Electrochemistry and Bioelectrocatalysis of Microperoxidase-11 Immobilized on Chitosan-Graphene Nanocomposite. *Electroanalysis*, 22(12), 1323–1328. doi:10.1002/elan.200900637

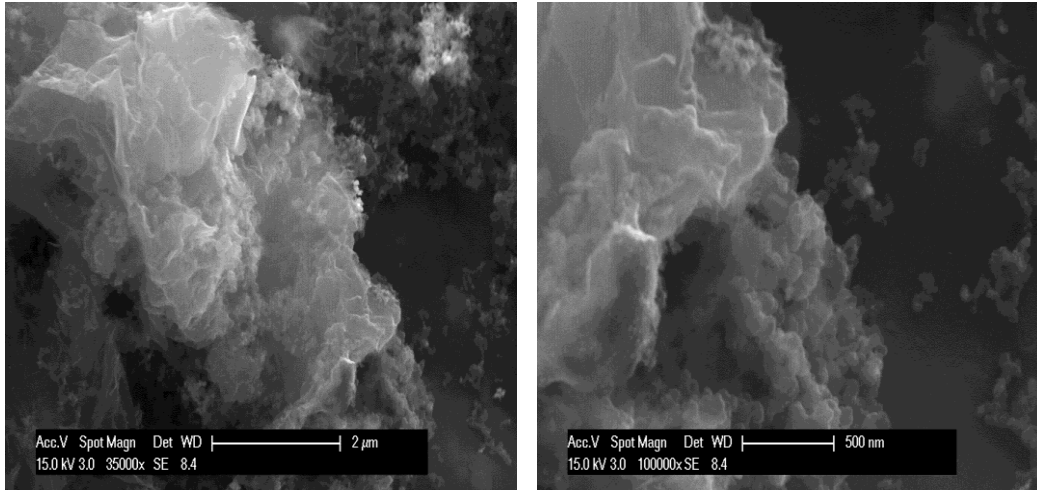
6. Appendix

Pt/(90%RGO+10%C)



Pt/(80%RGO+20%C)





Pt/(70%RGO+30%C)

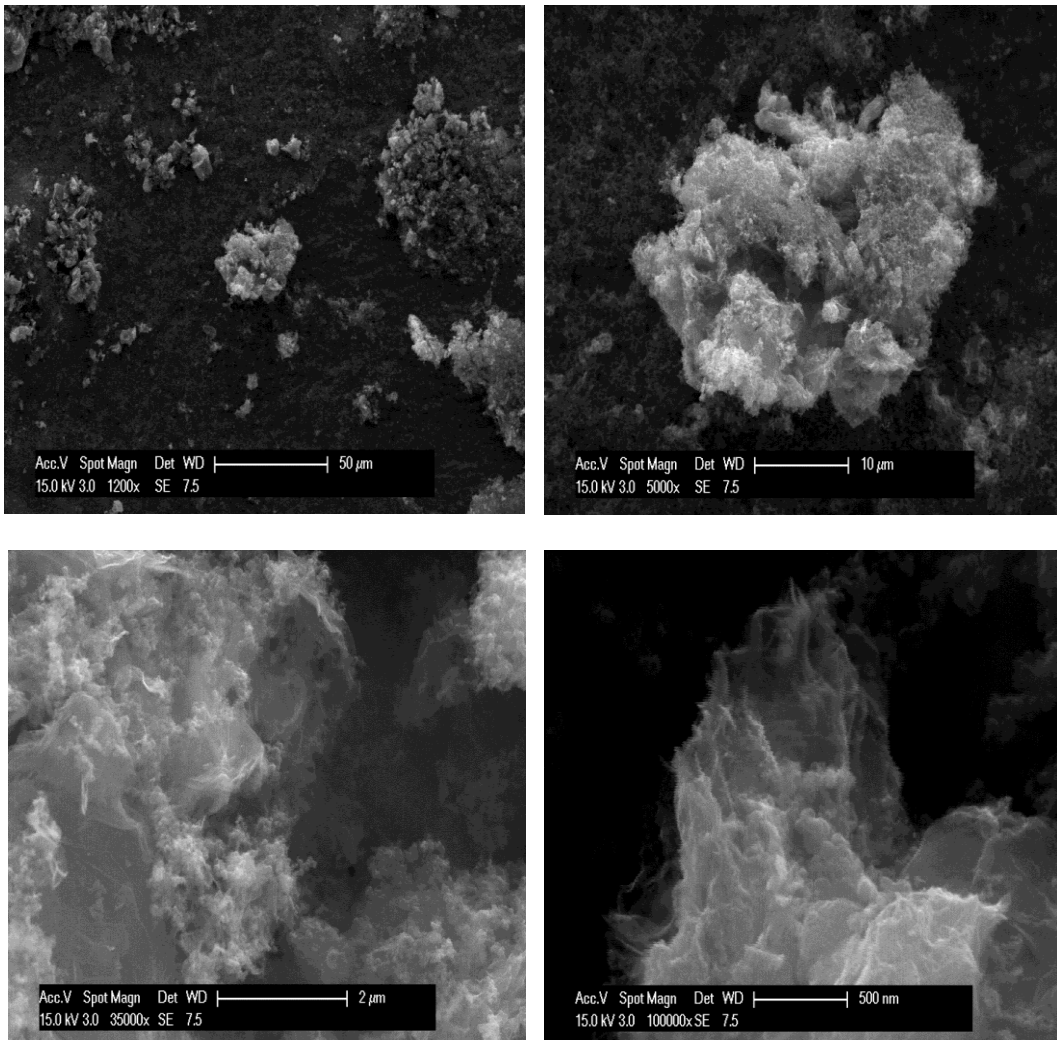
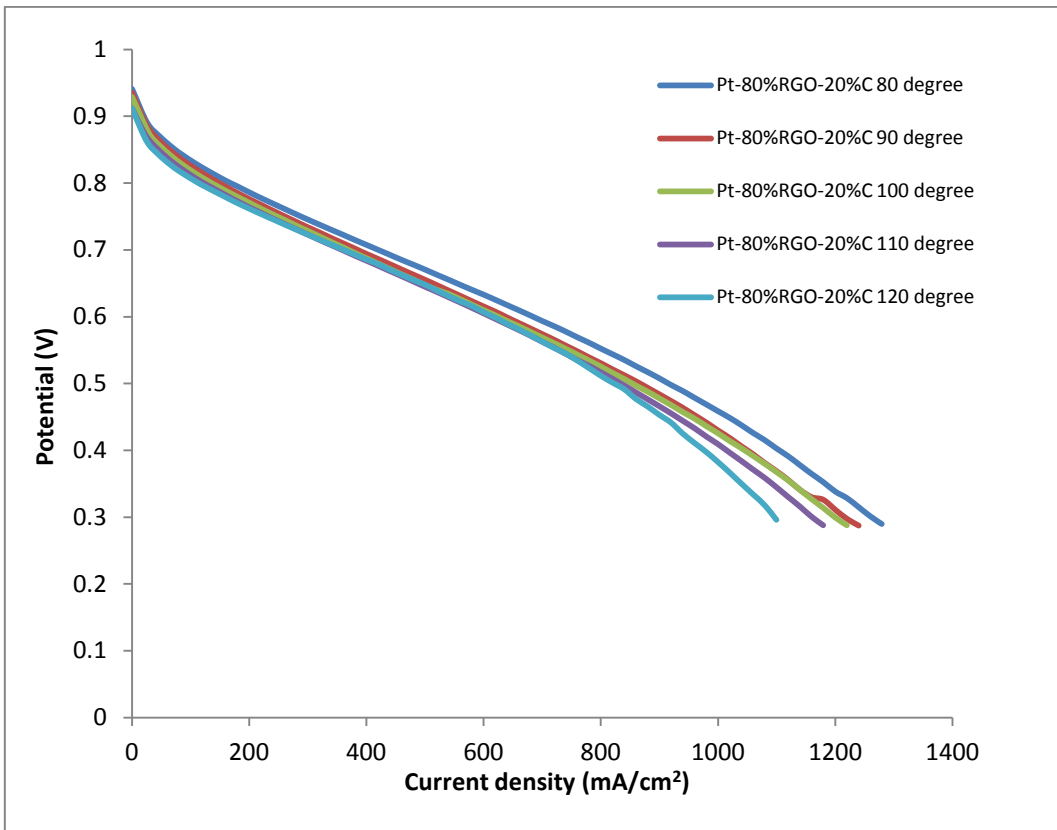
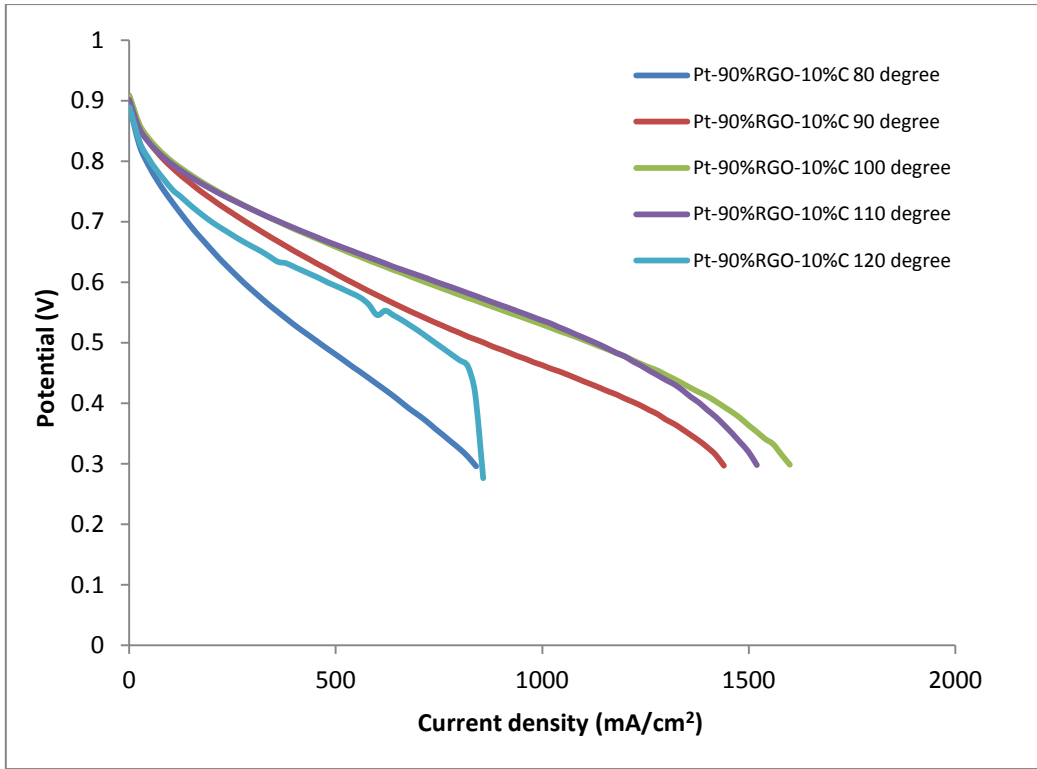


Figure.6.1. SEM of Pt-RGO-C catalysts with different carbon content



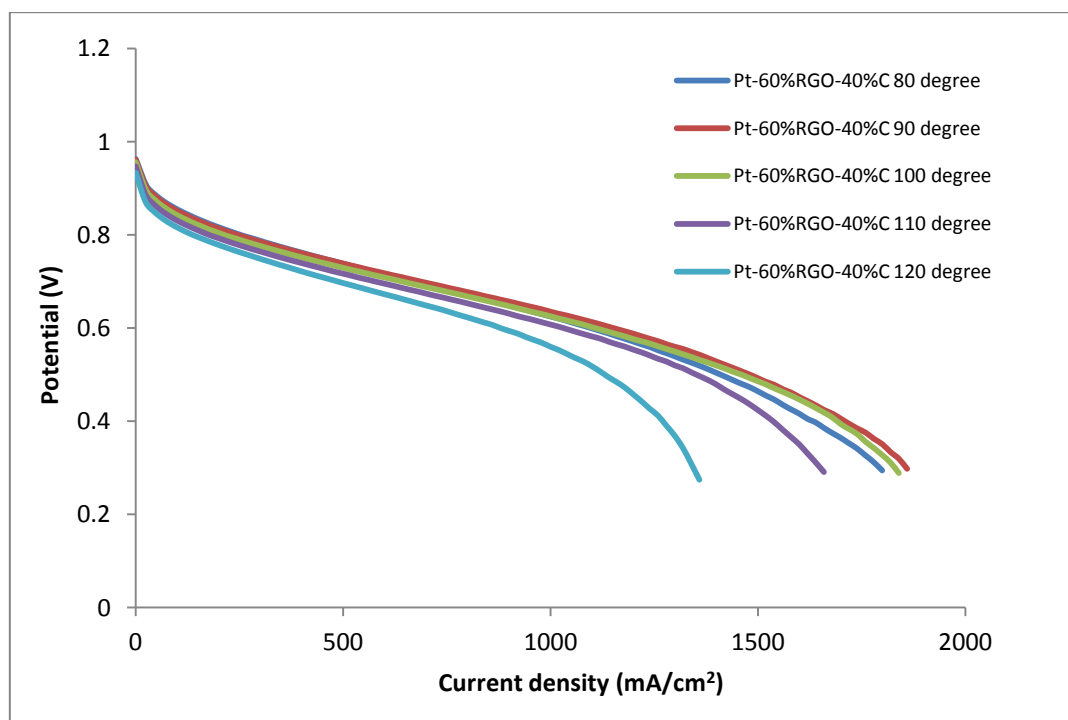
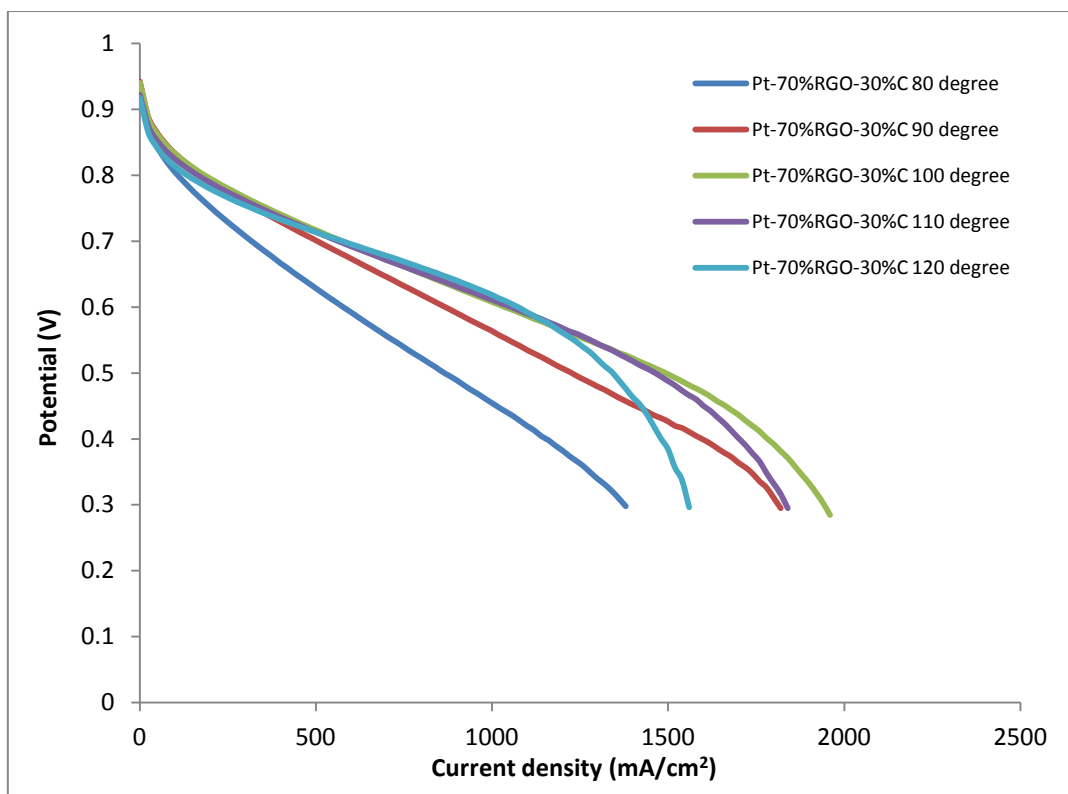


Figure.6.2. Polarization curves of Pt-RGO-C catalysts with different C content (10%, 20%, 30% and 40%) at various operation temperatures (80, 90, 100, 110 and 120 °C)